TÉCNICO LISBOA

Using 3D Cardiac Models derived from hPSCs for Cardiac Toxicity Studies during Heart Development

Tiago Alexandre Correia Nunes

Thesis to obtain the Master of Science Degree in

Biomedical Engineering

Supervisors: Doctor Mariana da Mota Veiga de Araújo Branco
Professor Dr. Maria Margarida Fonseca Rodrigues Diogo

Examination Committee

Chairperson: Professor Dr. Cláudia Alexandra Martins Lobato da Silva
Supervisor: Doctor Mariana da Mota Veiga de Araújo Branco
Member of the Committee: Doctor Hugo Machado Fernandes

November 2022

This work was created using LaTeX typesetting language
in the Overleaf environment (www.overleaf.com).

Preface

The work presented in this thesis was performed at the Stem Cell Engineering Research Group of the Institute for Bioengineering and Biosciences of Instituto Superior Técnico (Lisbon, Portugal), during the period March-October 2022, under the supervision of Prof. Margarida Diogo and Dr. Mariana Branco.

Declaration

I declare that this document is an original work of my own authorship and that it fulfills all the requirements of the Code of Conduct and Good Practices of the Universidade de Lisboa.

Acknowledgments

The journey that reaches its end with the conclusion of this dissertation was only possible due to the contribution of the many people that helped me during the years in one way or another. The following lines are my attempt at thanking them. Specifically, I would like to thank:

To Professor Joaquim Cabral for receiving me in SCERG.

To Professor Margarida Diogo, my supervisor, for introducing me to the world of stem cells; for, from the first interactions, always showing such a welcoming enthusiasm that made the work all the more rewarding; for believing that I was capable to undertake this project even when I didn't think the same; and for all the patience, wisdom and encouraging words that helped guide the work to its conclusion.

To Mariana Branco, my supervisor, for being the mentor that everyone wished they had; for all the knowledge transferred to me; for all the meetings with me squatting next to the desk while we were discussing the next experiments; for being there all the early mornings, the weekends, Easter and all the other holidays; and for the persistence when I thought I couldn't properly use a pipette.

To Miguel Tenreiro, for always being available to help the "masters" and for sharing the same morning grumpiness I have. To Ana Luísa for being my partner in crime during these last months; for all the pipette tips boxes that we filled; and for always taking the best side of the laminar flow hood.

To my MSc room colleagues, Iryna, João, and Beatriz, for the companionship and for the joint effort of making sure that none of us missed the shuttle; and to all the other SCERG group members.

To noc: Sara, Remco, Sofia, Ferrão, Andreia, and Ricardino. Thanks for all the amazing moments back in Tábua and all the crazy adventures in Coimbra. For the nights in the "cadeira" and the tears in the first days of university. A special thanks to Sara, Remco, and Joca, for always giving me shelter whenever I needed it and for helping make the most uncertain days look so easy.

To my university friends. I think it's fair to say that we were all lucky to find each other so fast after our academic journey began. A special thanks to Marta, Francisco, and Diogo for being amongst the most annoying people I have ever known. I think that is the reason we get along so well. I am also grateful to Dulce and the cats for all the allergies. Thank you all for the last five years and the many more to come.

Then, to my peoples in resi! Those who received me when I arrived in Lisbon and those I met from all over the world over the years. But particularly to those who eventually turned into my second family:

Bera, Gabi, Sara, Acácio, Jã Meguel, Catarina, Gonçalo, Ariana, and Pedro. We had a pretty good ride together. I could mention how much each one of you means to me but it would probably take a few pages. In summary, we learned together the most important things of the last five years and that makes it all worth it.

To Jorginho. I can imagine you are already complaining about not being on the previous list. It's for a good reason. Now that I think of it, it's a bit weird that you were the first person I met while enrolling in Técnico or the first person I met from RDP while buying groceries in the supermarket. But maybe there is such a thing as fate. In this case, it was for the best. Thank you for all the support and true friendship over the years.

Lastly, to Bruno, Ruca, and Andreia. Thank you for always believing in me and guiding me through life. To Mom and Dad, sorry for the long periods without going back home. Thank you for all the love and all the sacrifices. Without you, none of this would be possible. I will always keep you in my heart.

Abstract

The detection of cardiotoxic effects during drug development is a leading cause of attrition. Developmental cardiotoxicity assessment is particularly limited by the inability of pregnant women to participate in clinical trials, emphasizing the need to develop pre-clinical platforms able to accurately predict the drug's fetal safety profile. The use of human pluripotent stem cells (hPSCs) for engineering *in vitro* heart models is a promising solution. Although hPSC-derived cardiac models have considerably evolved into more physiological *in vivo*-like systems, the majority of the cardiotoxicity studies has been performed using 2D-based cardiac models which do not recapitulate the complex microenvironment of the heart. Furthermore, there is a lack of reliable studies focused on assessing functional and structural toxicity during the early stages of heart development. In this work, a 3D cardiac model was used to study the developmental cardiotoxicity of nine pharmaceutical compounds. The drug-induced impacts were assessed at the level of (i) mesoderm and endoderm progenitor population commitment, and (ii) cardiac cells specification into cardiomyocytes, using different drug exposure strategies. We observed that the timing of drug exposure had impact on the level of toxicity, and that early drug exposure could result in an imbalance of mesoderm and endoderm progenitor populations and a disruption of their spatial organization. The 3D cardiac model used in this study allowed to detect defects at the level of cavity formation, which was particularly relevant in the case of thalidomide. Thus, the presented platform has the potential to detect drug-induced cardiotoxicity during development at both structural and functional levels, and to help clarifying the mechanisms behind the detected toxicity.

Keywords

Human induced pluripotent stem cells; Cardiac models; Developmental cardiotoxicity; Mesoderm/endoderm commitment; Cardiomyocytes; Thalidomide.

Resumo

A cardiotoxicidade é uma das principais classes de efeitos adversos detetadas durante o desenvolvimento de novos fármacos. A avaliação da cardiotoxicidade durante desenvolvimento embrionário é particularmente limitada pela incapacidade de grávidas participarem em ensaios clínicos, enfatizando a necessidade de desenvolver plataformas pré-clínicas mais fidedignas. A utilização de células estaminais pluripotentes humanas (hPSC) para a engenharia de modelos cardíacos *in vitro* é uma solução promissora. Embora estes modelos tenham evoluído para sistemas mais fisiológicos, a maioria dos estudos de cardiotoxicidade são realizados utilizando modelos 2D que não recapitulam o complexo microambiente do coração. Além disso, há uma falta de estudos centrados na avaliação da toxicidade durante as fases iniciais do desenvolvimento do coração. Neste trabalho, foi utilizado um modelo cardíaco 3D para estudar a cardiotoxicidade do desenvolvimento de nove compostos farmacêuticos. Os impactos induzidos pelos fármacos foram avaliados ao nível do (i) comprometimento das populações progenitoras de mesoderme e endoderme, e (ii) da especificação das células cardíacas em cardiomiócitos. Observámos que o momento da exposição aos fármacos teve impacto no nível de toxicidade, e que uma exposição precoce poderia resultar num desequilíbrio entre as populações de progenitores e numa perturbação da sua organização espacial. O modelo cardíaco 3D utilizado neste estudo permitiu detetar impactos ao nível da formação de cavidades, o que foi particularmente relevante no caso da talidomida. Assim, a plataforma apresentada tem o potencial de detetar cardiotoxicidade induzida por fármacos durante o desenvolvimento e de clarificar os mecanismos por detrás desta.

Palavras Chave

Células estaminais pluripotentes induzidas humanas; Modelos cardíacos; Cardiotoxicidade do desenvolvimento embrionário; Comprometimento mesoderme/endoderme; Cardiomiócitos; Talidomida.

Contents

List of Figures

List of Tables

Acronyms

5-Fu	5-fluorouracil
ASA	acetylsalicylic acid
AP	action potential
ANOVA	analysis of variance
AVN	atrioventricular node
BMP	bone morphogenic protein
BSA	bovine serum albumin
cTNT	cardiac troponin T
CBZ	carbamazepine
CM	cardiomyocyte
CNNCs	cardiac neural crest cells
CAS	Chemical Abstracts Service Registry number
CSMC	coronary smooth muscle cell
DAPI	4',6-diamidino-2-phenylindole
DKK1	Dickkopf 1
DMSO	dimethyl sulfoxide
DOX	doxycycline hydrochloride
DMEM/F12	Dulbecco's Modified Eagle Medium/Nutrient Mixture F-12
PenStrep	penicillin/streptomycin
EAD	early after depolarization
EB	embryoid body
EC	endothelial cell
ECM	extracellular matrix

ESC embryonic stem cell

EHT engineered heart tissue

EMT epithelial-to-mesenchymal transition

EMA European Medicines Agency

EDTA ethylenediaminetetraacetic acid

EURL-ECVAM EU Reference Laboratory for Alternatives to Animal Testing

FDA Food and Drug Administration

FBS fetal bovine serum

FGF fibroblast growth factor

FHF first heart field

GSK3 glycogen synthase kinase-3

hADSC human adipose-derived stem cells

HCS high-content screening

HEK-293 human embryonic kidney 293

hERG human *ether-à-go-go*-related gene

hiPSC human induced pluripotent stem cell

hPSC human pluripotent stem cell

HUVEC human umbilical vein endothelial cell

ICM inner cell mass

IWP2 inhibitor of Wnt production-2

IWP4 inhibitor of Wnt production-4

JNK c-Jun NH2-terminal kinase

Klf4 Krüppel-like factor 4

KO-SR KnockOut™ serum replacement

LIF leukemia inhibiting factor

MAPK mitogen-activated protein kinase

mEST mouse embryonic stem cell test

NCE New Chemical Entity

Oct3/4 cctamer-binding transcription factor 3/4

PEG	polyethylene glycol
Pen G	benzylpenicillin sodium
PFA	paraformaldehyde
PAR	paroxetine hydrochloride
PDMS	polydimethylsiloxane
PBS	phosphate-buffered saline
PEO	proepicardial organ
ROCKi	Rho kinase inhibitor
ROS	reactive oxygen species
RyR	ryanodine receptor
SERCA	sarcoendoplasmic reticulum calcium ATPase
SR	sarcoplasmic reticulum
SV40	simian virus 40
SAN	sinoatrial node
SHF	second heart field
SMX	sulfamethoxazole
TBX5	T-box transcription factor
TdP	Torsades de Pointes
Thal	thalidomide
TMP	trimethoprim
TMP/SMX	co-trimoxazole
ULA	ultra-low attachment
WEC	whole embryo culture
Wnt	Wingless integrated

1

Introduction

Contents

1.1 Heart Development and Adult Heart

After implantation, the early embryo consists of a sphere of cells, the blastocyst, composed of an inner cell mass (ICM) and an outer layer, the trophoblast [Mahler and Butcher, 2011]. It is possible to assume that the process of cardiac development begins following gastrulation – the process by which the cells of the ICM are specified into three germ layers: ectoderm, mesoderm, and endoderm – with the formation of the cardiac mesoderm along the primitive streak. This series of events is primarily controlled by three families of signalling molecules: Wingless integrated (Wnt), fibroblast growth factor (FGF) and transforming growth factor-beta (TGF-β) superfamily ligands, which include bone morphogenic protein (BMP), Nodal and activin A. Later on, Wnt signalling plays once again an important role. This time, Wnt/β-catenin inhibition by Crescent and Dickkopf 1 (DKK1), expressed in the adjacent endoderm, induces specification of the cardiac mesoderm into cardiac progenitor cells [Miyamoto et al., 2021, Später et al., 2014].

Cardiac progenitor cells undergo complex processes of differentiation and migration. The cardiac mesodermal cells migrate towards the anterior side of the embryo and form the two main populations of progenitors: the first heart field (FHF) and second heart field (SHF). Co-migrating endoderm cells secrete factors that support this determination in a paracrine way, such as BMP and FGF [Lough and Sugi, 2000, Später et al., 2014]. The various steps of cardiac development include the formation of the cardiac crescent, mainly composed of FHF progenitors, which then rearranges to form the primitive heart tube. SHF progenitors play a role in heart tube elongation, which is followed by the looping of the heart tube. After this last step, other two progenitor populations become apparent, the proepicardial organ (PEO) and cardiac neural crest cells (CNNCs) [Später et al., 2014]. The heart eventually evolves into a four-chamber organ, composed of the right and left ventricles and the right and left atria (Figure 1.1).

The FHF will give rise to the left ventricle and parts of the atria, whereas the SHF forms the right ventricle, outflow tract, and parts of the atria [Protze et al., 2019]. The PEO is a cluster of mesothelial cells that will eventually attach and grow over the outer surface of the developing heart to form the epicardium [Meilhac and Buckingham, 2018]. CNNCs arise from the dorsal neural tube and migrate towards the heart. Their derivatives form the parasympathetic innervation of the heart, contribute to the valves and are part of the outflow tract patterning and septation [Protze et al., 2019].

The main cell types of the adult heart include (i) cardiomyocytes (CMs), about 75% in tissue volume but only 30% of the total number of cells; (ii) endothelial cells (ECs), 60% of the non-myocyte cell population; (iii) cardiac fibroblasts, 15% of non-myocyte cell population; (iv) coronary smooth muscle cells (CSMCs); and (v) epicardial cells [Branco et al., 2020a, Protze et al., 2019]. The CM population further divides into different subtypes, namely, right- and left-ventricular CMs, right- and left-atrial CMs, and CMs of the conduction system. The conduction system of the heart consists of the

sinoatrial node (SAN) pacemaker, the primary pacemaker, responsible for initiating the heart beat; the atrioventricular node (AVN) pacemaker, which conducts electrical signals from the atria to the ventricles; and the Bundles of His and Purkinje Fibers, fast conducting fibres that conduct the electrical pulse from the AVN to the apex of the ventricle where contraction is initiated [Protze et al., 2019].

The heart wall is divided into three distinct layers: (i) the endocardium, (ii) the myocardium and (iii) the epicardium. The endocardium consists of a specialized endothelial population that lines the lumen of the atria and ventricles and also gives rise to a portion of the coronary endothelium and to valvular endothelial and interstitial cells that form the major valves of the heart. It is also responsible for the induction of trabecular CMs at the early heart tube stage, which form structures known as trabeculae that develop within the lumen of the chambers and function to increase the surface area in the fetal heart [Protze et al., 2019]. The myocardium constitutes the middle layer of the heart wall. The epicardium is the epithelial layer that surrounds the myocardium. Some epicardial cells undergo an epithelial-to-mesenchymal transition (EMT) process and migrate into the myocardium as epicardium-derived cells, which eventually can give rise to other cell types, making the epicardium a primary source of cardiac fibroblasts and CSMCs [Protze et al., 2019, Später et al., 2014]. The epicardium plays a major role in supporting the proliferation of compact CMs, which form the thick compact layer of myocardium that provides the force generation required in the ventricles of the adult heart, gradually replacing the trabecular tissue [Protze et al., 2019].

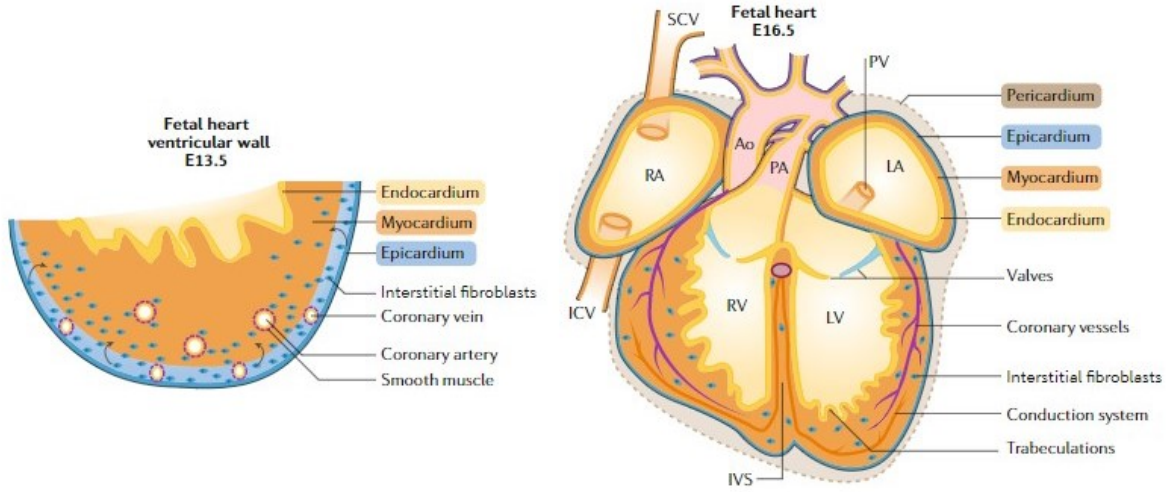

Figure 1.1: Late stages of cardiogenesis in the mouse embryo representing the cell type diversity of the heart. The heart wall is composed of three layers: the endocardium, the myocadium, and the epicardium. Some epicardial cells undergo EMT and give rise to interstitial fibroblasts (signalled with arrows on the left subfigure). The heart evolves into a four-chamber structure with two atria and two ventricles. Ao, aorta; ICV, inferior caval vein; IVS, interventricular septum; LA, left atrium; LV, left ventricle; OFT, outflow tract; PA, pulmonary artery; PV, pulmonary vein; RA, right atrium; RV, right ventricle; SCV, superior caval vein. Retrieved from [Meilhac and Buckingham, 2018].

1.2 Human Pluripotent Stem Cells and *In Vitro* Cardiac Models

1.2.1 Human Embryonic Stem Cells and Human Induced Pluripotent Stem Cells

The relevance of human pluripotent stem cells (hPSCs) in the biomedical research field is based on two main characteristics of these cells: long-term self-renewal capacity and pluripotency, the capability to differentiate into all mature cell types from the three primary germ layers of the embryo.

The isolation of mouse embryonic stem cells (ESCs) was first reported in 1981 [Evans and Kaufman, 1981]. However, it took more than a decade to obtain ESCs from the human blastocyst. This was performed by isolating and culturing cells from the ICM [Thomson et al., 1998] and opened new possibilities for human development research, among other fields of biology. Although a remarkable breakthrough, it also raised multiple ethical concerns related to the destruction and manipulation of human embryos.

The emergence of human induced pluripotent stem cells (hiPSCs), which are obtained after reprogramming adult somatic cells to a pluripotent state, allowed to circumvent these relevant issues. It also offers the possibility to generate human patient- and/or disease-specific cells [Brandão et al., 2017]. This major accomplishment was first reported using mouse somatic cells retrovirally transduced with the genes encoding four transcription factors – cctamer-binding transcription factor 3/4 (Oct3/4), Sox2, Krüppel-like factor 4 (Klf4), and c-Myc – which together became famously known as the *"Yamanaka factors"* [Takahashi and Yamanaka, 2006]. Just one year later, iPSCs were generated from human fibroblasts [Takahashi et al., 2007], effectively beginning the hiPSCs era, which resulted in a gradual replacement of the use of ESCs.

1.2.2 hPSC-derived Cardiac Models: from 2D Monolayer Models to Organoids

The first methods for CM differentiation from hPSCs were based on the formation of 3D embryoid bodies (EBs) which consist of spheroids that spontaneously differentiate into cells of the three germ layers. However, initial attempts lacked reproducibility and efficiency (EBs only contained $\approx$ 5-10% CMs). Some of the reasons behind the low efficiencies were the use of chemically undefined media such as fetal bovine serum (FBS) and the use of protocols based on undirected differentiation [Kehat et al., 2001].

Two-dimensional monolayer protocols using precise cocktails of morphogens capable of modulating the signalling pathways responsible for the induction of the mesodermal lineage eventually showed enhanced differentiation capacity leading to more enriched populations of CMs. Small molecules progressively replaced these growth factors due to their lower cost, faster production and reduced batch-to-batch variability. Lian and colleagues developed a growth factor-free protocol which relied on the temporal modulation of the canonical Wnt signalling pathway [Lian et al., 2012]. First, a step of Wnt signalling pathway activation was performed for mesendoderm induction (a bi-potent group of progenitors that can give rise to endoderm and mesoderm cells) through glycogen synthase kinase-3 (GSK3)

inhibition by CHIR99021, a step required for the translocation of β-catenin into the nucleus and transcriptional induction of genes controlled by the Wnt pathway. This is followed by Wnt's own inhibition for cardiac lineage specification using inhibitor of Wnt production-2 (IWP2) or inhibitor of Wnt production-4 (IWP4). This protocol, named GiWi protocol, was capable of producing a high yield of up to 98% CMs, a significant improvement over the initial methodologies.

However, the maturation level of hPSC-derived CMs was still in line with a fetal stage raising the need to develop more complex systems to surpass that limitation. Three-dimensional differentiation protocols would reveal enhanced features, such as more *in vivo*-like cell-to-cell interactions, to better recapitulate signalling events that occur during development [Branco et al., 2020a].

Size heterogeneity was one of the factors contributing to the low efficiencies of CM differentiation in early EB protocols. The use of forced aggregation platforms, including microwell plates, U- and V-shaped 96-well plates, and micropatterned surfaces, allowed to control the size of the aggregates by varying the cell seeding density in each well. This improved the efficiency and reproducibility of 3D CM differentiation protocols [Branco et al., 2020b].

By using a directed CM differentiation protocol, Bauwens and colleagues confirmed the link between aggregate size and homogeneity on CM differentiation efficiency. Moreover, the authors hypothesized a mechanistic link between CM differentiation efficiency and combined endoderm specification. Indeed, a variation of aggregate size affected not only the frequency of cardiac troponin T (cTNT)-positive cells at terminal differentiation but also the extent of endoderm layer formation early on, suggesting that a disturbance of the level of endoderm-secreted factors may be responsible for reduced efficiency [Bauwens et al., 2011].

More recently, Branco and colleagues developed a platform for cardiac cell differentiation based on the temporal modulation of the Wnt signalling pathway. The cells also grow as size-controlled aggregates using a forced aggregation platform. In this study, it was shown, through a transcriptomic analysis, that cells differentiated in 3D conditions revealed enhanced maturation compared to a 2D monolayer protocol. Before cardiac induction, a period of hiPSC expansion under 3D conditions primed the hiPSCs towards the mesendodermal lineage due to an up-regulation of mitogen-activated protein kinase (MAPK)/c-Jun NH2-terminal kinase (JNK), a stabilization of TGF-β/Nodal signalling and an increase in glycolysis metabolism, which was suggested to explain the differences detected when compared to 2D-differentiated cells [Branco et al., 2019].

Nonetheless, the heart's complex structure can not be recapitulated entirely with protocols that direct differentiation towards only CMs. Other tissue engineering strategies have been deployed to support the development of an array of cardiac cells. The definition of the various techniques used for cardiac tissue engineering varies from author to author. From here on, we followed Miyamoto and colleagues' classification of the current hPSC-derived 3D cardiac model assembly strategies [Miyamoto et al., 2021].

Microtissues are defined as models that incorporate already differentiated CMs with supporting cell types such as cardiac fibroblasts and ECs in three-dimensional structures. Since the aggregates are formed using cell types of different origins or independently differentiated, the recapitulation of heart development is limited. However, these models can help study the role of the different cardiac cell types in CM functionality.

Richards and colleagues used a mix representative of the main cardiac cell types, hiPSC-CMs, primary cardiac fibroblasts, and human umbilical vein endothelial cells (HUVECs) at a ratio of 5:4:1, respectively, to form microtissues using non-adhesive agarose hydrogel molds [Richards et al., 2017]. They also studied the inclusion of other cell types by adding human adipose-derived stem cells (hADSCs) to the mix due to their pro-angiogenic potential, resulting in increased number of CD31-positive cells and lumen formation capacity. When comparing to hiPSC-CMs-only aggregates, the microtissues showed increased levels of extracellular matrix (ECM) component collagen I, which was attributed to the presence of cardiac fibroblasts. A higher level of CM maturation within the microtissues was also observed as concluded from immunostaining analysis of sarcomere structure and a higher ratio of expression of cardiac troponin I (*TNNI3*) over slow, skeletal troponin I (*TNNI1*). These findings strengthen the idea that the presence of diverse cardiac cell types allows hPSC-based cardiac models to move one step closer towards mimicking the heart's microenvironment.

More recently, further advances have been achieved in recapitulating the structure of the early heart and its various developmental steps. Thus, the first cardiac organoids arose. Organoids can be defined as *in vitro* 3D miniaturized organ-like structures composed of multiple self-organizing cell types that pattern similarly to their *in vivo* equivalent and undergo *in vivo*-like developmental trajectories [Miyamoto et al., 2021]. Organoids reproducing multiple organ systems, such as specific regions of the brain [Qian et al., 2016] have been achieved. However, advancements in cardiac organoids lagged mainly due to the complexity of early heart morphogenesis.

A method of hPSC-derived developmental cardiac organoids, which presented both cardiac and endodermal lineages has been reported. This was performed by embedding aggregates in Matrigel followed by a two-step Wnt pathway modulation using CHIR and IWP2. The structures presented an inner endodermal core surrounded by endocardial-like cells, a dense cardiomyocyte layer, and cardiomyocytes interspersed with liver anlagen and septum transversum-like cells. The morphogenesis of these organoids is currently limited to very early developmental stages. Matrigel encapsulation was found to be indispensable for organoid formation [Drakhlis et al., 2021].

Although the previous model is capable of recapitulating early steps in development, it lacks a vital step unique to the heart: chamber formation. Lewis-Israeli and colleagues generated heart organoids following a differentiation protocol based on the temporal modulation of Wnt signalling in three steps: (i) Wnt pathway activation for mesodermal induction using CHIR, combined with BMP and Activin; (ii)

Wnt pathway inhibition for cardiac lineage specification using Wnt-C59; and (iii) an extra one-hour CHIR exposure to induce pro-epicardial organ specification. Epicardial-like cells were found on external layers of the organoid and adjacent to myocardial tissue. The final organoid structure featured the formation of microchambers. However, these were notably small and could not form a standardized pattern [Lewis-Israeli et al., 2021] .

At the same time, Hofbauer and colleagues reported a platform that recapitulates heart chamber formation, and how this process can be mechanistically modulated *in vitro*. Additionally, they explored the co-generation of an endocardial layer lining the cavity-like structure and described a strategy to induce epicardial layer formation through co-culture with pro-epicardial organ-like structures [Hofbauer et al., 2021].

Engineered heart tissues (EHT) use various tissue engineering approaches, such as mechanical stretch, electrical stimulation, and bioprinting, to help CMs reach a more adult-like state. These tissues can be distinguished from cardiac organoids since they usually present limited patterning and tissue-level scale. They are also different from microtissues since they are forced into a particular structure using biomimetic engineering solutions [Miyamoto et al., 2021].

Mills and colleagues designed a platform consisting of a 96-well plate with customized inserts containing two polydimethylsiloxane (PDMS) elastomeric posts that allowed the formation of dense muscle bundles around the scaffolds, forming a circular structure [Mills et al., 2017]. A mix of pre-differentiated cells composed by 70% hESC-CMs and $CD90^{+}$ stromal cells obtained from the same differentiation protocol was then mixed with a matrix containing collagen I and Matrigel. This system allows measurement of the force of contraction by automated tracking of the movement of the poles.

With the aim of performing direct measurement of organ-level and physiologically relevant ventricle contractile properties beyond beating frequency, Li and colleagues developed a custom construct in which previously differentiated CMs were re-suspended together with human dermal fibroblasts [Li et al., 2018]. This was performed using a spherical agarose mould containing a filled silicone balloon that allowed the formation of a chamber-like structure (with the balloon and the agarose mold providing an inner and outer boundary, respectively, for the cells to form a ventricle-like CM layer). However, while trying to mimic adult-like heart features, high-wall stress was detected and the cells showed limited maturity levels and random cell alignment.

Overall, the phenotypic characteristics of hPSC-derived CMs have similarities to primary human CMs in terms of molecular, electrophysiological and metabolic properties. Nonetheless, in general, such characteristics still point to an immature phenotype compared to adult CMs and closer to that of fetal CMs [Sayed et al., 2016]. If this diminishes their utility for adult-related applications, at least for now, it offers the opportunity to use these cells to study heart development and how it can be impaired.

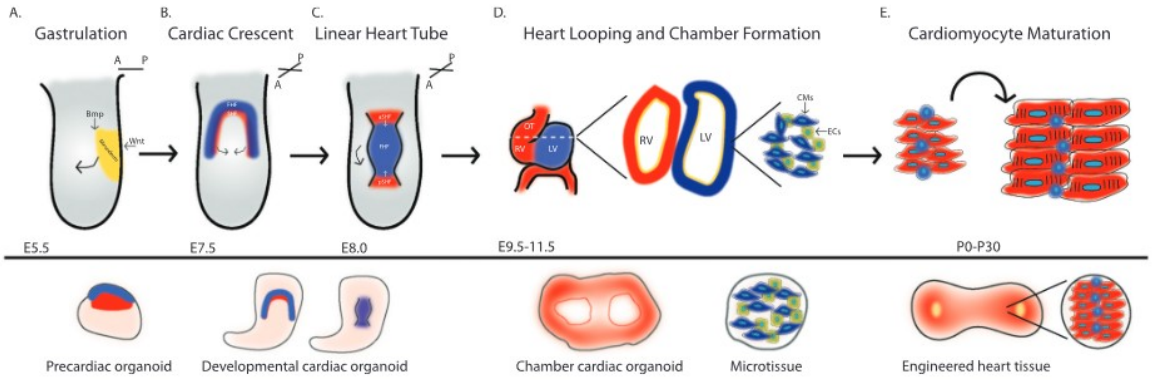

Figure 1.2: Key steps of cardiac development and corresponding hPSC-derived cardiac *in vitro* models. **A** - Gastrulation. Precardiac organoids model this stage but were not mentioned since the models in the literature use mouse ESC. **B, C** - Cardiac crescent formation and the linear heart tube step. Developmental cardiac organoids model this stage of development. **D** - Embryo undergoing rightward looping and chamber formation. Chamber cardiac organoids recapitulate this stage of development and microtissues offer insights into the cell type-cell type interactions between CMs and stromal cells. **E** - Maturation of cardiomyocytes to promote adult heart function. EHTs attempt to promote a more adult-like state of cardiac tissues. Retrieved from [Miyamoto et al., 2021].

1.3 Drug Development and Cardiotoxicity Screening

Assessment of potential toxicity caused by pharmacological compounds is a primary concern during drug development. This procedure is controlled by the responsible regulatory agency in the region where the drug is to be marketed, e.g. the European Medicines Agency (EMA) in the European Union and the Food and Drug Administration (FDA) in the United States. It can be divided into three pre-marketing steps and one post-marketing step. In the first pre-marketing step, Discovery and Development, a New Chemical Entity (NCE) (FDA's nomenclature) is developed or an already-approved drug may be repurposed based on a comprehensive understanding of the disease pathophysiology, and initial testing of the drug effects and efficacy is performed. This stage is followed by Pre-Clinical Research, where both *in vitro* and animal tests are carried out to evaluate pharmacokinetic, pharmacodynamic and toxicology parameters before first-in-human studies. The final pre-marketing step, Clinical Research, is commonly comprised of four phases carried out in increasing sets of healthy human volunteers and/or patients. Phase 1 aims to define the tolerability, pharmacokinetics and safety profile. Subsequently, phase 2 and 3 studies examine the therapeutic efficacy and safety in exploratory and confirmatory manners, respectively. Phase 4 and Post-Marketing surveillance establish a long-term safety profile and determine the efficacy and safety in different populations not included in phase 3 [Ovics et al., 2020].

One of the main therapeutic disasters that shaped this process was the *"Thalidomide Tragedy"* [Paine, 2017]. Thalidomide was patented in 1954 in Germany, having been developed as a possible antidote to nerve gas poisoning. However, by the time it was first marketed in 1957, it was used as a sedative, a pain killer and an anti-emetic appropriate for the treatment of nausea in pregnant women.

Soon, its use was widespread in Europe, Australia, and Japan. However, in 1961, the Australian obstetrician William McBride published a letter in *The Lancet* reporting an increase in the incidence of congenital abnormalities observed in babies delivered by women treated with thalidomide [McBride, 1961]. In fact, it has been reported that between its launch and withdrawal from the market in 1961, more than 10 000 children in 46 countries were born with congenital deformities, most commonly phocomelia (malformations of the limbs). Other birth defects included congenital heart disease, malformations of the inner and outer ear, and ocular abnormalities [Kim and Scialli, 2011, Lachmann, 2012]. In the pre-clinical testing, no tests were performed on pregnant animals to check possible effects on the fetus since it was thought that the human placenta gave perfect protection and was impermeable to toxic substances unless they were present at such large quantities that they would also kill the mother [Dally, 1998]. This prompted regulatory agencies to create more strict legislation requiring that all drugs be tested for teratogenicity through the analysis of possible ill effects on the fetus in pregnant animals [Lachmann, 2012].

Due to fear of such risks and the threat of legal liabilities, pregnant women have been excluded from clinical trials for nonobstetric conditions [Blehar et al., 2013]. A review of the industry-sponsored clinical trials in the US between 2011 and 2012 showed that 95% of them excluded pregnant women [Shields and Lyerly, 2013]. Furthermore, a 2011 study revealed that from the drugs approved by the FDA between 2000 and 2010, 97.7% did not have sufficient data regarding the teratogenic risk in human pregnancy [Adam et al., 2011]. On the flip side, the fact that the age at the time of pregnancy has been increasing along with the rates of comorbidities, such as hypertension and depression, is likely responsible for the fact that the rate of medication use during pregnancy has significantly increased [Ayad and Costantine, 2015]. For example, whereas the rate of pregnant women using antidepressants in 1996 was 2% this value was estimated to have risen to 7.5% only a decade later [Andrade et al., 2008]. In addition, changes in immunity and physiology during pregnancy can make pregnant women more susceptible to infectious diseases requiring the use of antibiotics [Jamieson et al., 2006]. From this, resulted the fact that, in 2015, almost half of pregnant women were using four or more drugs at some point during pregnancy. This increase is predominant in the first semester, a crucial period for organogenesis and, therefore, more susceptible to teratogen exposure [Ayad and Costantine, 2015, Mahler and Butcher, 2011].

1.3.1 Cardiotoxicity: The Most Common Cause for Drug Withdrawal

The drug development process is lengthy and costly, and the price tag increases exponentially as the drug progresses through the various stages of its development. Estimates predict that 70% of the toxicity detected in clinical trials could be identified in the preclinical phase using animal models and that a 10% increase in the capacity of preclinical models to predict such effects could save, on average, 100 million dollars per drug [Olson et al., 2000, Sasseville et al., 2004].

About 45% of all drugs withdrawn from the market and 30% of restrictions to drug application are due to unexpected toxic cardiovascular effects [Laverty et al., 2011]. This can be caused by drugs targeting both cardiac or non-cardiac cells after acute or chronic drug treatment, which means that drug side effects of cardiovascular nature can occur very late in the drug development process, endangering the patient's safety and increasing both the time and cost of marketing a new drug.

Moreover, developmental cardiotoxicity is particularly aggravated by the fact that severe cardiovascular dysfunction is lethal for embryos after approximately 3-4 weeks of gestation, which means that exposures that result in early miscarriage are challenging to identify and studies at birth would only capture a small part of possible outcomes [Mahler and Butcher, 2011].

Currently available *in vivo* and *in vitro* platforms for cardiotoxicity assessment are still regarded oversimplified and lacking specificity in detecting the cardiac safety profile of a drug when compared to its effects in humans.

1.3.1.A Cardiotoxicity at Two Different Levels: Structural and Functional

Drug-induced cardiac toxicity can be classified in terms of its effect on cell function, i.e., the structural and functional properties of cardiac cells.

Structural cardiotoxicity is mostly related to changes in the multiple cardiac cell types at the cellular and/or subcellular level, resulting in morphological defects [Cross et al., 2015]. Developmental cardiotoxicity is mainly a result of exposure to cardiac teratogens until the seventh week of gestation. Such toxicity during the organogenesis stage manifests predominantly as cardiac structural abnormalities due to impairment of the main steps of cardiac development (Figure 1.2). Firstly, the process of gastrulation is a very susceptible period for teratogenic effects. Then, after the formation of the cardiac crescent and, subsequently, the linear heart tube, the ventricular region of the heart tube begins to loop to the right as a result of the activation and/or inhibition of a cascade of signalling pathways. Disturbances to this process can cause abnormal looping. By day 28 of fertilization, endocardial cushions, the extracellular matrix swellings that develop in the valve-forming regions of the heart tube, the outflow tract, and the atrioventricular junction, arise. These will eventually originate the heart's valves and contribute to the interventricular and interatrial septa. Inadequate endocardial cushion fusion will lead to septal defects. When the heart finishes the looping period, the linear segments of the heart must be aligned with the atrial and ventricular chambers and aortic and pulmonary arteries. This requires remodelling of the inner curvature of the looped heart tube and, if done incorrectly, will result in an improper movement of the outflow tract over the atrioventricular canal resulting in outflow tract abnormalities, such as double-inlet left ventricle or double-outlet right ventricle, defects where the heart's two major arteries are both connected to the same ventricle [Mahler and Butcher, 2011].

After birth, the heart is still susceptible to drug-induced structural toxicity. Effects at the mature CM

level range (i) from non-lethal injuries, such as CM vacuolation, which can result from lipid accumulation, mitochondrial swelling or dilation of the sarcoplasmic reticulum (SR); to (ii) lethal injuries, including loss of membrane integrity and cell death [Walker et al., 2016].

Functional cardiac toxicity can be further divided based on its effects on cardiac electrophysiology and cardiac contractility. Normal electrophysiological cardiac function occurs through the concerted action of membrane ion channels and ion transporters that maintain ion homeostasis in CMs. Action potentials (AP), which will ultimately result in the contraction of CM, result from inward and outward ion fluxes. Briefly, sodium (Na^+) channels are the key players in inducing the depolarization of the cell membrane, calcium (Ca^{2+}) channels contribute to the maintenance of the plateau phase of action potentials (APs), and various types of potassium (K^+) channels participate in different phases of repolarization [Shi et al., 2020]. Drug off-target interactions with such ion channels are often the cause of aberrant CM function and can be the cause of endangering arrhythmias, namely, Torsades de Pointes (TdP). Drugs that induce QT prolongation are normally related with the inhibition of human *ether-à-go-go*-related gene (hERG)-related potassium channels. This can cause a delay of cardiac repolarization resulting in an inward depolarizing current known as early after depolarization (EAD). If these resulting EADs reach a large enough amplitude, they can generate ectopic beats, i.e., extra heart beats that occur just before a regular heart beat, leading to TdP, a potentially lethal tachycardia [Walker et al., 2016, Trinkley et al., 2013].

Cardiac contractility relates to the capacity of CMs to produce contractile force and shorten, and it is dependent on intra/extracellular calcium homeostasis. It is due to the process of excitation-contraction coupling that rhythmic electrical stimulation (APs) translates into mechanical force and contraction. Calcium entry through L-type Ca^{2+} channels after depolarization triggers the release of Ca^{2+} from the terminal cisternae of the SR via ryanodine receptors (RyRs) present in the T-tubules. The increase in the internal concentration of this ion allows it to bind to troponin-C, which induces a conformational change in the troponin complex allowing myosin to bind to actin, and the movement of actin relative to myosin will lead to contraction. Relaxation occurs by removing Ca^{2+} from the cytosol either by returning to the SR through the sarcoendoplasmic reticulum calcium ATPase (SERCA) or by extrusion to the extracellular space through Ca^{2+} pumps [Klabunde, 2011]. Drugs producing an imbalance in calcium handling and/or sensitivity and with effects on the overall contractile mechanisms can increase (positive inotropy) or decrease (negative inotropy) cardiac contractility, which might lead to increased heart stress and reduced perfusion of extremities, respectively [Walker et al., 2016].

1.3.1.B Drug Classes Associated with Cardiotoxicity

Drug-induced cardiotoxic events can occur during development, caused by treatment of the pregnant woman, or affect the heart's normal function as a consequence of exposures after birth.

A teratogen is defined as “any agent that acts during embryonic or fetal development to produce an alteration of form or function” [Lynch and Abel, 2015]. Three main classes of pharmacological compounds have been linked to structural cardiac defects arising during pregnancy: (i) antidepressants, (ii) anticonvulsants, and (iii) antibiotics.

Regarding antidepressants, paroxetine, a selective serotonin reuptake inhibitor, has been reported to increase the risk of cardiac malformations with a higher risk if such exposure occurs during the first trimester. Such impacts include abnormalities in *bulbus cordis* (transient developmental heart structure), cardiac septal closure, atrial septal defects, and right ventricular outflow tract defects [Bérard et al., 2016]. Fluoxetine and sertraline have also been associated with cardiac malformations. Bupropion, used for smoking cessation and mild depression, has been linked with left outflow tract defects. Nonetheless, data regarding antidepressants’ teratogenicity lacks confirmation [Lynch and Abel, 2015].

Valproic acid has the most consistent data regarding its teratogenicity within the class of anticonvulsants [Hernández-Díaz et al., 2012]. It has been primarily linked to neural tube defects. Nonetheless, cardiovascular deffects have also been reported, including atrial and ventricular septal defects, tetralogy of Fallot (a birth defect made up of four heart and heart blood vessel defects: ventricular septal defect, narrowing of the pulmonary valve and pulmonary artery, enlargement of the aortic valve which seems to open from both ventricles, and right ventricle hypertrophy), pulmonary valve atresia (lack of formation of the pulmonary valve), and hypoplastic right heart syndrome (a range of defects where the right-sided structures of the heart are underdeveloped). Once again, exposure during the first trimester is also accompanied by increased teratogenic risk [Jentink et al., 2010]. Carbamazepine is another anticonvulsant associated with developmental cardiotoxicity. Cardiovascular defects, including septal defects, patent ductus arteriosus (an opening between the aorta and the pulmonary artery) and tetralogy of Fallot, were found to be the major congenital abnormalities arising after treatment with this drug during pregnancy in a meta-analysis of 1255 cases of exposure [Matalon et al., 2002]. Other anticonvulsants such as phenobarbital and phenytoin have also been linked to congenital heart disease [Lynch and Abel, 2015].

The use of some antibiotics during pregnancy has also been reported to potentially cause cardiovascular malformations. A recent population-based cohort study associated doxycycline exposure with increased risk of circulatory system malformations, cardiac malformations, and ventricular/atrial septal defects. It also identified clindamycin use as a possible cause of ventricular/atrial septal defects, among other malformations [Muanda et al., 2017]. The association of doxycycline with cardiac malformations was later questioned [Cao and Xu, 2020] due to a lack of a “sufficient number of events to adjust for confounding” among other confounders. The authors answered these concerns by pointing to animal studies that also showed the drug’s teratogenicity and to the fact that doxycycline has also been linked to an increased risk of spontaneous abortion, which might explain a smaller number of reported

birth defects [Muanda et al., 2020]. Trimethoprim/sulfamethoxazole, also known as co-trimoxazole, is a broad-spectrum antimicrobial drug used to treat a variety of bacterial infections, including urinary tract and respiratory tract infections [Church et al., 2015]. Animal studies have shown adverse effects on the fetus, primarily neural tube and cardiac defects and its use is not recommended in the first trimester, and after 32 weeks of gestation [Bookstaver et al., 2015].

Other teratogenic drugs linked to congenital heart disease outside of these three classes include: lithium, used as a mood stabilizer in bipolar disease; isotretinoin, used for acne treatment; mycophenolate; and, of course, thalidomide [Lynch and Abel, 2015].

Regarding drugs that affect the adult heart, they can be divided according to their effect on (i) electrophysiology, (ii) contractility, and (iii) structural toxicity. QT prolongation and/or TdP have been associated with a wide range of drugs, including antiarrhythmics, antibiotics, antipsychotics, antihistamines, and antimalarials [Walker et al., 2016]. Drugs with known effects on specific ion channels include lidocaine, a sodium channel blocker; quinidine, an antiarrhythmic drug with known blocking effects on the sodium and repolarizing potassium channels; nifedipine, a blocker of the cardiac L-type calcium channel; and E-4031, a hERG-type potassium channel blocker [Mandenius et al., 2011]. Cardiac contractility can also be affected. Isoproterenol is a nonselective β-adrenergic agonist capable of causing positive ionotropy [Takeda et al., 2018]. Both anthracyclines, such as doxorubicin, and tyrosine kinase inhibitors, such as sunitinib, are known for being structural cardiotoxins [Archer et al., 2018, Walker et al., 2016].

1.3.1.C Most Commonly Used Models During the Pre-clinical Phase: Animal and *In Vitro* Models and Their Limitations

The first and most common cardiotoxicity models resorted to the use of animals. In fact, heart development is highly conserved across species, especially through the linear heart tube phase into the early stages of looping morphogenesis [Mahler and Butcher, 2011].

Mammalian models of cardiotoxicity include small animals, such as the mouse (*Mus musculus*), and larger animals. Mice are the most commonly used mammalian research model, having a relatively similar sequence of cardiac development [Krishnan et al., 2014]. Relevant drawbacks include the fact that mouse embryos are of difficult access inside the uterus, preventing non-invasive *in vivo* imaging of cardiac function during early embryonic stages [Kheradvar et al., 2017] and offering low-throughput drug toxicity screening. Among other limitations, mice have almost ten times faster heart rates compared to humans and differential gene expression of ion channels like the $K_V7.1$ and hERG-related potassium channels [van Meer et al., 2016]. In fact, species differences are the reason behind the fact that thalidomide is teratogenic in humans but not rodents [Kazuki et al., 2016].

Non-mammalian model organisms include zebrafish (*Danio rerio*), fruit fly (*Drosophila melanogaster*), frog (*Xenopus laevis*), and chicken (*Gallus gallus*) [Xia et al., 2020]. Of these, the zebrafish, a small

tropical fish, has unique characteristics. The fact that embryos develop externally and have a small size allows chemical compounds to be directly diluted into water and diffuse into embryos. Early optical transparency also gives the opportunity to optically monitor the dynamic cellular events of cardiac morphogenesis. Besides, heart development starts very early in zebrafish development, just 5 hours post fertilization, leading to reduced experiment time [Zakaria et al., 2018]. Overall, this makes it a higher-throughput and low-cost model organism, giving it advantages over other animal models. However, zebrafish have a single circulation system and a two-chambered heart, with the single atrium and ventricle connected by an atrioventricular valve, and are evolutionary further away from humans [Xia et al., 2020]. Other limitations include differences in calcium handling and Na^+ current [Heijman et al., 2014].

The use of animal models in biomedical research during the late twentieth and early twenty-first centuries has been very successful in many areas. However, besides the briefly mentioned bottlenecks, there are obvious ethical concerns attached to it. Following the 3R principles (Reduction, Refinement, and Replacement), *in vitro* cardiotoxicity assessment provides an alternative to animal testing [Lilienblum et al., 2008].

Three *in vitro* teratogenicity testing platforms have been validated by EU Reference Laboratory for Alternatives to Animal Testing (EURL-ECVAM) for assessment of developmental toxicity. These include (i) whole embryo culture (WEC), (ii) limb bud micromass culture, and (iii) the mouse embryonic stem cell test (mEST) [Scialli, 2008].

The whole embryo culture uses explanted rodent embryos that are prepared with the visceral yolk sac and ectoplacental cone intact. Embryos are cultured in rotated culture bottles for 48 hours, although cultures can be extended for up to 72 hours. At the beginning of the culture, test compounds are added to the culture medium at various concentrations and embryos are examined for abnormalities of developmental morphology and overall embryonic growth after treatment. The rate of malformation and dead embryos of each test group can be used to determine parameters such as the half-maximal inhibitory concentration (IC_{50}) [Augustine-Rauch et al., 2010, Scialli, 2008]. A primary advantage of this model includes the fact it provides well-controlled experimental conditions, and embryos are easily accessible and manipulated during culture. However, embryos can only be cultured for short durations (2-3 days). This window of time represents a critical step of organogenesis and sensitivity to teratogens, but the effects may not manifest morphologically until a later time in embryonic development. Another limitation is that this model still requires animal sacrifice [Augustine-Rauch et al., 2010].

Micromass culture is based on the primary culture of limb bud cells of mammalian origin and re-establishment of a tissue-like system *in vitro*. In chick embryonic CM micromass culture, 5-day-old CMs are cultured at a very high cell density which forces cells to proliferate and differentiate to form *loci* which show phases of contraction and relaxation. The cells are then exposed to chemicals, and

cytotoxicity is assessed using relevant endpoints such as contractile activity, cell viability, and reactive oxygen species (ROS) production. The chick micromass model has the advantage of not requiring the sacrifice of the mother to access the embryo [Mohammed and Pratten", 2019].

The validated mEST uses a permanent line of mouse ESC maintained in a de-differentiated state by leukemia inhibiting factor (LIF). After LIF removal, the embryonic cells spontaneously produce beating CMs. The test compares the concentration of the test chemical at which differentiation is inhibited with the concentration at which growth and viability of a cultured fibroblast cell line are reduced. Fibroblasts are used as a surrogate for toxicity in the pregnant woman. The growth rate and viability of the embryonic cells are also taken into consideration. The test classifies drugs as not embryotoxic, weakly embryotoxic, or strongly embryotoxic as a result of the comparison to toxic concentrations in adult fibroblasts. By using established cell lines, it is possible to avoid the use of additional animals [Scialli, 2008].

The *in vitro* assessment of drug-induced toxicity in adult cardiac cells includes the use of (i) expression systems, (ii) primary CMs, and (iii) CM cell lines.

Expression systems consist of genetically manipulated cells to express a certain protein [Fisher et al., 2016]. Screening for hERG-interaction in the preclinical phase of drug development is mandatory, with several testing systems already approved by the regulatory agencies, which include hERG-expressing human embryonic kidney 293 (HEK-293) cells [Hoffmann and Warner, 2006]. However, the use of non-cardiac cells lacks predictive capacity since several drugs inhibit the hERG-related potassium channel but are safe in humans, and others interact with other ion channels or lead to multichannel blockages that cannot be detected [Eder et al., 2016].

As CMs are the main cardiac cell type affected by cardiotoxicity, these are the ideal test-bed for simple cardiotoxicity models. Primary CMs are directly harvested from the cardiac tissue, either of animal or human origin, and then cultured *in vitro*. However, CMs have characteristically low proliferation rates, finite lifespan, and there are no abundant sources of primary CMs as these can only be obtained from small, rarely performed cardiac biopsies [Eder et al., 2016].

One solution to this problem would be the creation of CM cell lines, i.e. genetically manipulating the cells to obtain unlimited expansion capacity. AC16 is the result of the fusion between primary ventricular CMs with a simian virus 40 (SV40) transformed fibroblast cell line [Davidson et al., 2005]. It expresses cardiac-specific markers and has been used in studying the cardioprotective effects of spinochrome D against doxorubicin-induced toxicity [Yoon et al., 2019]. However, cell function may be impacted by the genetic manipulation required for immortalization, pointing to the need for new strategies that can mimic the human heart with higher accuracy.

1.4 hPSC-derived Cardiac Models and *In Vitro* Cardiotoxicity Screening

1.4.1 Developmental Cardiotoxicity Screening

Species differences between the human heart and animal models have previously been responsible for the lack of detection of drug-induced teratogenicity. Among other applications, hPSC-derived models offer the opportunity to complement the data obtained from animal toxicological studies. Various hPSC-based studies which study the effect of drug exposure throughout differentiation have been described in the literature. In this section, we present them in an order based on which stage of cardiac development is being analyzed. The focus is first on studies using 2D monolayer differentiation protocols and then on the 3D strategies applied to cardiac developmental toxicity assessment.

Kameoka and colleagues focused on assessing toxicity-induced effects on mesendoderm differentiation. This was performed using a 3-day monolayer differentiation which was achieved after a 24h exposure to Wnt 3a, for activation of the Wnt pathway, and a 72h exposure to Activin A, for activation of the Nodal pathway [Kameoka et al., 2014]. Quantification of SOX17 expression through high-content screening (HCS) was chosen as the sole endpoint. First, the platform was trained using 71 drugs with known *in vivo* effects and 15 environmental toxicants. A compound concentration was classified as toxic if its exposure resulted in a 50% inhibition of SOX17 relative to vehicle control. An IC_{50} of 30µM was used as a teratogenicity threshold and resulted in a 94% accuracy for predicting developmental toxicity when compared to the published literature. Then, a screening of 300 kinase inhibitors was performed to test the suitability of the test for high-throughput screening. This protocol has the advantages of being fast and straightforward, simplifying the teratogenicity classification process. It also allows the identification of toxicity events occurring very early in development. However, its simplicity is also a limitation. Namely, the 2D monolayer system does not allow for recapitulation of the interactions between the different cell types in the early embryo. Besides this, it does not allow the prediction of drug-induced effects on terminally differentiated cardiac cells.

Liu and colleagues studied the molecular mechanisms of 13-*cis*-retinoic acid toxicity during development and found the disruption of an event occurring later in development: mesodermal differentiation. For that, testing was performed using a 2D monolayer differentiation protocol towards CM with samples being collected at different periods of differentiation to assess effects on mesoderm formation and CM progenitors [Liu et al., 2018]. The authors found reduced levels of expression of mesodermal marker Brachyury on treated cells, which resulted in minimal levels of TNNT2 later on compared to the control condition. However, the authors did not observe perturbations of CM differentiation if the drug was added only after mesoderm formation. Separately, the effects of exposure on endoderm and ectoderm individual cultures were tested, and a possible disturbance of endoderm formation was identified. RNA

seq analysis pointed to a deregulation of pathways involved in early mesodermal differentiation, such as TGF-β. Using ATAC-seq, which allows assessing genome-wide chromatin accessibility, it was possible to identify transcription factors with enhanced chromatin accessibility at binding events after drug exposure, namely, HNF1B, SOX10 and NFIC which can implicate that these are regulatory factors involved in the disturbance of mesoderm formation. The limitations of simple 2D models become apparent in this study as it would be of interest to examine the interaction between mesodermal and endodermal cells since an effect on the latter was also identified.

Ribavirin is an antiviral drug with potential anti-cancer effects that has been linked with congenital malformations. Ye and colleagues evaluated the possible developmental cardiac toxicity of the drug on 2D monolayer hiPSC-derived CMs on three different phases of differentiation, from pluripotent status to mesoderm, then to cardiac progenitor cells, and finally to CMs, and concluded that the drug inhibited proliferation and differentiation in the last two stages but not in the first one [Ye et al., 2020]. Increases in ROS content during differentiation from mesoderm to cardiac progenitor cells were detected through DCFH-DA fluorescent staining, and resulting DNA damage was assessed by analysing γH2AX staining and p53 expression levels in this phase of differentiation. Overexpression of long noncoding RNAs Gas5 and HBL1 was detected in the mid- and late-phases and only in the mid-phase of differentiation, respectively. However, their role in ribavirin-induced toxicity was not disclosed. Overall, these results suggested that ribavirin may be detrimental to cardiac proliferation and differentiation during the mid- and late-phase stages of differentiation.

Intending to validate a hiPSC-based toxicity test with features similar to the mEST, Jamalpoor and colleagues tested eleven well-established *in vivo* teratogens and ten non-teratogenic compounds. After a preliminary cell viability test, the assessment was performed at non-cytotoxic concentrations to ensure that the effect seen was not caused by a highly cytotoxic concentration that affected stem cell differentiation by compromising viability without adding relevant information about their teratogenic potential. The authors analyzed the effects on mesoderm- and endoderm-derived cell lineages by comparing drug toxicity on CM and hepatocyte 2D cultures. Teratogenicity classification was performed based on analysis of time-dependent biomarker expression (BMP4 at day 7 and MYH6 at day 14 of differentiation for CMs and FOXA2 at day 7 and AFP at day 21 for hepatocyte cultures) after a drug exposure during differentiation. CM contractile function and morphological abnormalities were also used as secondary readouts. Further testing of the remaining drugs resulted in an accuracy of 91% [Jamalpoor et al., 2022]. The visual scoring of contraction and morphology are the main limitations of the platform.

Developmental toxicity studies have mainly relied on the use of two-dimensional cultures. However, the limitations of such strategies have already been discussed. Besides, as discussed in the previous section, drug-induced teratogenicity usually manifests as structural malformations during development. More recently, 3D models, which can give some insights into these processes, have started to be applied

to these experiments.

One field of stem cell biology that has recently garnered attention is the recapitulation of early embryo development. “Gastruloids” are a model system that mimics some of the events of gastrulation, including symmetry break, axial elongation and differentiation towards the three germ layers. These structures can be evaluated regarding morphological changes, germ layer proportions and spatiotemporal gene expression. Mantziou and colleagues performed a proof-of-concept study testing a set of 7 drugs including all-*trans*-retinoid acid, valproic acid, thalidomide and penicillin G (negative control) [Mantziou et al., 2021]. This was performed on both mouse and human systems through analysis of the morphological shape of the aggregates (qualitatively and quantitatively), marker gene expression (SOX2 for neuroectoderm, SOX17 for endoderm and Brachyury for mesoderm, in human gastruloids) and cytotoxicity. The platform seemed sensible to species differences as thalidomide exposure did not affect mouse gastruloids but showed increased SOX2 expression in human gastruloids. One of the drawbacks of using 3D systems for toxicology studies is the reduced throughput. This platform is based on 96-well plates, and the morphological assessment was semi-automated, offering higher throughput. Further automation is required to make 3D models more suitable for this kind of assays. Once again, analysis at such early development steps needs to be complemented with studies on specific cell lineages.

Nonetheless, teratogenicity studies using 3D hPSC-derived models still focus mainly on assessing toxicity at the CM level. Lauschke and colleagues relied on the use of 96-well plates for the formation of 3D aggregates from three different hiPSC lines and subsequent CM differentiation using a chemically defined medium containing FGF, Activin, BMP, and CHIR [Lauschke et al., 2020]. A preliminary cell viability test was performed to assess non-cytotoxic testing concentrations. Developmental toxicity was modelled using a quantitative assay of contraction based on the manual assessment of a beat score. Aggregate volume was also assessed. Thalidomide, valproic acid, and rodent toxicant epoxiconazole were tested in the model, and the lowest observable effect (LOEC) and IC_{25} were computed. These values varied significantly between cell lines with the IC_{25} of thalidomide ranging from 2.0 µM to 36 µM, the maximum concentration tested. The manual assessment of contractility is very limited and subject to bias, and the measurement of aggregate volume gives little to no mechanistic information.

Hoang and colleagues provided a better characterization of the morphological and functional properties of hiPSC-CMs using a more complex platform [Hoang et al., 2021]. The cells grew geometrically confined and attached to a polyethylene glycol (PEG)-based micropatterned substrate, and the aggregate starts to form upwards. By day 12 of differentiation, the cardiac tissue compacted to the centre, forming a structure with some degree of structural organization. Smooth muscle-like stromal cells were positioned in the outermost section of the aggregate. The model was used to test the teratogenic potential of nine compounds spanning different FDA pregnancy categories by analysing the aggregates at the end of culture. Cardiac differentiation efficiency measurement was performed by flow cytometry

and also by calculating an “area ratio” defined by the authors as the ratio between the beating tissue region over the entire pattern. Morphological parameters such as the height of the aggregates and the full width at half-maximum (FWHM) were also used as endpoints of toxicity and functional analysis was performed using motion tracking analysis. The authors finished the work comparing the results obtained with a zebrafish WEC. As expected, the model showed higher sensitivity to species differences than the zebrafish culture, namely, after thalidomide treatment. This platform presents a significant improvement over the previously discussed ones both in terms of model complexity, being composed of more than one cardiac cell type, and in terms of readout reliability. The main limitation is attached, quite literally, to the fact that these aggregates grow upon and are confined to a biomaterial substrate, restricting the stem cells’ self-organization capacity.

It can be concluded that, besides classifying the different hPSC-derived developmental cardiotoxicity platforms based on the culture format or the cardiac developmental stage being studied, two different goals may be aimed: (i) developing a platform with simple readouts capable of serving as a classification test for compounds with unknown toxicity or (ii) designing the study to provide mechanistic information of a particular individual or group of drugs. Both types of platforms can certainly co-exist and are complementary to one another.

Table 1.1: Summary of the main strategies used for characterization of drug-induced toxicity in developmental cardiotoxicity studies using hPSC-derived models of cardiac development. CM: cardiomyocyte.

Study	Drug Exposure	Culture Format	Developmental Stage Studied	Main Endpoints	Strengths	Limitations
[Kameoka et al., 2014]	Developmental	2D	Mesendoderm	SOX17 expression	Fast protocol; Allows the identification of early toxicity events.	Monolayer is too simplistic; Not possible to assess which cell lineages and/or signalling pathways are affected.
[Liu et al., 2018]	Developmental	2D	Mesoderm	Expression levels of stage specific markers; RNA-Seq; ATAC-Seq.	Allows the identification of early toxicity events. Mechanistic insights.	Monolayer is too simplistic.
[Ye et al., 2020]	Developmental	2D	Mesoderm Cardiac progenitors CM	Proliferation; Expression levels of stage specific markers; ROS levels.	Assessment of toxicity throughout differentiation.	Monolayer is too simplistic.
[Jamalpoor et al., 2022]	Developmental	2D	Mesoderm CM	Expression levels of stage specific markers; Contraction (manual); Cell morphology.	Focus on two mesendoderm-derived cell lineages (CMs and hepatocytes).	Visual scoring of contraction and morphology.
[Mantziou et al., 2021]	Developmental	3D Gastruloid	Gastrulation	Aggregate morphology; Expression levels of germ layer specific markers.	Recapitulation of early embryo development.	Not possible to assess how different cell lineages are affected.
[Lauschke et al., 2020]	Developmental	3D Aggregate	CM	Contraction (manual); Aggregate volume.	Three-dimensional differentiation of CMs.	Limited and subjective endpoints.
[Hoang et al., 2021]	Developmental	3D Organoid	CM	Differentiation efficiency; Quantification of macrostructure features; Contraction velocity and beat rate.	Presence of more than one cell type; Objective structural and functional analysis.	Assessment is only performed at the end of differentiation; Limited self-organization of hPSCs as the aggregates grow attached to biomaterial.

1.4.2 Adult Cardiotoxicity Screening

Unlike the previous examples, the goal of adult cardiotoxicity studies is to assess the effects of post-birth drug exposures. The use of hPSC-derived models for the detection and study of mechanisms involved in such cases is more established when compared to teratogenicity studies.

Two-dimensional CM cultures offer higher throughput and may be more suitable to this type of studies since many adult cardiotoxicity-caused diseases affect mostly CM functional and structural properties, whereas developmental toxicity is more macrostructural in nature. Sharma and colleagues described a protocol in which monolayer hiPSC-CMs were used to classify compound cardiotoxicity using a "cardiac safety index" (CSI) as the metric. This value results from a mathematical equation that combines the effects on CM viability and various contractility parameters and normalizes its value to the *in vivo* C_{max} reported in pharmacokinetic models [Sharma et al., 2018]. Through high-content screening it was possible to use such a classification method on a vast set of tyrosine kinase inhibitors [Sharma et al., 2017]. However, the requirement for expensive HCS systems is a limitation preventing its widespread utilization.

Nonetheless, one of the most prominent limitations of hiPSC-CMs is their lack of maturity. As discussed, by adding predifferentiated supporting cell types, microtissues allow taking the maturation level one step forward. Richards and colleagues used a previously established microtissue [Richards et al., 2017] to be able to model the structure of the human heart after myocardial infarction as well hypoxia-enhanced doxorubicin cardiotoxicity. Doxorubicin was exposed to fully differentiated microtissues for two days. Drug-induced toxicity was determined by assessing a number of features that supported the idea that patients with pre-existent cardiovascular conditions may be more susceptible to detrimental drug effects. This included the impact of increasing drug doses on the contraction amplitude of both control and infarct organoids, which was measured using threshold edge detecting on videos of contracting microtissues, and the impact on the CM population by radial-density-profile plots of the intensity of α-sarcomeric actinin immunostaining. Other endpoints measured were the levels of apoptotic cell death and the levels of doxorubicin-induced cardiac fibrosis by quantifying the level of the vimentin-covered area [Richards et al., 2020].

Archer and colleagues characterized microtissues containing hiPSC-CMs, primary human cardiac microvascular endothelial cells and human cardiac fibroblasts combined at a ratio of 4:2:1, respectively. The model was validated for the assessment of structural toxicity by testing 15 FDA-approved structural cardiotoxins and 14 non-structural cardiotoxins. The detection of known soluble cardiac biomarkers released from CMs upon damage was based on the measurement of the levels of cardiac troponin I (cTNI), creatine phosphokinase muscle/brain (CK-MB), and fatty acid-binding protein-3 (FABP-3) which, if increased, are suggestive of morphological damage. Using high content screening, the authors assessed internal structure through the fluorescence intensity analysis of the integrity of the endoplasmic reticu-

lum and the mitochondria membrane potential ($\Delta\Psi m$) using the fluorescent probes ER-Tracker blue and TMRE, respectively. The analysis was complemented by the assessment of cell viability [Archer et al., 2018].

EHTs allow to bring cardiac cells to a more adult-like maturation level as well as assess features that are not yet possible to detect in hiPSC-based models without resorting to more complex tissue engineering solutions. After characterizing their biomimetic ventricle-like model, Li and colleagues then tested the response of the model to pharmacological compounds, including positive and negative inotropes. Contractile properties such as frequency of contraction, heart-chamber pressure, and cardiac output were measured after treatment with isoproterenol, digoxin, verapamil, nifedipine, and disopyramide. The electrophysiological function of the cells was characterized using voltage-sensitive dyes, and parameters like upstroke time and AP amplitude were measured after exposure to isoproterenol, flecainide and verapamil, following described outcomes [Li et al., 2018]. However, drug-induced macrostructural abnormalities are impossible to assess using such models as there is little room for stem cell self-organization. The complex EHT formation system also prevents higher-throughput adoption of the model for drug toxicity screening.

As highlighted by the last example, the assessment of contractile and electrophysiological properties is required for a full characterization of the functional properties of cardiac cells after drug exposure, as this might allow the identification of any disruption of the process of excitation-contraction coupling. Notably, van Meer and colleagues developed a system capable of the simultaneous measurement of AP, Ca^{2+} transients and contraction using a VSD (ANNINE-6plus), a calcium-sensitive dye (Rhod3), and a cell membrane label (CellMask Deep Red). It was then possible to extract kinetic parameters and concentration-response plots per kinetic parameter. A hypothesis-based statistical algorithm to identify mechanisms of action was also developed. Then, drugs representative of the main mechanisms of action affecting contractility were tested in order to validate the setup and the algorithm. These results were compared with the individual assessment of each parameter, and it was concluded that the simultaneous measurements led to more consistent responses and better identification of the mechanism of action [van Meer et al., 2019]. It must be noted that although the authors claim that this setup is applicable to 3D aggregates, it was only tested in monolayer cultures of hiPSC-CMs.

Table 1.2: Summary of the main strategies used for characterization of drug-induced toxicity in adult cardiotoxicity studies using hPSC-derived cardiac models. EHT: engineered heart tissue. CM: cardiomyocyte.

Study	Drug Exposure	Culture Format	Main Endpoints	Strengths	Limitations
[Sharma et al., 2018]	Adult	2D	Viability; Contractile parameters.	Use of multiple toxicity readouts for the computation of an index that allows quick classification of drug toxicity.	Requirement of expensive HCS systems.
[Richards et al., 2020]	Adult	3D Microtissue	Contraction amplitude; CM structural organization; Impact on ECM components.	Allows to assess impact on different cell types.	Formed by a mix of pre-differentiated cells with different origin.
[Archer et al., 2018]	Adult	3D Microtissue	Detection of CM damage biomarkers; Mitochondrial membrane potential; Endoplasmic reticulum integrity.	Analysis of structural features at a subcellular level.	Focused only on structural toxicity.
[Li et al., 2018]	Adult	3D EHT	Contraction parameters (frequency of contraction, heart-chamber pressure, cardiac output); Electrophysiology parameters.	Assessment of chamber-level features.	Complex system prevents higher-throughput;
[van Meer et al., 2019]	Adult or Developmental	2D or 3D Aggregates	Action potential; Calcium flux; Contraction.	Simultaneous measurement of the 3 endpoints allows better identification of toxicity mechanisms.	Use of dyes may induce CM toxicity.

2

Aims of the Study

Contents

2.1 Aims of the Study

Most studies using hiPSC-derived models for cardiotoxicity studies still rely on the use of 2D-based differentiation protocols. Since drug-induced developmental toxicity usually results in congenital heart defects caused by structural abnormalities, the use of 3D-based models provides a closer recapitulation of these events. Furthermore, the early developmental stages are the most sensitive to such effects. For that reason, studying the impacts of drug exposure in the different cell populations throughout development can enlighten the mechanisms and the periods of exposure most susceptible to toxicity.

In this work, we aimed at adapting a 3D cardiac model previously established and characterized [Branco et al., 2019] for developmental cardiotoxicity studies. To overcome some of the limitations detected in the literature, the platform was developed in order to allow the assessment of toxicity at the different stages of cardiac cell differentiation, ranging from mesendoderm specification to CM commitment, taking advantage of the cell type diversity and structural organization of the model. A group of nine drugs representative of different pregnancy risk levels was chosen to assess the predictability of the platform.

In the first step, the cytotoxic potential of the nine compounds was tested to ensure that the outcomes of drug exposure were not caused by generalized cell death but through specific teratogenic mechanisms affecting cardiac cell lineages. Then, the intent was to characterize the impact of drug treatment at two different stages of differentiation. First, an assessment was performed at an early stage of differentiation, focused on mesendoderm specification. Later, we aimed to evaluate the impact of drug treatment only until the progenitor stage or further prolonging it until terminally differentiated CMs, on the macrostructure of the cardiac aggregates and on the sarcomere structure and proliferative capacity of CMs. Lastly, and to completely disclose the dependency of exposure timing on the observed drug-induced defects, we tested drug exposure starting later on without affecting early differentiation process.

3

Materials and Methods

Contents

3.1 Expansion of Human Induced Pluripotent Stem Cells

3.1.1 Cell Line

The experiments were performed using the hiPSC line iPS-DF6-9-9T.B, provided by WiCell Bank (Wisconsin, USA). This cell line is vector free and was reprogrammed from foreskin fibroblasts with a karyotype 46, XY that were collected from healthy donors using defined factors in the Laboratory of Dr. James Thomson, at University of Wisconsin.

3.1.2 Cell Thawing and Maintenance

A Matrigel® matrix (Corning, #354277) was used as adhesion substrate for hiPSCs culture. Matrigel® was aliquoted and stored at –20 °C. Aliquots were thawed on ice and a 1:100 (v/v) dilution in cold Dulbecco's Modified Eagle Medium/Nutrient Mixture F-12 (DMEM/F12) (Thermo Fisher Scientific, #32500-035) was prepared. This was used to coat 6-well tissue culture plates (Corning) that were left at room temperature for at least two hours, or stored at 4 °C for later use up to 2 weeks.

mTeSR™1 medium (STEMCELL Technologies, #85850) was used as hiPSCs expansion medium. mTeSR™1 5$\times$ supplement was thawed at room temperature or at 4 °C overnight and mixed with basal medium. The final formulation was aliquoted and stored at –20 °C. Aliquots were thawed overnight at 4 °C and supplemented 1:200 (v/v) with penicillin/streptomycin (PenStrep) (Thermo Fisher Scientific, #15140122). mTeSR™1 was pre-warmed at room temperature before use.

At the beginning of each experiment, cells cryopreserved in liquid nitrogen at –196 °C were thawed at 37 °C. The cryovial was transferred to a laminar flow hood when its content started to thaw and the cells were gently re-suspended in culture medium in a conical tube and centrifuged at 210 $\times$ g for 3 min. The cell pellet was re-suspended in culture medium and the cell suspension was seeded onto a Matrigel® plate to a final volume of 1.5 mL/well. The cells were kept in a CO_2 incubator at 37 °C, 5% CO_2 and 20% O_2. Culture medium was changed every 24 h.

Once cells achieved 70-80% confluence, the cells were passaged at a split ratio between 1:3 and 1:4 to new Matrigel®-coated 6-well tissue culture plates. Enzyme-free cell passaging was performed using a 0.5 mM ethylenediaminetetraacetic acid (EDTA) solution (Thermo Fisher Scientific, #15575-038). Cells were washed and then incubated with EDTA for 5 min at room temperature. After EDTA removal, the cells were flushed with culture medium and collected to a conical tube. The cell suspension was distributed to each Matrigel®-coated well.

3.1.3 Cell Cryopreservation

Whenever required, hiPSCs were cryopreserved for cell banking purposes. The cells were washed and then incubated with EDTA for 5 min at room temperature. After EDTA removal, the cells were flushed with culture medium, collected to a conical tube and centrifuged at 210 $\times$ g for 3 min. The cell pellet was re-suspended in KnockOut™ serum replacement (KO-SR) (Thermo Fisher Scientific, #10828028) diluted with 1:10 (v/v) of dimethyl sulfoxide (DMSO) (Sigma-Aldrich, #276855). A cell density of about 1.5×10^6 cells/vial was used for a final volume of 250 µL/vial. A cryovial was filled with the cell suspension and stored in a freezing container at –80 °C for 24 h followed by storage in liquid nitrogen at –196 °C.

3.1.4 Cell Counting

To calculate cell density, cell counting was performed diluting the cell suspension in 1:4 to 1:8 ratios in Trypan Blue (Thermo Fisher Scientific, #15250-061). After homogenization, cells were counted using a hemocytometer under an inverted optical microscope.

3.2 Citoxicity Assessment

3.2.1 Formation of hiPSC Aggregates

Once hiPSCs reached approximately 70% confluence, the cells were washed with phosphate-buffered saline (PBS) (Sigma-Aldrich, #D8662) and incubated with Accutase® solution (Sigma-Aldrich, #A6964) at 37 °C for 7 min for single-cell formation. The cells were flushed with Accutase® solution and collected to a conical tube with two times the volume of culture medium for inactivation of enzymatic digestion. After centrifugation at 210$\times g$ for 3 min, the cell pellet was re-suspended in culture medium supplemented 1:1000 (v/v) with a Rho kinase inhibitor (ROCKi), Y-27632 (STEMCELL Technologies, #72304) for a concentration of 10 µM. The cell seeding density was optimized so that the size of hiPSC aggregates was equivalent to that of CM aggregates at day 9 of differentiation as drug exposure occurred from day 1 to day 15 of differentiation. Seeding densities of 5×10^3 up to 7×10^4 cells/well were tested and a density of 2×10^4 cells/well was chosen based on statistical analysis (Supplemental Figure A.1). The cell suspension was seeded onto V-shaped 96-well ultra-low attachment (ULA) culture plates for a final volume of 100 µL/well. The culture plate was centrifuged at 210 $\times$ g for 3 min and the cells were kept in a CO_2 incubator at 37 °C, 5% CO_2 and 20% O_2. This corresponded to Day –2 of the cytotoxicity experiment. Culture medium was changed after 24 h (Day –1) to culture medium without ROCKi.

3.2.2 Drug Set

Drugs stocks were prepared in DMSO at a concentration of 2 mM. Nine compounds were tested: benzylpenicillin sodium (Pen G) (Chemical Abstracts Service Registry number (CAS) #69-57-8); acetylsalicylic acid (ASA) (CAS #50-78-2); trimethoprim (TMP) (CAS #738-70-5); co-trimoxazole (TMP/SMX) (CAS #8064-90-2); carbamazepine (CBZ) (CAS #298-46-4); paroxetine hydrochloride (PAR) (CAS #78246-49-8); doxycycline hydrochloride (DOX) (CAS #10592-13-9); 5-fluorouracil (5-Fu) (CAS #51-21-8); and thalidomide (Thal) (CAS #50-35-1). TMP/SMX is combination drug commercially prepared at a 1:5 ratio of TMP and sulfamethoxazole (SMX). However, the serum concentration of the combination drug is at ratio of 1:20 due to a higher volume of distribution of TMP (the drug has a higher propension to move to the extravascular compartments) [Castro and Morrison-Bryant, 2010]. For that reason, TMP/SMX was prepared as a 1:20 dilution of TMP and SMX.

Table 3.1: Drug compounds tested and corresponding medicinal use, former FDA pregnancy category and therapeutic peak plasma *in vivo* concentration (C_{max}) reported in the literature.

Drug	Medicinal Use	FDA Pregnancy Category	C_{max} (µM)	C_{max} Reference
Benzylpenicillin Sodium (Pen G)	Antibiotic	B	135	[Palmer et al., 2013]
Acetylsalicylic Acid (ASA)	Analgesic	C	301	[Nagelschmitz et al., 2014]
Trimethoprim (TMP)	Antibiotic	C	3.55	[FDA, NA]
Co-trimoxazole (TMP/SMX)	Antibiotic	C	13.8 (TMP) 197 (SMZ)	[Reeves and Wilkinson, 1979]
Carbamazepine (CBZ)	Anticonvulsant	D	47.0	[Mahmood and Chamberlin, 1998]
Paroxetine Hydrochloride (PAR)	Antidepressant	D	0.0850	[Bourin et al., 2001]
Doxycycline Hydrochloride (DOX)	Antibiotic	D	31.8	[Agwuh and MacGowan, 2006]
5-Fluorouracil (5-Fu)	Antineoplastic	D	4.25	[Öman et al., 2005]
Thalidomide (Thal)	Myeloma, Inflammation	X	7.74	[Teo et al., 2004]

3.2.3 Cytotoxicity Assay

On Day 0, the cells were exposed to drugs diluted in culture medium at five different concentrations ranging from 0.1 to 50 µM. Vehicle control samples were supplemented with DMSO at concentrations corresponding to each drug concentration (Figure 3.1). The culture medium was changed 24 h later (Day 1) with medium containing fresh drug dilutions. On Day 2, a cytotoxicity assay was performed using the alamarBlue™ Cell Viability Reagent (Thermo Fisher Scientific, #DAL1100), a resazurin-based solution that allows the quantification of cell viability by the measurement of the fluorescence of resorufin

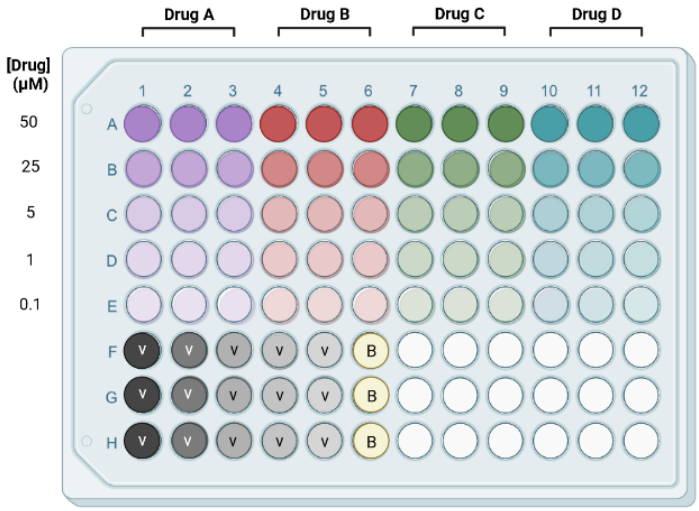

Figure 3.1: Simplified pippeting scheme for the cytotoxicity assay. Rows A-E contained the five dilutions of the test drug (0.1, 1, 5, 25, and 50 µM), and this series was repeated every three columns for each drug to create three technical replicates per drug. Rows G-H contained the corresponding vehicle dilution (0.005, 0.05, 0.25, 1.25, and 2.5 % (v/v) DMSO). B, blank (culture medium without cells).

(highly fluorescent) which is the product of the reduction of resazurin (non-fluorescent) upon entering living cells. The cells were incubated with a 1:10 dilution of alamarBlue™ in culture medium for 3h at 37 °C. The medium was transferred to a Nunc™ F96 MicroWell™ black polystyrene plate (Thermo Fisher Scientific) and fluorescence was measured on a Infinite® 200 PRO (Tecan) microplate reader using excitation/emission wavelengths of 560 and 590 nm, respectively. The cell viability values for each drug dose were normalized with the corresponding DMSO concentration. A testing dose of 2 µM for each drug was chosen and its toxicity-induced effects were assessed during CM differentiation.

3.3 3D Differentiation of hiPSC in Cardiomyocytes

3.3.1 Predifferentiation Culture

Once hiPSCs reached approximately 70% confluence, the cells were washed with PBS and incubated with Accutase® solution at 37 °C for 7 min for single-cell formation. The cells were flushed with Accutase® solution and collected to a conical tube with two times the volume of culture medium for inactivation of enzymatic digestion. After centrifugation at 210 $\times$ g for 3 min, the cell pellet was re-suspended in culture medium supplemented 1:1000 (v/v) with ROCKi. Prior to cell seeding, a AggreWell™800 plate (STEMCELL Technologies) containing 0.5 mL/well of culture medium was centrifuged at 4500 $\times$ g for 3 min. The cell suspension was seeded onto the AggreWell™800 plate with a cell density of 1.14 $\times$ 10^6 cells/well (3.8 $\times$ 10^3 cells/microwell) for a final volume of 1.5 mL/well. The culture plate was centrifuged at 210 $\times$ g for 3 min. The cells were kept in a CO_2 incubator at 37 °C, 5% CO_2 and 20% O_2. This step

corresponded to Day –3 of differentiation. Culture medium was changed after 24 h and 48h (Day –2, Day –1, respectively) to culture medium without ROCKi.

3.3.2 3D Differentiation of hiPSC in Cardiomyocytes

RPMI 1640 (Thermo Fisher Scientific, #11875-093) was used as a basal medium during differentiation. From Day 0 to Day 6, basal medium was supplemented with B-27™ Supplement minus insulin (Thermo Fisher Scientific, #A1895601) whereas from Day 6 onward, basal medium was supplemented with B-27™ (Thermo Fisher Scientific, #17504001)). RPMI 1640 was aliquoted and supplemented accordingly. Each final formulation was stored at 4 °C for up to 1 month. Culture medium was pre-warmed at room temperature before use. The differentiation protocol is based on two steps of Wnt signalling modulation. On Day 0, 11 µM CHIR99021 was addded to the culture medium to act as a Wnt pathway activator in order to promote mesendoderm induction. CHIR was removed 24 h later, on Day 1, as culture medium was changed. On Day 3, Wnt pathway inhibition was performed for cardiac lineage specification. IWP4 at a concentration of 5 µM was added to a combined medium composed in equal parts by exhausted medium and culture medium. IWP4 exposure lasted 48h and, on Day 5, the aggregates were transferred from the AggreWell™800 plate to a 6-well ULA culture plate (Corning) with a final volume of 2mL/well of culture medium. Culture medium was refreshed on Day 6 and, afterwards, every 72 h (Day 9 and Day 12) until aggregates were harvested at Day 15.

3.3.3 Re-aggregation of Progenitor Aggregates

Drug exposure from Day 6 onward was performed in V-shaped 96-well ULA culture plates to increase throughput. Re-aggregation was performed on Day 5. The aggregates were flushed from the AggreWell™800 plate, collected to a conical tube, washed with PBS and incubated with Accutase® solution at 37 °C for 5 min. The enzymatic digestion was stopped by dilution with two times the volume of culture medium supplemented 1:10 with FBS (Gibco, #10270-106). After centrifugation at 210 $\times$ g for 3 min, the cell pellet was re-suspended in culture medium supplemented 1:1000 (v/v) with ROCKi. The cell seeding density was optimized so that the size of the aggregates after re-aggregation was equivalent to that of non-re-aggregated aggregates at the same stage of differentiation. Seeding densities of 2×10^4 up to 8×10^4 cells/well were tested and a density of 3×10^4 cells/well was chosen based on statistical analysis (Supplemental Figure A.5). The cell suspension was seeded onto V-shaped 96-well ULA culture plates for a final volume of 100 µL/well. The culture plate was centrifuged at 210 $\times$ g for 3 min. The cells were kept in a CO_2 incubator at 37 °C, 5% CO_2 and 20% O_2.

3.3.4 Drug Exposure

Drug treatment was performed using three different exposure periods: (i) from Day 1 to Day 15, in order to mimic continuous drug exposure during fetal development (figure 3.2A); (ii) from Day 1 to Day 5, to study the impact of toxicity-induced effects on mesendoderm specification and its consequences in CMs (Figure 3.2B); and (iii) from Day 6 to Day 15, to isolate possible toxicity-induced events occurring after mesendoderm specification on CM commitment (Figure 3.2C). No drugs were added to the culture medium on Day 0, the day of CHIR exposure, as previously done by Hoang and colleagues using a similar differentiation protocol [Hoang et al., 2021]. Drug exposure was also not performed from Day 5 to Day 6 as the re-aggregation process was occurring.

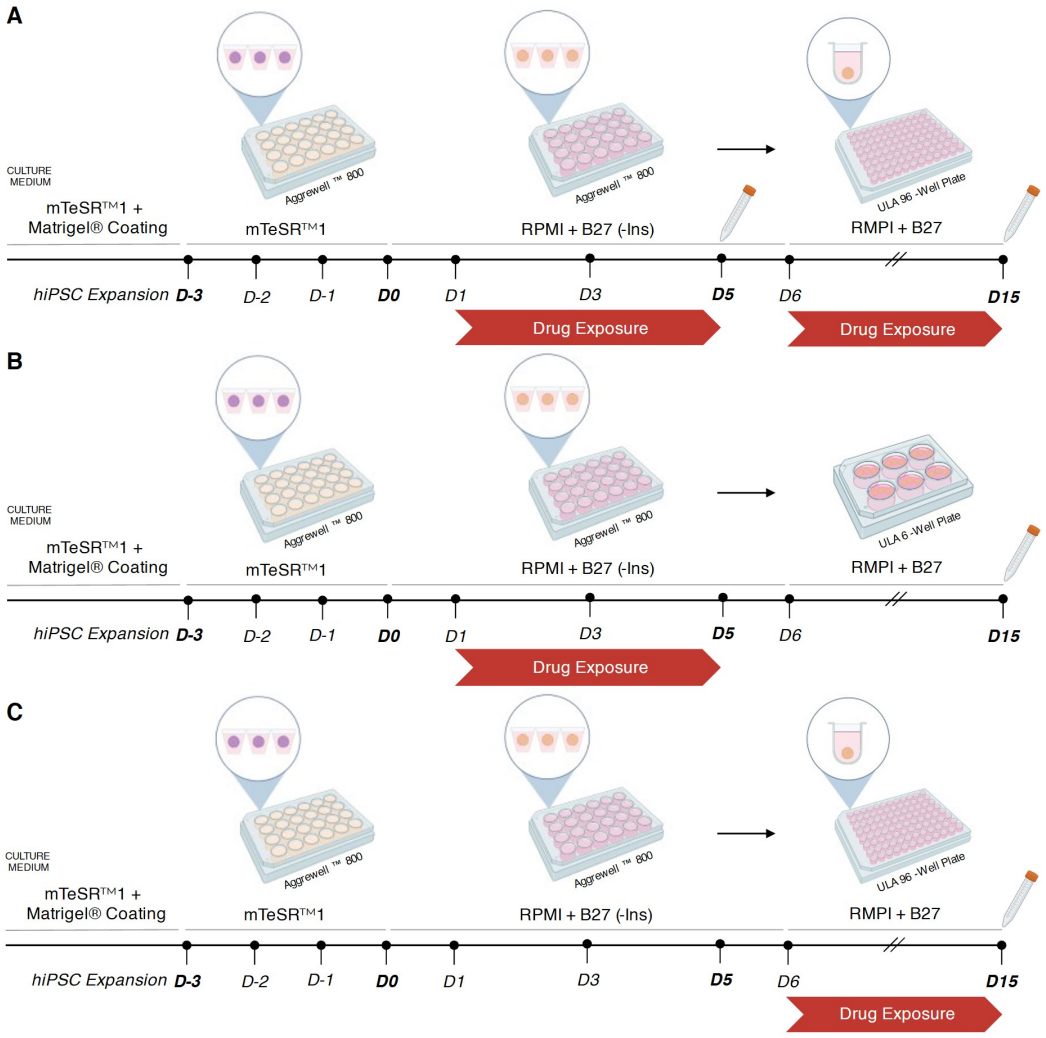

Figure 3.2: The three different drug exposure strategies used during differentiation. **A** - Drug exposure from Day 1 to Day 15 mimicking continuous exposure during fetal development. **B** - Drug exposure from Day 1 to Day 5 in order to study the impact of toxicity-induced effects on mesendoderm specification and its consequences in CM. **C** - Drug exposure from Day 6 to Day 15 in order to study the impact of toxicity-induced events occurring after mesendoderm specification on CM commitment.

3.4 Cell Characterization

3.4.1 Aggregate Size Analysis

Aggregate sizes were monitored throughout culture by the acquisition of several images using a Leica DMI 3000B microscope with a Nikon DXM 1200F digital camera. The Feret diameter of the aggregates, the longest distance between any two points of the aggregates' surface, was measured using ImageJ Software.

3.4.2 Flow Cytometry Analysis

For flow cytometry, cell samples of selected days of differentiation were collected. The cells were washed with PBS and incubated with TrypLE™ Express Enzyme (1X) (Thermo Fisher Scientific, #12604013) for 5 mins at 37 °C, in the case of Day 5 aggregates, or with 0.25% (v/v) trypsin-EDTA (Thermo Fisher Scientific, #R001100), in PBS for 7 mins at 37 °C in the case of Day 15 aggregates. The enzymatic digestion was stopped by dilution with two times the volume of culture medium supplemented 1:10 with FBS. After centrifugation at 210 $\times g$ for 3 min, the cell pellet was washed with PBS and centrifuged again at 210 $\times g$ for 3 min. The cell pellet was fixed by re-suspension in 2% (wt/v) paraformaldehyde (PFA) (Sigma-Aldrich, #158127) in PBS for 20 min at room temperature and stored at 4 °C until analysis up to one week.

3.4.2.A Surface Markers (CXCR4 and c-KIT)

Fixed cells from Day 5 aggregates were centrifuged at 210 $\times g$ for 5 min. The cells were washed 3 times with PBS and centrifuged at 210 $\times g$ for 5 min, each time. The cell pellet was re-suspended and incubated with 2% bovine serum albumin (BSA) in PBS containing a 1:20 (v/v) dilution of the primary antibody mouse IgG2a anti-CXCR4 (Santa Cruz, #Sc-12764), for 30 min at room temperature in the dark. The cells were washed with PBS and centrifuged at 210 $\times g$ for 5 min. The cell pellet was re-suspended and incubated with 2% BSA in PBS containing a 1:1000 (v/v) dilution of the secondary antibody Alexa Fluor™ 488 goat anti-mouse IgG (Thermo Fisher Scientific, #A11001) for 20 min at room temperature in the dark. The cells were washed with PBS and centrifuged at 210 $\times g$ for 5 min. The cell pellet was re-suspended and incubated with 2% BSA in PBS with a 1:10 (v/v) dilution of the primary antibody PE mouse IgG1 anti-c-KIT (Biolegend, #313204), for 30 min at room temperature in the dark. The cells were washed 2 times with PBS and the cell pellet was re-suspended in PBS in Falcon® round-bottom tubes. Flow cytometry was performed using a FACSCalibur™ flow cytometer (Becton Dickinson) and data analysis using FlowJo software.

3.4.2.B Intracellular Markers (cTNT)

Fixed cells from Day 15 aggregates were centrifuged at 200 $\times$ g for 5 min. The cell pellet was re-suspended and incubated in 90% (v/v) cold methanol in Milli-Q® water at 4 °C for 15 min. The cells were washed 3 times with washing buffer 1, containing 0.5% (v/v) BSA (Sigma-Aldrich, #A8327) diluted in PBS, and centrifuged at 210 $\times$ g for 5 min, each time. The cell pellet was re-suspended and incubated with washing buffer 2, containing 0.1% (v/v) Triton™ X-100 (Sigma-Aldrich, #T9284) diluted in washing buffer 1, with a 1:800 (v/v) dilution of the primary antibody mouse IgG anti-cTNT (Thermo Fisher Scientific, #MA5-12960), for 1 h at room temperature in the dark. The cells were washed 2 times with washing buffer 2 and the cell pellet was re-suspended and incubated in washing buffer 2 containing a 1:1000 dilution of the secondary antibody Alexa Fluor™ 488 goat anti-mouse IgG, for 30 min at room temperature in the dark. The cells were washed with washing buffer 2 twice and the cell pellet was re-suspended in PBS in Falcon® round-bottom tubes. Flow cytometry was performed using a FACSCalibur™ flow cytometer (Becton Dickinson) and data analysis using FlowJo software.

3.4.3 Immunostaining Analysis

3.4.3.A Sample Preparation

For immunostaining analysis, cell samples of selected days of differentiation were harvested. For aggregate slices, the aggregates were collected to a conical tube, washed with PBS and incubated in 4% (wt/v) PFA in PBS for 30 min at room temperature. After PFA removal, the fixed aggregates were stored in PBS at 4 °C. For analysis of the fixed aggregates, the cells were incubated with 15% (wt/v) sucrose solution (Sigma-Aldrich, #S7903) overnight at 4 °C, and with gelatin block solution, containing 15% (wt/v) sucrose and 7.5% (wt/v) gelatin (Sigma-Aldrich, #G6144) in PBS, for 1 h at 37 °C. The aggregates were embedded in gelatin blocks, placed on top of a drop of Tissue-Tek® (Sakura, #4583) and frozen in isopenthane (Carlo Erba Reagents, #528492) at –80 °C. The blocks were cut in 10/12 µm sections using a cryostat-microtome (Leica CM3050S, Leica Microsystems) and collected on Superfrost™ Microscope Slides (Thermo Scientific). The slides were stored at –20 °C. The sections were degelatinized in PBS for 30 min at 37 °C before immunostaining.

For replated aggregates, the aggregates harvested on Day 15 were washed with PBS and incubated with 0.25% (v/v) trypsin-EDTA in PBS for 7 mins at 37 °C. The enzymatic digestion was stopped by dilution with two times the volume of culture medium supplemented 1:10 with FBS. After centrifugation at 210 $\times$ g for 3 min, the cell pellet was washed with PBS and centrifuged again at 210 $\times$ g for 3 min. The cell pellet was re-suspended in culture medium supplemented 1:1000 (v/v) with ROCKi and the cell suspension was seeded onto a 24-well culture plate (Corning) coated with Matrigel® and coverslips. Culture medium was changed after 24 h (Day 15 + 1). On Day 15 + 2, the cells were incubated in 4%

(wt/v) PFA in PBS for 20 min at room temperature and stored in PBS at 4 °C.

3.4.3.B Immunostaining

Aggregate sections and replated cells in coverslips were incubated with 0.1 M Glycine (Sigma-Aldrich, #G8898) for 10 min at room temperature to remove PFA residues, permeabilized with 0.1% Triton X-100 in PBS at room temperature for 10 min and incubated with blocking solution, containing 10% (v/v) FBS in TBST (20 mM Tris-HCl pH 8.0 (Sigma-Aldrich), 150 mM NaCl and 0.05% (v/v) Tween-20 (Sigma-Aldrich), for 30 min at room temperature. The cells were incubated with the primary antibodies, diluted to the appropriate working concentration (Table 3.2), overnight at 4 °C. The cells were then incubated with the secondary antibodies, diluted to the appropriate working concentration (Table 3.2), for 30 min at room temperature in the dark, and with 0.15% (v/v) 4',6-diamidino-2-phenylindole (DAPI) dye (Sigma-Aldrich, #D9542) in PBS, for nuclear counterstaining, for 10 min at room temperature in the dark. Immunostaining images were acquired with a LSM 710 Confocal Laser Point-Scanning Microscope (ZEISS). Image analysis was performed using ZEISS ZEN software.

Table 3.2: Antibodies used for flow cytometry (FC) and immunostaining analysis (IS).

Antibody	Isotype	Source (Reference)	Dilution (v/v)
Primary Antibody			
c-KIT-PE	Mouse IgG1	BioLegend (313204)	1:10 (FC)
CXCR4	Mouse IgG2a	Santa Cruz (Sc-12764)	1:20 (FC)
cTNT	Mouse IgG	Thermo Fisher (MA5-12960)	1:400 (FC) 1:200 (IS)
ISL1	Rabbit IgG	Abcam (ab178400)	1:200 (IS)
SOX17	Mouse	Abcam (ab224637)	1:200 (IS)
PAX6	Rabbit IgG	BioLegend (901302)	1:200 (IS)
SOX2	Mouse IgG2a	ReD Systems (MAB2018)	1:200 (IS)
CDX2	Rabbit IgG	Abcam (ab76541)	1:200 (IS)
CD34	Mouse IgG1	BioLegend (343502)	1:25 (IS)
CD31	Mouse IgG	Dako (M0823)	1:50 (IS)
NKX2.5	Rabbit IgG	Abcam (ab97355)	1:200 (IS)
α-actinin	Mouse IgG1	Sigma-Aldrish (A7811)	1:200 (IS)
NG2	Rabbit IgG	Abcam (ab275024)	1:50 (IS)
CX43	Rabbit IgG	Sigma-Aldrish (C6219)	1:400 (IS)
Fibronectin	Mouse IgG1	Abcam (ab253288)	1:300 (IS)
Laminin	Rabbit IgG	Abcam (ab11575)	1:300 (IS)
MLC2V	Rabbit IgG	Proteintech (10906-1-AP)	1:200 (IS)
Ki-67	Rabbit IgG	Abcam (ab833)	1:50 (IS)
Ki-67	Mouse IgG1	BD Pharmingen (550609)	1:50 (IS)
Caspase-3	Rabbit IgG	Cell Signaling (9661S)	1:400 (IS)
Secondary Antibody			
Alexa Fluor™ 488	Goat Anti-Mouse IgG	Thermo Fisher (A11001)	1:1000 (FC)
Alexa Fluor™ 488	Goat Anti-Rabbit IgG	Thermo Fisher (A11008)	1:500 (IS)
Alexa Fluor™ 546	Goat Anti-Mouse IgG	Thermo Fisher (A11003)	1:500 (IS)

3.4.3.C Quantification of Sarcomere Length

Immunostaining images of replated cells stained with the Z-line protein α-actinin (Table 3.2) were used for the quantification of sarcomere length. For each condition, ten to fifteen images were taken using a Plan-Apochromat 63×/1.4 Oil DIC M27 objective (ZEISS). Image analysis was performed using the ImageJ software. Segmentation of each image into 5 × 5 matrices and quantification of the segment's sarcomere length was performed using the SotaTool software [Stein et al., 2022]. Each segment with a sarcomere length between 1.2 and 2.2 µm (adult human CM sarcomere length) was visually assessed for the existence of an organized sarcomere and, if so, was used for sarcomere length quantification.

3.4.3.D Quantification of Ratio of Proliferating Cells

Immunostaining images of replated cells stained with proliferation marker Ki-67 and cardiac markers NKX2.5 or α-actinin (Table 3.2) were used for the quantification of the ratio of proliferating CMs. For each condition, four to five images were taken using a Plan-Apochromat 20×/0.8 M27 objective (ZEISS). Image analysis was performed using the ImageJ software.

3.5 Statistical Analysis

Statistical analysis was performed using the GraphPad Prism software. Half-maximal inhibitory compound doses of cytotoxicity (IC_{50}) were determined from concentration-response curves generated using a $\log(\text{inhibitor})$ vs $\text{normalized response}$ nonlinear regression (Equation 3.1).

$$\text{Cell Viability } (\%) = \frac{100}{1 + 10^{\log([\text{drug}]) - \log(\text{IC}_{50})}} \tag{3.1}$$

For single comparisons between two individual groups, a two sided Student's t-test was used. For comparisons between more than two groups, one-way analysis of variance (ANOVA) was performed. ANOVA was supplemented with Dunnett's multiple comparison tests to determine significance between test groups and the control group. A p value ≤ 0.05 was considered significant. p values of $p < 0.05$ are indicated with *, $p < 0.01$ with **, and $p < 0.001$ with *** in the figures.

4

Results and Discussion

Contents

4.1 Cytoxicity Testing and Dose Selection

Nine drugs were chosen for the assessment of developmental toxicity, comprising different former FDA pregnancy categories: Pen G (category B); ASA, TMP, and TMP/SMX (category C); CBZ, PAR, DOX, and 5-Fu (category D); and Thal (category X) (Table 3.1). These categories, which accompanied drug labels until they started to be phased out in 2015, were determined on the basis of the reliability of the available data regarding the teratogenic potential of the drug and the risk-to-benefit ratio. For drugs classified as category A, no risk in human and animal studies was identified. For category B drugs, there are no well-controlled studies in pregnant women, but animal studies failed to demonstrate teratogenic risk. For category C drugs, the risk cannot be ruled out as animal studies have demonstrated a risk to the fetus, although there are no adequate studies in pregnant women, so the drug must be prescribed only when it is considered that the benefits outweigh the risk. In the case of category D drugs, there has also evidence of teratogenic risk in pregnant women, but there are some situations when it is considered that drug treatment may still be more beneficial than the risks it presents. Category X drugs are contraindicated during pregnancy [Leek and Arif, 2022]. Although this classification refers to overall embryotoxicity, all the drugs in this list have been linked to specific teratogenic defects leading to congenital cardiac malformations (Section 1.3.1.B).

Following one of the most famous principles of toxicology, *"the dose makes the poison"*, in the present work, a cell viability test for the nine selected drugs in a range of concentrations was performed before initiating the assessment of drug-induced developmental toxicity, This was done to ascertain that the potential impact that a studied drug would have on normal cardiac differentiation was not hindered by a highly cytotoxic drug concentration that would impair normal stem cell differentiation regardless of cell lineage.

As described in Section 3, cell viability was measured after a 48 h drug exposure to hiPSC aggregates (Figure 4.1A). A clear cytotoxic effect of 5-Fu, in the range of the tested concentrations, was observed upon macroscopic observation of the aggregates, which presented a considerable reduction in aggregate size compared with the control condition, for the three highest concentrations tested (Supplemental Figure A.2J). Aggregates exposed to the highest concentration of 5-Fu (50 µM) were 5-times smaller than aggregates exposed to the smallest (0.1 µM) (Supplemental Figure A.2I). The cell viability assay revealed an IC_{50} of 14.08 µM (Figure 4.1B). This follows what was expected as 5-Fu is an antineoplastic drug used as a monotherapy or in combination with other agents during chemotherapeutic treatment. Its cytotoxic effect is caused by the inhibition of cellular thymidylate synthase, which prevents DNA replication and the inhibition of RNA synthesis due to the integration of its metabolites into RNA after intracellular activation [Ghafouri-Fard et al., 2021].

5-Fu and Pen G were part of the list of drugs tested in the ECVAM validation study of the mEST [Genschow et al., 2004] and have been used as negative and positive controls of cytotoxicity, respectively, in

order to validate platforms for teratogenicity studies [Seiler and Spielmann, 2011, Walker et al., 2021]. In agreement with that, no significant cytotoxicity was detected after treatment with Pen G (Figure 4.1C). Hence, the cytotoxicity assay was able to reproduce the expected outcome after exposure to 5-Fu and Pen G.

Additionally, Thal treatment did not show cytotoxicity effects at the concentrations tested (Figure 4.1D), being in agreement with what was previously reported upon exposure of hiPSCs to this drug [Jamalpoor et al., 2022, Lauschke et al., 2020]. No cytotoxicity was detected after TMP (Figure 4.2A) and TMP/SMX exposure (Figure 4.1E).

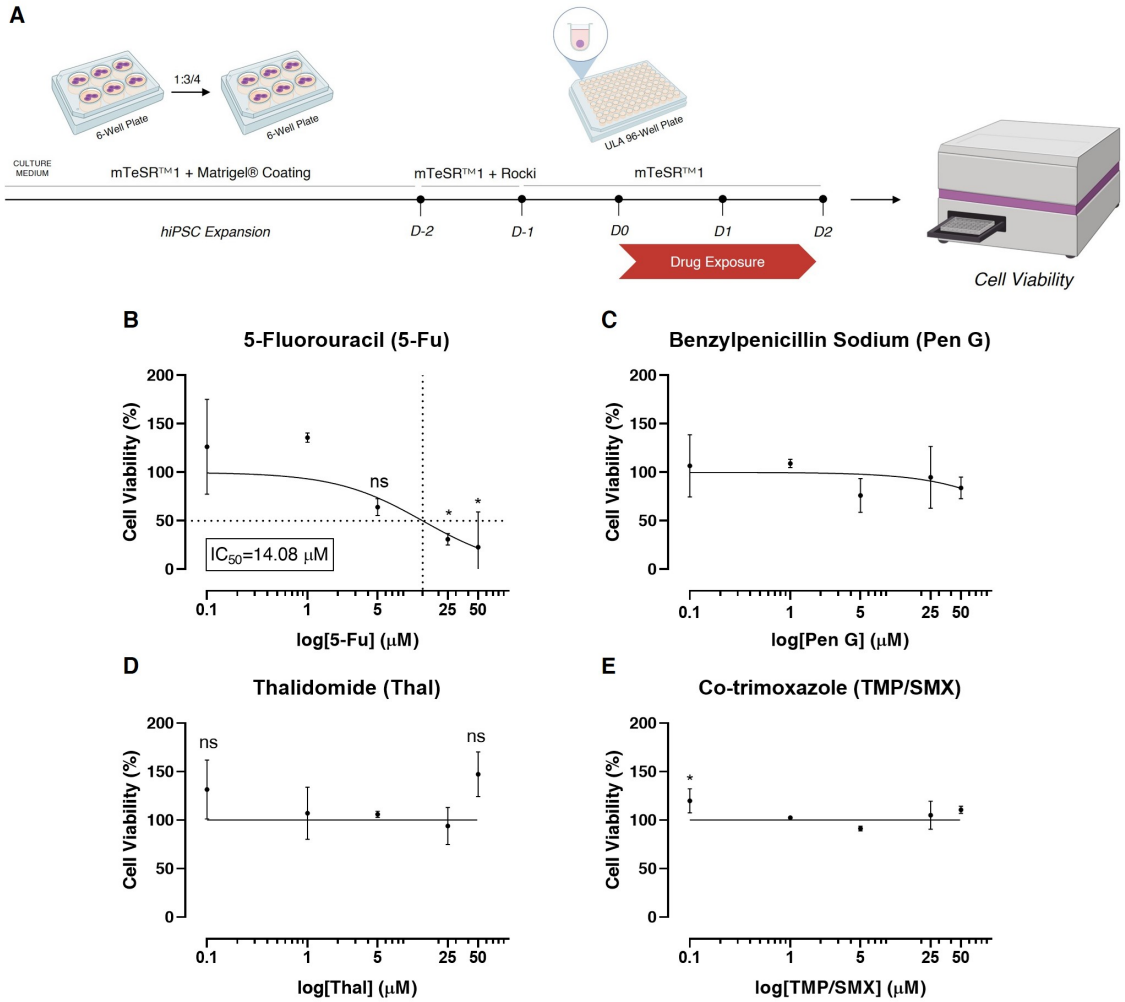

Figure 4.1: Cytoxicity assessment of 5-Fu, Pen G, Thal, and TMP/SMX. **A** - Schematic representation of the platform used for hiPSC cytotoxiciy testing after a drug exposure of 48 h. **B-E** - Concentration-viability curves obtained after exposure to 5-Fu, Pen G, Thal, and TMP/SMX, respectively. A IC_{50} of 14.08 µM was determined for 5-Fu. Mean $\pm$ SD; n $= 1$ experiment for each condition with technical replicates ranging from N $= 2 - 3$. Statistical analysis was performed based on ANOVA with Dunnett's multiple comparisons test comparing each condition with the control condition (*p = 0.0280 between exposure to 25 µM 5-Fu and control; *p = 0.0157 between exposure to 50 µM 5-Fu and control).

DOX exposure produced a significant reduction in cell viability at concentrations above 5 µM and resulted in an IC_{50} of 42.15 µM (Figure 4.2B). DOX acts as an antibiotic by inhibiting the synthesis of bacterial proteins through binding to the 30S ribosomal subunit. Reduced proliferation of human cell lines after DOX exposure has also been reported. The mechanisms behind this remain elusive, although cell cycle stage G_1 arrest and increased apoptotic cell death have been described [Ahler et al., 2013]. Based on statistical analysis, a decrease of viability was also detected after treatment with 50 µM ASA, 50 µM PAR, and with 25 µM or more CBZ (Figure 4.2C,D,E).

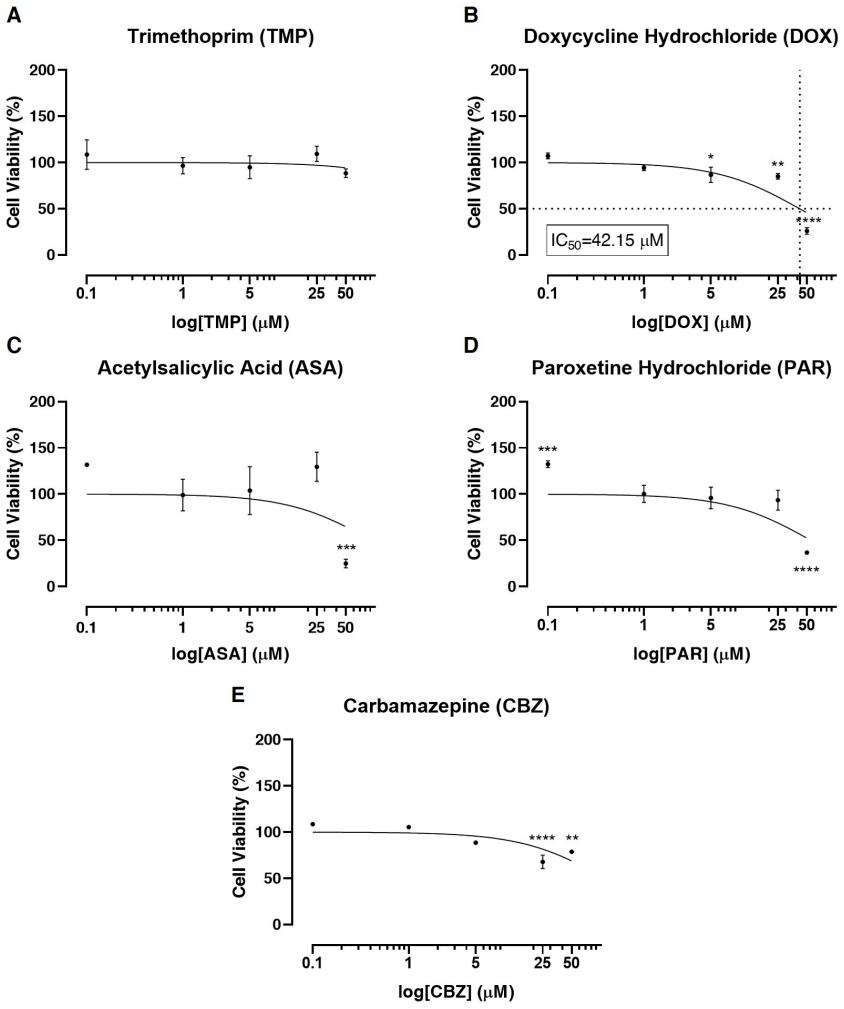

Figure 4.2: Cytoxicity assessment of TMP, DOX, ASA, PAR, and CBZ. **A-E** - Concentration-viability curves obtained after exposure to TMP, DOX, ASA, PAR, and CBZ, respectively. A IC_{50} of 42.15 µM was determined for DOX. Mean $\pm$ SD; n $= 1$ experiment for each condition with technical replicates ranging from N $= 2-3$. Statistical analysis was performed based on ANOVA with Dunnett's multiple comparisons test comparing each condition with the control condition (*p = 0.0129 between exposure to 5 µM DOX and control; **p = 0.0054 between exposure to 25 µM DOX and control; ****p <0.0001 between exposure to 50 µM DOX and control; ***p = 0.0006 between exposure to 50 µM ASA and control; ***p = 0.0004 between exposure to 0.1 µM PAR and control; ****p <0.0001 between exposure to 50 µM PAR and control; ****p <0.0001 between exposure to 25 µM CBZ and control; **p = 0.0013 between exposure to 50 µM CBZ and control).

Overall, the effects on cell viability were consistent with a decrease in aggregate size (Supplemental Figure A.2).

The cell viability data presented was normalized with the corresponding concentration of the vehicle. Nonetheless, an effect of vehicle-induced toxicity was detected. Vehicle concentrations higher than 5 µM led to significantly reduced aggregate size (Supplemental Figure A.2). Hence, the chosen tested drug concentration was not only set in a non-cytotoxic value per se but also taking into consideration a top concentration of DMSO of 0.1% (v/v), as previously performed in other two- and three-dimensional hiPSC-based models of developmental cardiac toxicity [Hoang et al., 2021, Palmer et al., 2013, Jamalpoor et al., 2022].

Additionally, testing at doses below the therapeutic maximum serum concentration (C_{max}) of the drug was considered important to ensure that the effects described were physiologically relevant. A testing dose of 2 µM was chosen for the nine drugs, which was below the reported therapeutic C_{max} value for all the drugs except PAR (Table 3.1).

4.2 Characterization of the 3D Differentiation into Cardiomyocytes

The platform for 3D cardiac differentiation used in this work was previously established and characterized in [Branco et al., 2019]. A detailed protocol is available [Branco et al., 2020b]. In the present work, we performed further molecular and structural characterization of this cardiac model.

From Day 0 to Day 5 of differentiation, the aggregates progressively increased in size to an average of 404.3 $\pm$ 26.02 µm on Day 5. Flow cytometry analysis revealed that on Day 5, the aggregates were composed of 78.3 $\pm$ 1.83 % $CXCR4^{+}$c-KIT^{-} cells, indicative of mesoderm-derived progenitors; 17.2 $\pm$ 2.10 % $CXCR4^{+}$c-KIT^{+} cells, indicative of endoderm-derived progenitors; and 3.79 $\pm$ 2.03 % $CXCR4^{-}$c-KIT^{-} cells, i.e., an unknown population of cells (Figure 4.3B).

Morphologically, Day 5 aggregates consistently presented a slightly elongated shape. By immunostaining analysis of Day 5 aggregate sections, a $SOX17^{+}$ layer was identified surrounding the aggregate and dividing $ISL1^{+}SOX17^{-}$ and $ISL1^{-}SOX17^{-}$ regions. This degree of polarity was reproducible throughout three independent experiments. The spatial organization of endoderm cells surrounding mesoderm progenitors seems to recapitulate the adjacent positioning of the endoderm population to cardiac mesoderm during development [Lough and Sugi, 2000]. In an attempt to characterize the identity of the $ISL1^{-}SOX17^{-}$ cell population, the aggregates were stained for the pluripotency and neuroectoderm induction marker SOX2, revealing no staining, and definitive endoderm marker CDX2, which resulted in staining of a small number cells within that specific region. $CD34^{+}$ cells were detected in a minor number dispersed throughout the aggregate (Figure 4.3B).

From Day 5 onward, the cells progressed through CM commitment. On Day 6, the aggregates were

transferred to low-attachment cell culture plates. Spontaneous contraction usually started around Day 9. Aggregate size increased and the structures became less dense (Figure 4.3C). CM differentiation efficiency was quantified at 84.3% by flow cytometry analysis of CM marker cTNT on Day 15 (Figure 4.3D). Immunostaining analysis of sections of Day 15 aggregates confirmed the cardiac cell identity by the presence of CM markers cTNT and NKX2.5. Laminin expression was also detected. This glycoprotein is an extracellular matrix (ECM) component produced mainly by cardiac fibroblasts. Thus, this points to the presence of other cardiac cell types in the aggregate. This and other ECM components have been shown to support CM maturation by providing structure and harbouring growth factors and other signalling proteins [Eghbali, 1992, Guo and Pu, 2020]. Furthermore, one of the unique features of this model is the capacity to form cavity-like structures. Interestingly, an accumulation of laminin was found predominantly lining the cavities of the aggregates, whose formation mechanism is still to be disclosed. Some $ISL1^{+}$ progenitor cells were still present, usually arranged in a core at the centre of the aggregate. The aggregates also stained positively for the endothelial marker CD31, confirming the presence of endothelial cells (Figure 4.3D).

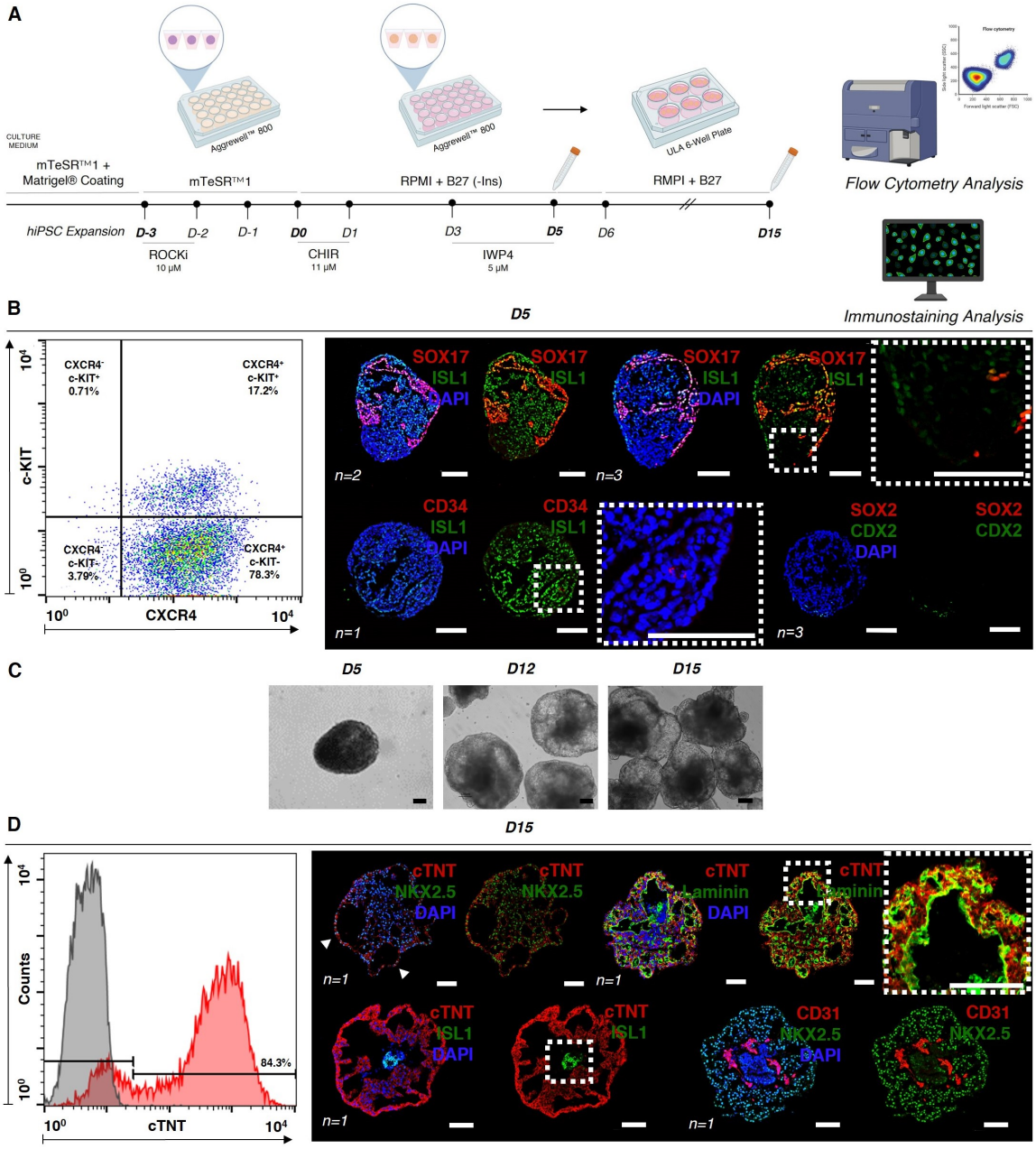

Figure 4.3: The 3D microwell platform for CM differentiation. **A** - Schematic representation of the platform used for CM differentiation and the differentiation protocol. Analysis of the aggregates was performed on Day 5 and Day 15 of differentiation through flow cytometry and immunostaining analysis. **B** - (**Left**) - Quantification of progenitor cell populations of Day 5 aggregates by flow cytometry analysis. CXCR4^{+}c-KIT^{-}: mesoderm-derived progenitors; CXCR4^{+}c-KIT^{+}: endoderm-derived progenitors; CXCR4^{-}c-KIT^{-}: other cells. n $= 3$ independent experiments. **(Right)** - Representative immunostained sections of Day 5 aggregates highlighting the existence of a SOX17^{-}ISL1^{-} region and the presence of CD34^{+} cells. n $= 3$ independent experiments. **C** - Representative bright-field images of the evolution of the aggregates from Day 5 to Day 15 of differentiation. **D** - **(Left)** - Differentiation efficiency determine by flow cytometry analysis of cTNT^{+} cells on Day 15. n $= 1$ experiment. **(Right)** - Representative immunostained sections of Day 15 aggregates. Arrows highlight the cavity-like structures. Dashed squares highlight the accumulation of laminin lining the cavities (top) and the presence of a core of ISL1^{+} cells at the center of the aggregate (bottom). n $= 1$ experiment. Scale bars represent 100 µm.

4.3 Developmental Cardiotoxicity at the Level of Mesendoderm Specification

4.3.1 Drug-caused Imbalance of the Progenitor Populations After Mesendoderm Specification

The first step of the developmental cardiotoxicity study was to expose the aggregates to the nine selected drugs and study their impacts on mesendoderm specification on Day 5 of differentiation.

The effect of drug exposure on aggregate size was first assessed. The vehicle condition (0.1% (v/v) DMSO) showed no toxicity-induced repercussions regarding aggregate size when compared to the control. Aggregate formation was not completely impaired in any of the conditions (Figure 4.4A). However, upon exposure to 5-Fu, the aggregates presented a significantly smaller size, 330.7 $\pm$ 59.95 µm, and higher levels of accumulation of cell death compared with the control condition. DOX exposure also resulted in a statistically significant reduction in aggregate size to 380.7 $\pm$ 48.30 µm, even though these values show some degree of variability (Figure 4.4B). This denotes that the two compounds seem to still have an impact on cell proliferation and viability of differentiating cells, likely through the mechanisms previously mentioned in Section 4.1.

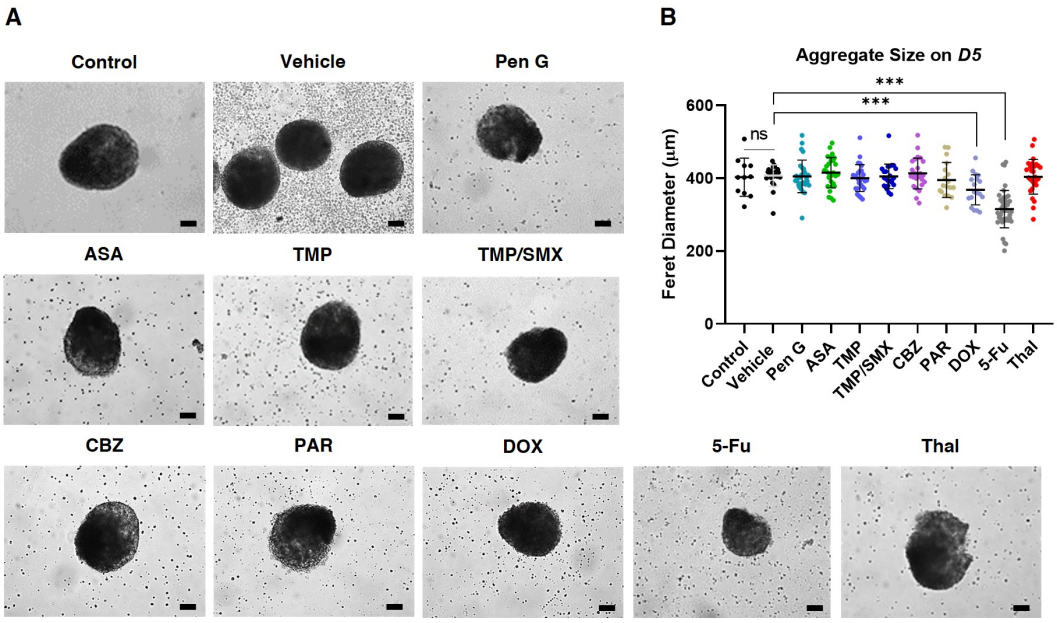

Figure 4.4: Effect of exposure to the nine selected drugs on morphology and size of hiPSC-derived aggregates on Day 5 of cardiac differentiation. **A** - Representative bright-field images of Day 5 aggregates exposed to the nine selected drugs. Scale bars represent 100 µm. **B** - Aggregate size on Day 5 determined by Feret diameter measurement. Mean $\pm$ SD; n $= 2 - 3$ independent experiments for each drug with technical replicates ranging from N $= 11 - 42$. Statistical analysis was performed using Student's t-test comparing each drug with vehicle (***p <0.001 between both 5-Fu and DOX and vehicle).

Flow cytometry analysis of the levels of mesoderm- and endoderm-derived progenitors denoted a more prominent impact on the endoderm population for the tested drugs. A minor dissimilarity was detected between the vehicle condition and the control, although it was not considered significant after statistical analysis (Figure 4.5A). TMP- and TMP/SMX-treated aggregates contained a slightly higher percentage, and similar between the two drugs, of endoderm progenitors when compared to the vehicle condition. This may suggest that the TMP/SMX-induced impact at this level is mainly caused by TMP. CBZ seemed to not have an impact on the percentage of $CXCR4^{+}$c-KIT^{+} endoderm cells compared to the control condition. DOX treatment resulted in highly variable results, so no conclusions could be taken at this stage.

Notably, a significant number of drugs showed a decreased amount of $CXCR4^{+}$c-KIT^{+} endoderm cells when compared to the control, namely, Pen G, ASA, PAR, 5-Fu, and Thal. In the case of 5-Fu-treated aggregates, this effect seems to be mostly compensated by a higher proportion of mesoderm-derived cells. Aggregate size on early differentiation has been shown to impact the efficiency of CM differentiation in this model [Branco et al., 2019]. Thus, the impact of 5-Fu on cell proliferation early on may be responsible for the impairment of the formation of the endoderm layer and reduce differentiation efficiency due to a lack of endoderm-secreted factors, although it is impossible to assess its effects on CMs at this stage. Unlike this drug, Pen G, ASA, PAR, and Thal seemed to redirect differentiation towards other cell types and not towards the mesoderm ($CXCR4^{-}$c-KIT^{-} cells) (Figure 4.5). These results are summarized in Supplemental Table A.1.

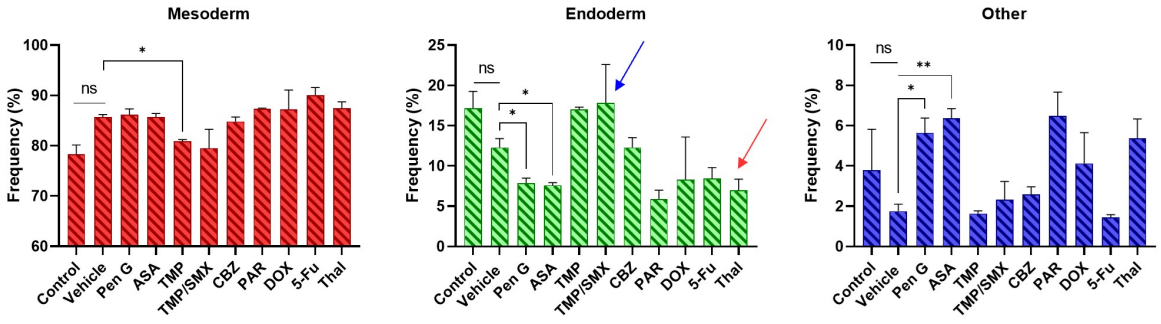

Figure 4.5: Effect of exposure to the nine selected drugs on on hiPSC-derived progenitor populations on Day 5 of cardiac differentiation by flow cytometry analysis. TMP/SMX and TMP treatment caused a slight increase in the endoderm progenitor population whereas other drugs caused a significant reduction of the percentage of these cells, namely, Pen G, ASA, PAR, 5-Fu, and Thal. $CXCR4^{+}$c-KIT^{-}: mesoderm-derived progenitors; $CXCR4^{+}$c-KIT^{+}: endoderm-derived progenitors. $CXCR4^{-}$c-KIT^{-}: other cells. Mean $\pm$ SEM. n $= 2 - 3$ independent experiments. Statistical analysis was performed using Student's t-test comparing each drug with vehicle (*p = 0.017 between TMP and vehicle's mesoderm population; *p = 0.03 between Pen G and vehicle's endoderm population; *p = 0.015 between ASA and vehicle's endoderm population; *p = 0.029 between Pen G and vehicle's other cells; **p = 0.006 between ASA and vehicle's other cells). Arrows highlight two drugs that led to an increase and a decrease in the endoderm-derived progenitor population: TMP/SMX (blue arrow) and Thal (red arrow), respectively.

Figure 4.6 highlights the differences detected in the levels of the endoderm population after treatment with TMP/SMX and Thal, two drugs that led to an increase and a decrease in this population, respectively.

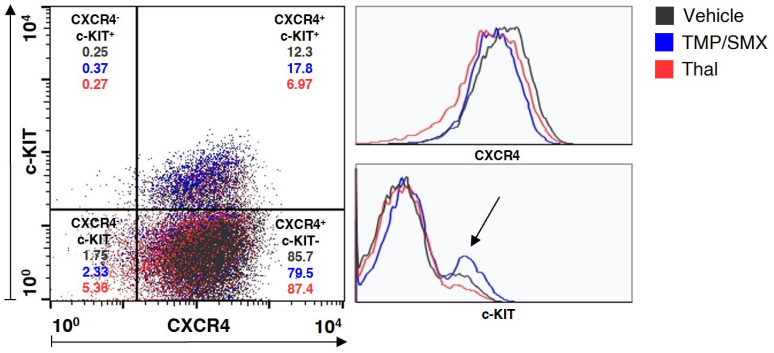

Figure 4.6: Exposure of hiPSC-derived aggregates to TMP/SMX and Thal led to an increase and a decrease, respectively, of the number of endoderm progenitor cells on Day 5 of cardiac differentiation, compared to vehicle-treated cells. $CXCR4^{+}$c-KIT^{-}: mesoderm-derived progenitors; $CXCR4^{+}$c-KIT^{+}: endoderm-derived progenitors. $CXCR4^{-}$c-KIT^{-}: other cells. Arrow highlights a difference in the $CXCR4^{+}$c-KIT^{+} population between the different conditions. n $= 2 - 3$ independent experiments.

Immunostaining analysis of aggregate sections allowed to assess if the aggregate macrostructure identified in the control condition was compromised by drug treatment. The aggregates treated with the group of drugs that showed slightly higher (TMP and TMP/SMX) or similar (CBZ) levels of endoderm progenitors, as well as DOX-treated cells, were able to maintain the three well-defined regions present in the control condition: $SOX17^{+}$ endoderm cells formed a structure that surrounded a part of the aggregate with a protuberance that divided $ISL1^{+}$ mesoderm cells from a $SOX17^{-}ISL^{-}$ region (highlighted with arrows in Figure 4.7). The region negative for both markers also showed higher levels of caspase, suggesting increased apoptosis occurring in this area. Compared to the control condition, TMP, TMP/SMX, and DOX showed higher levels of SOX17 expression and, in some cases, $SOX17^{+}$ were present as an almost or completely closed circle (Supplemental Figure A.6G-I). In order to evaluate if the $SOX17^{-}ISL^{-}$ area was the result of a redirection of the differentiation towards other germ layers, the sections were once again stained for CD31, CDX2, SOX2, as well as PAX6, a neuroectoderm marker also known to be involved in gastrointestinal development. The cells were negative for these four markers.

On the other hand, cells treated with Pen G, ASA, PAR, 5-Fu and Thal showed a reduced expression of SOX17. $SOX17^{+}$ cells were still found assembled together but in smaller clumps and were not able to properly form the structures evident in the previous conditions. This disarrangement varied in degree. Pen G, ASA, and Thal treatment still led to the formation of a $SOX17^{-}ISL1^{-}$ region but the $SOX17^{+}$ clusters were less organized (Figure 4.8A-C). PAR-treated aggregates showed smaller clumps

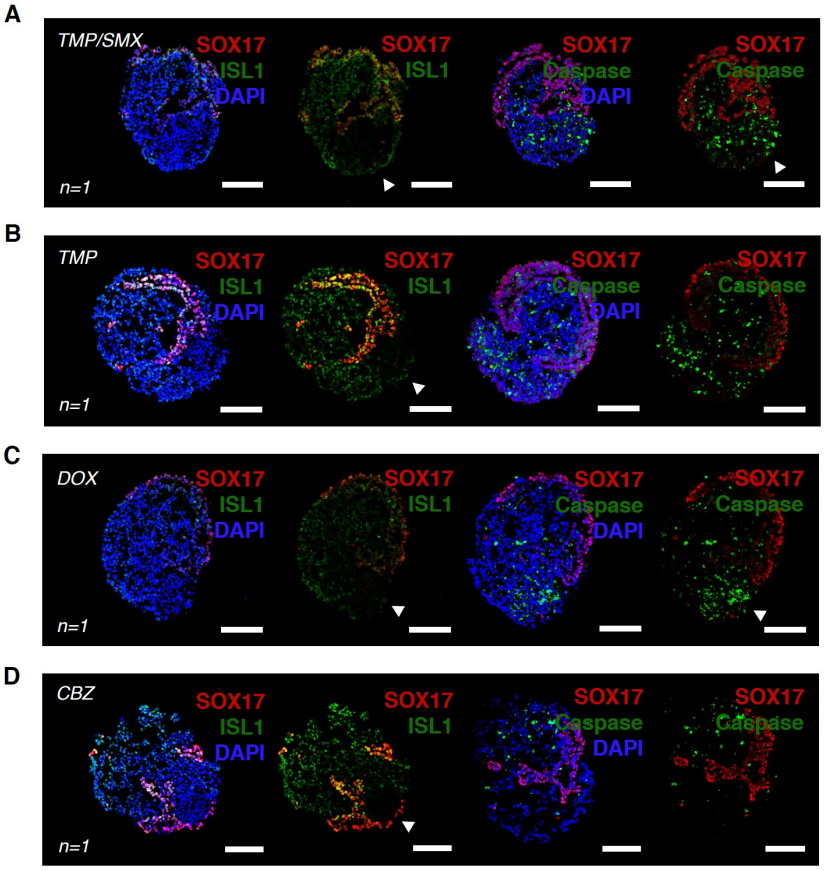

Figure 4.7: Exposure to TMP/SMX, TMP, DOX, and CBZ preserved the spatial organization of progenitor populations on hiPSC-derived aggregates on Day 5 of cardiac differentiation. **A-D** - Representative immunostained sections of Day 5 aggregates treated with TMP/SMX, TMP, DOX, and CBZ, respectively. Arrows highlight the presence of a $SOX17^{-}ISL^{-}$ region. $n = 1$ experiment. Scale bars represent 100 µm.

of $SOX17^{+}$ cells dispersed over the aggregate section (Figure 4.8D). After 5-Fu treatment, $SOX17^{+}$ cells still clustered in the outer layer of the aggregates but did not form a protuberance and the $SOX17^{-}ISL1^{-}$ region was absent (Figure 4.8E).

Kameoka and colleagues previously described a 50% reduction in the number of $SOX17^{+}$ cells in a 2D mesendodermal culture after treatment with 0.6 µM 5-Fu and 0.5 µM Thal [Kameoka et al., 2014]. However, unlike 5-Fu, Thal's effect was not accompanied by increased cell death. This can also be assumed to be the case in our study as Thal-treated aggregates did not show any significant reduction in size, unlike the ones exposed to 5-Fu. Furthermore, the same authors also reported decreased expression of *WNT5B* and *FZD8*, two genes that encode a Wnt signalling pathway ligand and receptor, respectively, after treatment with 5 µM Thal (a dose similar to the one tested in this study) pointing to some level of Wnt signalling pathway impairment. It will be interesting to assess, in the future, if Day 5 aggregates show compromised Wnt signalling activation after Thal exposure. One of the known mechanisms of Thal-induced teratogenicity is the binding of this drug to CRBN, a component of the E3

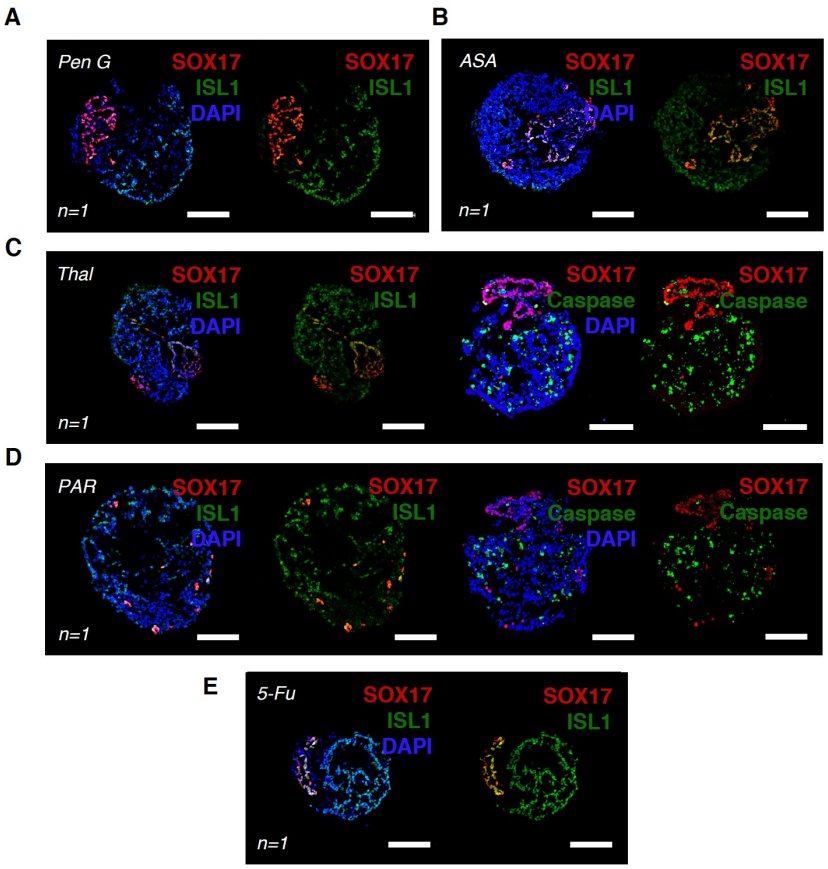

Figure 4.8: Exposure to Pen G, ASA, Thal, PAR, and 5-Fu led to a disruption of the spatial organization of progenitor populations of hiPSC-derived aggregates on Day 5 of cardiac differentiation. **A-E** - Representative immunostained sections of Day 5 aggregates treated with Pen G, ASA, Thal, PAR, and 5-Fu, respectively. n $= 1$ experiment. Scale bars represent 100 µm.

ubiquitin ligase complex, preventing auto-ubiquitination, which can induce CRBN-mediated degradation of target proteins. Belair and colleagues suggested that the inhibition of SOX17 expression upon Thal exposure is caused by Thal-binding to CRBN, which induces SALL4 degradation [Belair et al., 2020]. In fact, interaction of SALL4 with the SOX17 promotor had been previously reported and, besides this, SALL4-knockout mouse ESCs failed to express SOX17 [Lim et al., 2008, Miller et al., 2016].

Moreover, Xing and colleagues detected a Thal-induced disruption of the Brachyury (T) spatial expression pattern on micropatterned hiPSC colonies differentiated towards mesendoderm for 3 days, pointing to the existence of drug-induced morphological changes during this stage of differentiation. However, Pen G treatment did not induce such changes in the spatial organization of T^+ cells, which was expected as the drug has no reported teratogenicity. Nonetheless, a small but not statistically significant reduction of SOX17 expression was detected by RT-PCR after treatment with both drugs, with a more prominent effect on Thal-treated cells [Xing et al., 2015]. Our data suggests a slight impact on Pen G-treated aggregates, but further experiments need to be performed to prove this.

Nonetheless, our results after treatment with 5-Fu and Thal, two well-known teratogens, are in agreement with what has previously been described at a similar stage of hiPSC development using simpler 2D models. Thus, we decided to continue the study with the goal of understanding if and how these morphological defects can impact differentiation towards cardiac cells.

4.3.2 Thalidomide Exposure During Mesendoderm Specification Impairs the Formation of Cavity-like Structures at the End of Differentiation

To better understand the impact that an imbalance of the two progenitor populations has on CM differentiation, we decided to focus on two drugs that showed increased and decreased levels of endoderm progenitors, namely, TMP/SMX and Thal, respectively. Two different exposure strategies were performed: (i) drug treatment from Day 1 to Day 5 and (ii) prolonged exposure from Day 1 to Day 15.

As the aggregates were transferred from the AggreWell™ 800 plates on Day 5, re-aggregation onto V-shaped 96-well ULA culture plates was performed to increase the throughput for drug exposure. Aggregates whose drug treatment was terminated on Day 5 were transferred to ultra-low 6-well plates (Figure 4.9A). First, to discern the impact that the re-aggregation of progenitors on Day 5 could have on Day 15 aggregates, immunostained slices at the end of differentiation were analyzed and compared with those of non-re-aggregated Day 15 aggregates. It was possible to conclude that the re-aggregation experimental procedure introduced differences compared with the control. The main effect detected was the loss of cavity-like structures after re-aggregation. The levels of $CD31^{+}$ cells were also reduced compared with the non-re-aggregated condition, which is the basis for the assumption that the process of re-aggregation introduced some degree of CM purification. The loss of other cardiac cell types combined with the disassembly of the ECM formed until re-aggregation was considered to be the cause for the loss of the capacity to re-form cavity-like structures. Nonetheless, no major morphological differences were detected between control and vehicle-treated aggregates with or without re-aggregation (Figure 4.9B-C).

Comparing the impact of drug treatment between Day 1 and Day 5 on Day 15 CM aggregates, it was observed that (Thal *D1-D5*)-treated aggregates started contracting on Day 8 whereas (TMP/SMX *D1-D5*) and control aggregates began contraction on Day 9. Thal-exposed aggregates showed abnormal contraction profiles upon visual assessment, although a proper functional analysis is required to confirm this assumption. Furthermore, (Thal *D1-D5*) aggregates were considerably smaller and denser (Figure 4.10A).

Regarding aggregate growth rate, a continuous treatment with TMP/SMX until Day 15 led the aggregates to reach maximum size earlier than in the case of the (TMP/SMX *D1-D5*) condition hinting at a possible decrease of cell proliferation caused by continuous drug exposure. No major differences were detected macroscopically between the two Thal exposure conditions (Figure 4.10B-C).

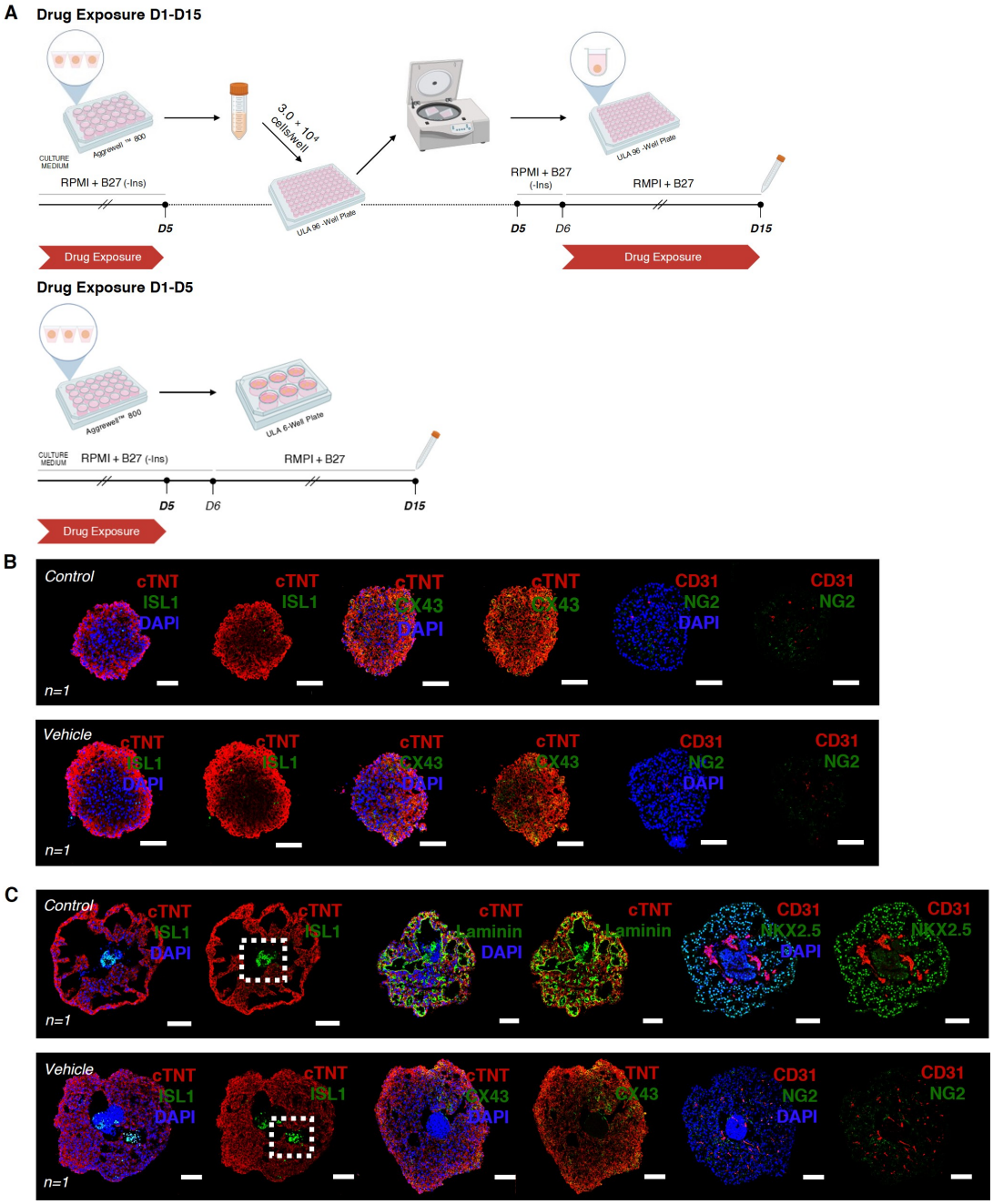

Figure 4.9: Adaptation of the differentiation protocol for higher-throughput drug exposure from Day 5 to Day 15 of differentiation. **A** - For drug exposure from Day 1 to Day 15, the aggregates were re-aggregated onto 96-well ULA culture plates with a cell seeding density of 3.0×10^4 cells/well. For drug exposure from Day 1 to Day 5, the aggregates were transferred from the AggreWell™ 800 plate to 6-well ULA culture plates. Analysis of the aggregates was performed on Day 15. **B** - Representative immunostained sections of Day 15 aggregates after re-aggregation. Re-aggregation resulted in a loss of cell type diversity and capacity of formation cavity-like structures. No major differences were detected between the control and vehicle conditions. **C** - Representative immunostained sections of Day 15 aggregates without re-aggregation. No major differences were detected between the control and vehicle conditions. $n = 1$ experiment. Scale bars represent 100 µm.

Notably, Thal exposure during the first five days of differentiation was enough to impair the formation of cavity-like structures which did not occur in TMP/SMX-treated aggregates, as confirmed by analysis of immunostained aggregate sections (Figure 4.10D).

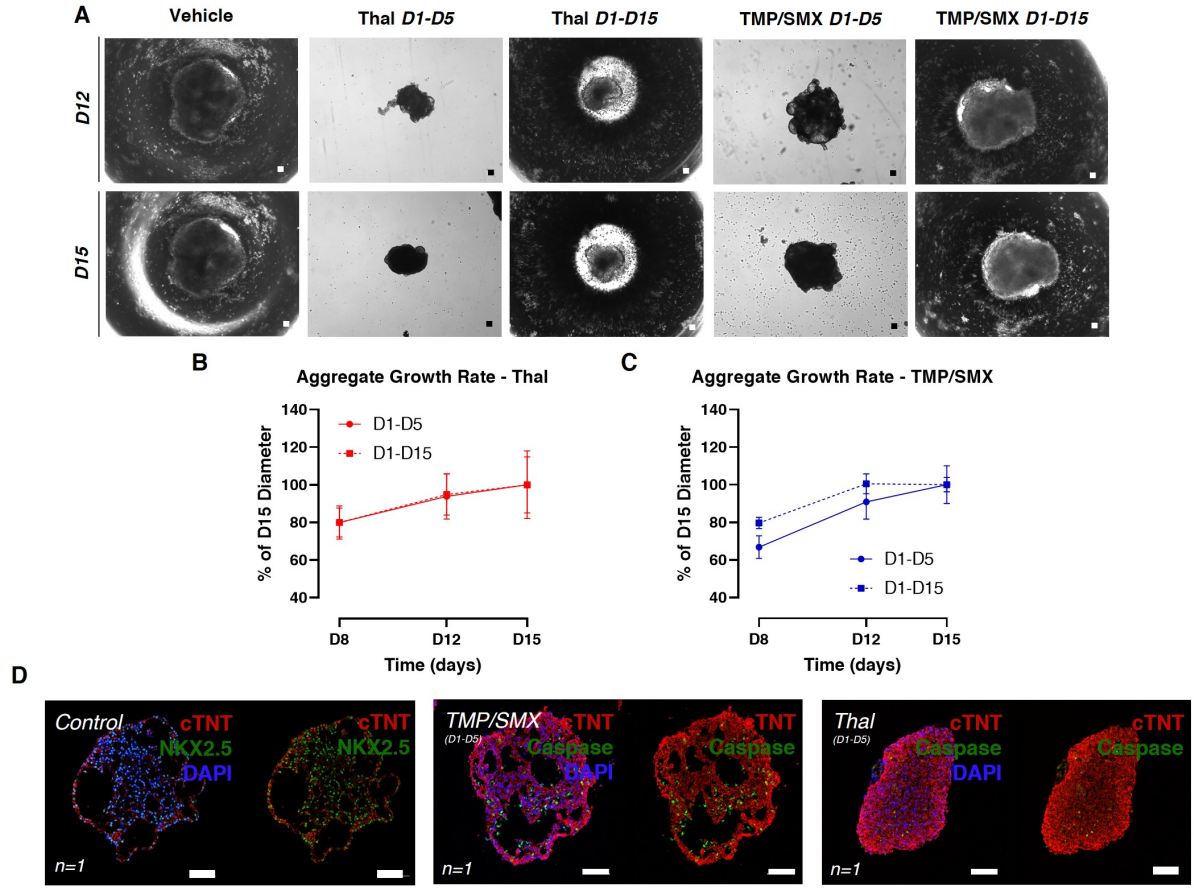

Figure 4.10: Comparison of the effects of Thal and TMP/SMX prolonged exposure *vs* exposure until mesendoderm specification on aggregate growth throughout cardiac differentiation, and effect of exposure until mesendoderm specification on chamber formation analyzed on Day 15. Thal treatment until mesendoderm specification was enough to impair the formation of cavity-like structures. **A** - Representative bright-field images of the evolution of aggregates treated with vehicle, Thal from Day 1 to Day 5 (Thal *D1-D5*), Thal from Day 1 to Day 15 (Thal *D1-D15*), TMP/SMX from Day 1 to Day 5 (TMP/SMX *D1-D5*), and TMP/SMX from Day 1 to Day 15 (TMP/SMX *D1-D15*), until Day 15 of differentiation. **B-C** - Aggregate growth rate after treatment with Thal and TMP/SMX, respectively. Each data point represents the mean percentage of final Feret diameter (Day 15) of the aggregates on the corresponding day. Mean $\pm$ SD. n $= 1$ experiment with technical replicates ranging from N $= 6 - 16$. **D** - Representative immunostained sections of Day 15 aggregates treated with TMP/SMX and Thal from Day 1 to Day 5. n $= 1$ experiment. Scale bars represent 100 µm.

Besides the already mentioned mechanisms responsible for Thal toxicity, this drug has been reported to decrease the expression of FGF through binding to GC boxes present in the FGF2 promoter [Stephens et al., 2000]. Altough the majority of the cardiac fibroblasts arise from the epicardium, it has been also shown that cardiac fibroblasts can be differentiated *in vitro* from SHF progenitors after FGF2 signal-

ing pathway activation [Zhang et al., 2019]. Therefore, it can be hypothesized that a defect in cardiac fibroblast specification in our cardiac model after Thal treatment, and consequently imbalanced ECM production can, e.g., compromise laminin production, which was detected lining the cavities. The lack of proper ECM components may be one of the reasons behind the loss of capacity of chamber formation. On the other hand, [Khalil et al., 2017] concluded that Thal binds to the amino acids required for DNA binding of T-box transcription factor (TBX5), a protein expressed in FHF-like derived populations (cells which also express left ventricular CM marker HAND1) [Branco et al., 2020a]. Inhibition of the interaction between TBX5 and HAND2 was also hypothesized as the amino acids through which TBX5 binds to DNA, and that become bound to Thal upon drug exposure are also the ones involved in the binding with HAND2. Interestingly, Hofbauer and colleagues inferred that inhibiting HAND1 expression in their chamber-forming cardiac organoids resulted in an incapacity to form cavities [Hofbauer et al., 2021]. Although the mechanisms of chamber formation remain elusive, an inactivation of TBX5 action by Thal and inhibition of its binding to HAND family transcription factors can also be involved in the events behind the loss of cavity formation capacity despite the fact that this requires confirmation. Both raised hypotheses should be further explored in the future, particularly to clarify the dependency of the observed toxicity-induced defects on FHF and/or SHF progenitors and their derivatives specification.

For both drug exposure strategies, on Day 15, the aggregates were replated onto Matrigel®-coated 24-well culture plates for analysis of sarcomeric structure. On Day $15 + 2$, a significant number of cells of the (Thal *D1-D5*) condition had detached from the coating matrix and formed 3D-structures with clumps of cells connected by CM-like individual cells (Figure 4.11A). Thal is still on the market for cancer treatment. One of the reasons behind this is its capacity to inhibit the binding of tumour cells to the stroma through modelling of the expression of cell surface adhesion molecules such as tumor necrosis factor (TNF-α), intercellular adhesion molecule-1 (ICAM-1), and vascular cellular adhesion molecule-1 (VCAM-1) [Kumar et al., 2004] which could eventually explain the reduced adhesion to the substrate after replating.

Sarcomere alignment disruption was not detected for any condition (Figure 4.11B). Sarcomere length of adult CMs is usually $\simeq$ 2.2 µm [Stein et al., 2022]. However, hiPSC-derived CMs are more immature and this value is lower. Day $15 + 2$ control CMs had a sarcomere length of 1.53 ± 0.06 µm. This value compared favourably to vehicle-treated CMs which had a value of 1.51 ± 0.15 µm. No significant impact on this parameter was detected upon exposure to (Thal *D1-D5*), (TMP/SMX *D1-D5*), and (TMP/SMX *D1-D15*) (Figure 4.11C). On the other hand, using NKX2.5 or α-actinin to specifically label CMs and Ki-67 as a marker of cell proliferation, a higher level Ki-67$^+$ cells was detected for the (Thal *D1-D15*) condition (42.3 ± 4.72 %) when compared to (TMP/SMX *D1-D5*) and (TMP/SMX *D1-D15*) (23.7 ± 4.16 % and 14.3 ± 3.56 %, respectively) (Figure 4.11D-E). Unfortunately, the levels of Ki-67$^+$ cells in the control condition were not measured, but a value of 11.9 ± 0.60% was previously reported in the model [Branco

et al., 2019]. Thus, a higher number of Ki-67^{+} cells after drug exposure, particularly evident in Thal treated cells, can indicate a less mature phenotype caused by drug treatment. Nonetheless, the data requires further validation.

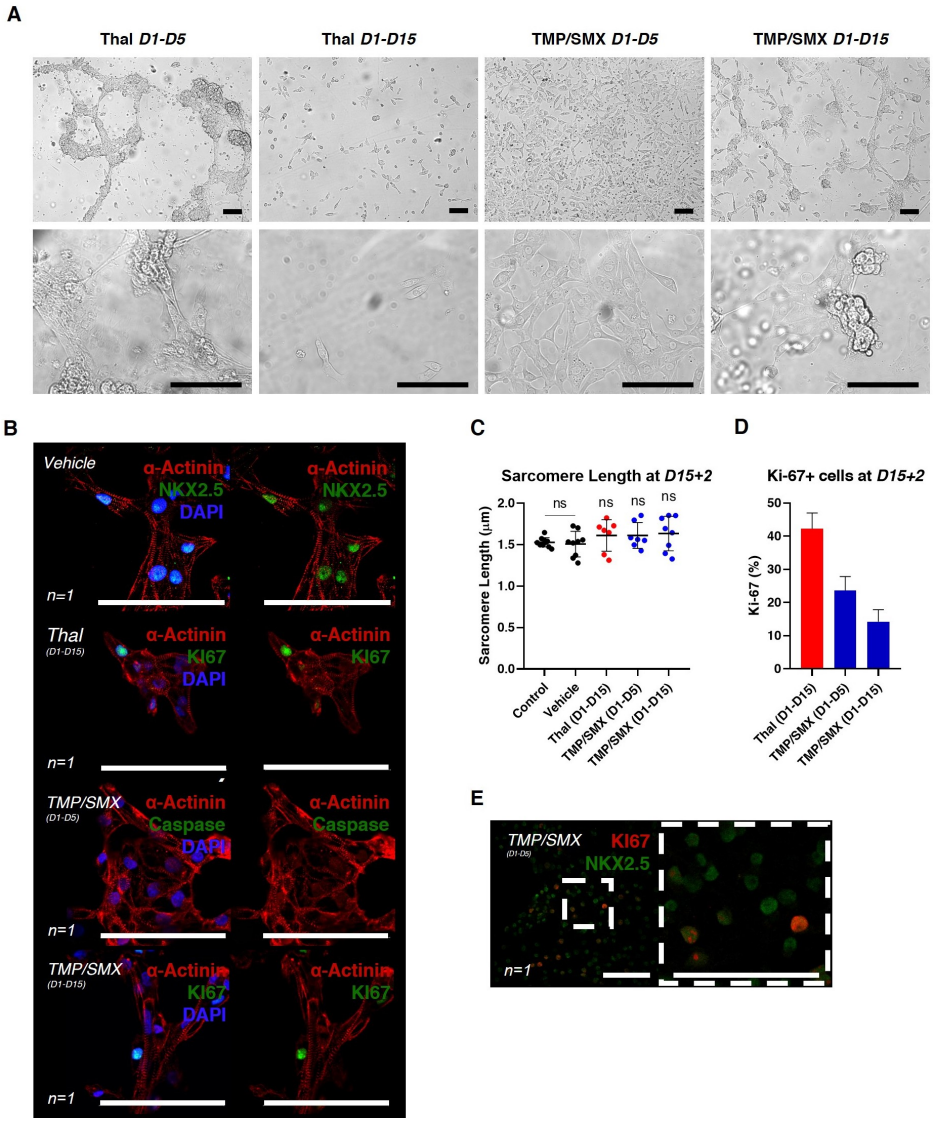

Figure 4.11: Comparison of the effects of Thal and TMP/SMX prolonged exposure *vs* exposure until mesendoderm specification on cell morphology, sarcomere length, and ratio of proliferative cells. Overall, Thal-treated cells were more proliferative on Day $15+2$ than cells exposed to TMP/SMX. **A** - Representative bright-field images of replated cells on Day $15+2$ after treatment with Thal from Day 1 to Day 5 (Thal *D1-D5*), Thal from Day 1 to Day 15 (Thal *D1-D15*), TMP/SMX from Day 1 to Day 5 (TMP/SMX *D1-D5*), and TMP/SMX from Day 1 to Day 15 (TMP/SMX *D1-D15*). **B**- Representative immunostaining images of replated cells on Day $15+2$ after treatment with vehicle, (Thal *D1-D15*), (TMP/SMX *D1-D5*), and (TMP/SMX *D1-D15*). n $= 1$ experiment. **C** - Sarcomere length quantification of Day $15+2$ cells of the control condition and after treatment with vehicle, (Thal *D1-D15*), (TMP/SMX *D1-D5*), and (TMP/SMX *D1-D15*). Mean $\pm$ SD. n $= 1$ experiment with technical replicates ranging from N $= 8-10$. Statistical analysis was performed using Student's t-test comparing each condition with vehicle. **D** - Percentage of Ki-67^{+} Day $15+2$ cells after treatment with (Thal *D1-D15*), (TMP/SMX *D1-D5*), and (TMP/SMX *D1-D15*). Mean $\pm$ SD. n $= 1$ experiment with technical replicates ranging from N $= 4-5$. **E** - Representative immunostaining image used for quantification of Ki-67^{+} cells. Scale bar represents 100 µm.

Collectively, the platform and drug exposure strategies tested in the present work allowed to highlight the teratogenic effect of Thal and TMP/SMX and corroborate previously described findings obtained in other *in vitro* models. Our data suggests that Thal toxicity seems to act mainly at the mesendoderm specification stage, as an exposure terminated on Day 5 seemed to be enough to disrupt normal cardiac development. The results regarding TMP/SMX treatment suggested some effect on the proliferation rate of cells that suffered a prolonged exposure which might indicate a drug-induced impact on CM differentiation that still needs to be further characterized.

4.4 Developmental Cardiotoxicity at the Level of Cardiomyocyte Commitment

In order to assess the effects that Thal exposure has on cardiac development if mesendoderm induction and specification were not compromised, we exposed the aggregates to the drug only from Day 6 forward.

Later onset of drug exposure did not result in any major macroscopic morphological changes when compared to the control condition (Figure 4.12A-B). However, upon immunostaining analysis of replated CMs some differences were detected. Different subtypes of CMs were observed with some presenting organized sarcomeres and others an abnormal and hypertrophic morphology. In the latter, the sarcomeres seemed to be concentrated around the nuclei and had a disarrayed structure (Figure 4.12C). This heterogeneous CM population may be a consequence of the diffusional gradients across the aggregate. Thal treatment from Day 6 to Day 15 seemed to also affect sarcomere length, showing a statistically significant increase in this value, 1.67 $\pm$ 0.08 µm, when compared to the control and vehicle conditions, 1.53 $\pm$ 0.06 µm and 1.51 $\pm$ 0.06 µm, respectively (Figure 4.12D). However, this was highly affected by the CM phenotypical heterogeneity, which precluded the measurement of the sarcomeres of CMs that presented morphological abnormalities introducing bias in the quantification.

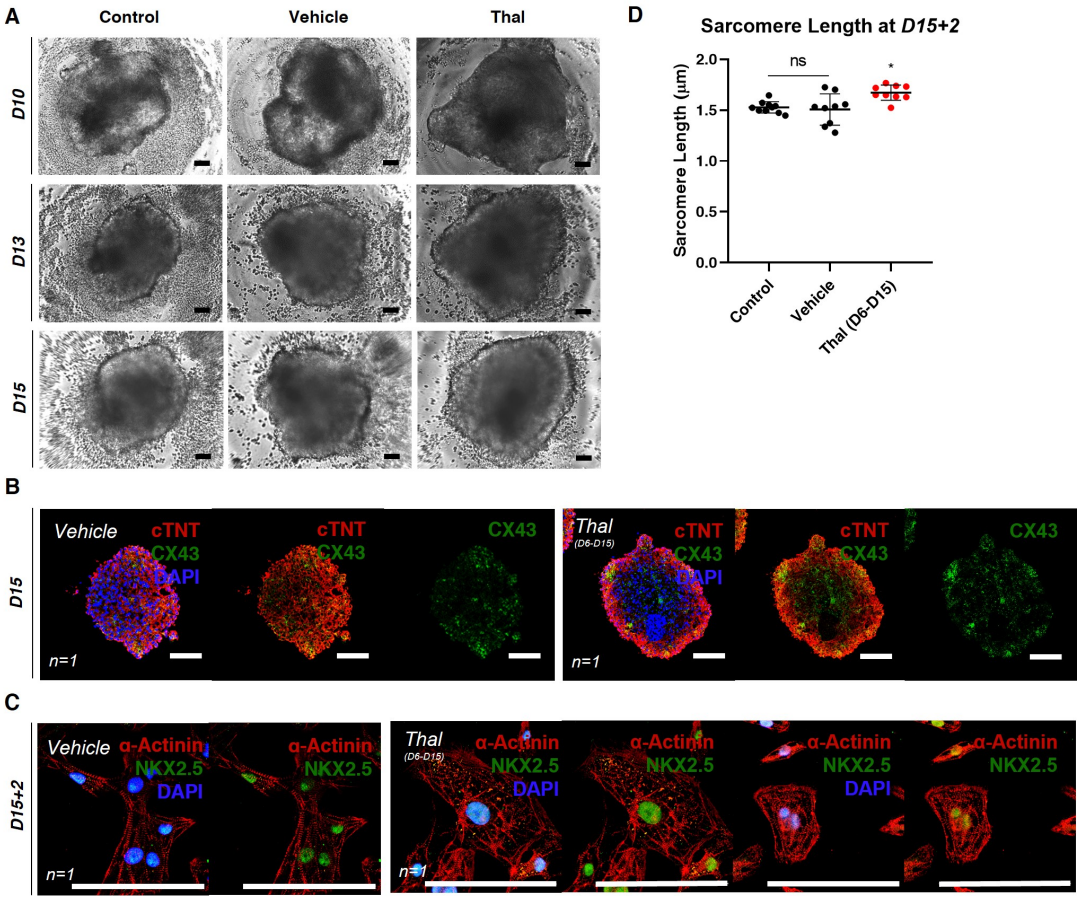

Figure 4.12: Effects of Thal exposure with onset after mesendoderm specification on aggregate and cell morphology, and sarcomere length. A subset of CMs presenting abnormal morphology was detected after treatment with Thal. **A** - Representative bright-field images of the evolution of aggregates treated with Thal from Day 6 to Day 15. Each photo corresponds to the evolution of the same aggregate throughout time within conditions. **B** - Representative immunostained sections of Day 15 aggregates treated with vehicle and Thal from Day 6 to Day 15. n $= 1$ experiment. **C** - Representative immunostaining images of replated cells on Day 15 $+$ 2 after treatment with vehicle and Thal from Day 6 to Day 15. n $= 1$ experiment. Scale bars represent 100 µm. **D** - Sarcomere length quantification of Day 15 $+$ 2 cells of the control condition and after treatment with vehicle and Thal from Day 6 to Day 15 (Thal *D6-D15*). Mean $\pm$ SD. n $= 1$ experiment with technical replicates ranging from N $= 9 - 10$. Statistical analysis was performed using Student's t-test comparing each condition with vehicle (*p = 0.011 between (Thal *D6-D15*) and vehicle).

5

Conclusions and Future Work

Contents

5.1 Conclusions

Developmental toxicology has still resorted mainly to the use of animal models to predict and evaluate the toxicity mechanisms behind teratogenic malformations. However, the 1960s *"Thalidomide Tragedy"* raised attention to the fact that some drugs may be toxic for some species but not others. The impossibility of pregnant women to take part in clinical trials makes human cell-based *in vitro* platforms the only viable alternative. Nowadays, stem cell based-models offer the opportunity to study human development at an organ level. Since heart-related defects are some of the most commonly reported birth pathologies, cardiac models are of great interest in the toxicology field. Until recently, hiPSC-derived models of developmental cardiotoxicity were still mainly based on 2D differentiation protocols. However, since congenital cardiac defects usually manifest as structural malformations (such as septal defects, atrial or ventricular underdevelopment, ...), 3D models, although far from recapitulating such events, can detect toxicity impacts that simply do not occur in 2D models and offer a further mechanistic understanding of such effects.

The organogenesis stage is the most sensitive to drug teratogenicity. For that reason, the use of models that allow tracking down possible toxicity events through development and, at the same time, assessing its effect on terminally differentiated cardiac cells offers a more comprehensive way to perform teratogenicity studies. To our knowledge, the hiPSC-derived model used in this study is the only 3D model that presents both mesoderm- and endoderm-derived progenitor populations that has been used for developmental cardiotoxicity studies. Here, we characterized those populations and detected a reproducible spatial clustering of these cells in a specific way. Furthermore, we detected that some drugs had the capacity to imbalance the specification into these two populations with a special impact on the endoderm progenitor population. A reduction of the levels of endoderm progenitors resulted in the loss of the spatial progenitor pattern identified. No direct link between this and effects on terminally differentiated cardiac cells can be assumed so far. However, we hypothesize that a disruption of this arrangement might affect the way the endoderm-derived progenitors provide cues for the differentiation of mesoderm-derived progenitors and their progress through normal development.

Exposure to thalidomide only until the mesendoderm specification stage was enough to impair the formation of cavity-like structures, one of the main features of the model here described. We identified a variety of mechanisms through which thalidomide might cause this that have been described in the literature, such as the inhibition of the expression of FGF or TBX5 and its effect on HAND family transcription factors. However, a direct mechanism of thalidomide-mediated inhibition of SOX17 expression has also been reported. SOX17 is required for endoderm formation in *Xenopus* and zebrafish embryos and in maintaining definitive endoderm in a progenitor state in mouse embryos. It is also associated with the expression of cardiogenic factors in mouse embryos [Pfister et al., 2011]. Thus, a combination of these events, along with the described loss of progenitor polarity, might be responsible for the loss of chamber

formation capacity and, eventually, for fetal heart abnormalities that have been described after pregnant women were treated with thalidomide. The different drug exposure strategies that we applied allowed to strengthen the hypothesis that thalidomide treatment has an impact mainly until the mesendoderm specification stage, confirming the idea that drug toxicity is dependent on the stage of development in which exposure occurs.

Thus, it can be concluded that the platform employed here offers unique features that are of interest for developmental cardiotoxicity testing. The model was capable of reproducing previously described thalidomide-induced toxicity effects. At the same time, the analysis of progenitor populations may offer a simplified early endpoint of toxicity as the differentiation towards endoderm- and mesoderm-derived progenitors is faster. Besides this, an impact of drug-induced toxicity on the capacity to form cavity-like structures was detected, which offers both the ability to obtain a better mechanistic understanding behind heart congenital malformations but also the possibility to enlighten the own mechanisms behind the formation of such structures.

5.2 Future Work

The present data requires, in most cases, further confirmation to increase the statistical power of the results and provide a more solid basis to assert the hypotheses that have been put forward in this work. It will be necessary to confirm that an effect on the progenitor populations assessed on Day 5 of differentiation is enough to predict cardiac toxicity. Besides this, a prolonged culture of the aggregates will allow the characterization of possible effects on cardiomyocyte maturation that were hinted in this work.

Furthermore, the analysis herein performed was mainly based on the assessment of structural features. In order to obtain a full characterization of the drugs' effects on CMs, a functional assessment based on calcium transient analysis will be performed. This will be complemented by testing different specific channel-blocker drugs to validate the functional properties of the CMs.

Bibliography

[Adam et al., 2011] Adam, M. P., Polifka, J. E., and Friedman, J. (2011). Evolving knowledge of the teratogenicity of medications in human pregnancy. *American Journal of Medical Genetics Part C: Seminars in Medical Genetics*, 157(3):175–182.

[Agwuh and MacGowan, 2006] Agwuh, K. N. and MacGowan, A. (2006). Pharmacokinetics and pharmacodynamics of the tetracyclines including glycylcyclines. *Journal of Antimicrobial Chemotherapy*, 58:256–265.

[Ahler et al., 2013] Ahler, E., Sullivan, W. J., Cass, A., Braas, D., York, A. G., Bensinger, S. J., Graeber, T. G., and Christofk, H. R. (2013). Doxycycline alters metabolism and proliferation of human cell lines. *PLoS ONE*, 8:e64561.

[Andrade et al., 2008] Andrade, S. E., Raebel, M. A., Brown, J., Lane, K., Livingston, J., Boudreau, D., Rolnick, S. J., Roblin, D., Smith, D. H., Willy, M. E., Staffa, J. A., and Platt, R. (2008). Use of antidepressant medications during pregnancy: a multisite study. *American Journal of Obstetrics and Gynecology*, 198:194.e1–194.e5.

[Archer et al., 2018] Archer, C. R., Sargeant, R., Basak, J., Pilling, J., Barnes, J. R., and Pointon, A. (2018). Characterization and validation of a human 3d cardiac microtissue for the assessment of changes in cardiac pathology. *Scientific Reports*, 8:10160.

[Augustine-Rauch et al., 2010] Augustine-Rauch, K., Zhang, C. X., and Panzica-Kelly, J. M. (2010). In vitro developmental toxicology assays: A review of the state of the science of rodent and zebrafish whole embryo culture and embryonic stem cell assays. *Birth Defects Research Part C: Embryo Today: Reviews*, 90(2):87–98.

[Ayad and Costantine, 2015] Ayad, M. and Costantine, M. M. (2015). Epidemiology of medications use in pregnancy. *Seminars in Perinatology*, 39(7):508–511.

[Bauwens et al., 2011] Bauwens, C. L., Song, H., Thavandiran, N., Ungrin, M., Massé, S., Nanthakumar, K., Seguin, C., and Zandstra, P. W. (2011). Geometric control of cardiomyogenic induction in human pluripotent stem cells. *Tissue Engineering Part A*, 17:1901–1909.

[Belair et al., 2020] Belair, D. G., Lu, G., Waller, L. E., Gustin, J. A., Collins, N. D., and Kolaja, K. L. (2020). Thalidomide inhibits human ipsc mesendoderm differentiation by modulating crbn-dependent degradation of sall4. *Scientific Reports*, 10:2864.

[Blehar et al., 2013] Blehar, M. C., Spong, C., Grady, C., Goldkind, S. F., Sahin, L., and Clayton, J. A. (2013). Enrolling Pregnant Women: Issues in Clinical Research. *Women's Health Issues*, 23(1):e39–e45.

[Bookstaver et al., 2015] Bookstaver, P. B., Bland, C. M., Griffin, B., Stover, K. R., Eiland, L. S., and McLaughlin, M. (2015). A review of antibiotic use in pregnancy. *Pharmacotherapy: The Journal of Human Pharmacology and Drug Therapy*, 35:1052–1062.

[Bourin et al., 2001] Bourin, M., Chue, P., and Guillon, Y. (2001). Paroxetine: A review. *CNS Drug Reviews*, 7:25–47.

[Branco et al., 2020a] Branco, M. A., Cabral, J. M., and Diogo, M. M. (2020a). From Human Pluripotent Stem Cells to 3D Cardiac Microtissues: Progress, Applications and Challenges. *Bioengineering*, 7(3):92.

[Branco et al., 2019] Branco, M. A., Cotovio, J. P., Rodrigues, C. A., Vaz, S. H., Fernandes, T. G., Moreira, L. M., Cabral, J. M., and Diogo, M. M. (2019). Transcriptomic analysis of 3d cardiac differentiation of human induced pluripotent stem cells reveals faster cardiomyocyte maturation compared to 2d culture. *Scientific Reports*, 9:1–13.

[Branco et al., 2020b] Branco, M. A., Dias, T. P., Cotovio, J. P., Rodrigues, C. A. V., Fernandes, T. G., Cabral, J. M. S., and Diogo, M. M. (2020b). 3d microwell platform for cardiomyocyte differentiation of human pluripotent stem cells. *Methods in Molecular Biology*, pages 127–143.

[Brandão et al., 2017] Brandão, K. O., Tabel, V. A., Atsma, D. E., Mummery, C. L., and Davis, R. P. (2017). Human pluripotent stem cell models of cardiac disease: from mechanisms to therapies. *Disease Models & Mechanisms*, 10:1039–1059.

[Bérard et al., 2016] Bérard, A., Iessa, N., Chaabane, S., Muanda, F. T., Boukhris, T., and Zhao, J. P. (2016). The risk of major cardiac malformations associated with paroxetine use during the first trimester of pregnancy: a systematic review and metaanalysis. *British Journal of Clinical Pharmacology*, 81:589.

[Cao and Xu, 2020] Cao, B. L. and Xu, C. (2020). Challenges in assessing the use of antibiotics during pregnancy and risk of congenital malformations. *British Journal of Clinical Pharmacology*, 86:620–621.

[Castro and Morrison-Bryant, 2010] Castro, J. and Morrison-Bryant (2010). Management of pneumocystis jirovecii pneumonia in hiv infected patients: current options, challenges and future directions. *HIV/AIDS - Research and Palliative Care*, page 123.

[Church et al., 2015] Church, J. A., Fitzgerald, F., Walker, A. S., Gibb, D. M., and Prendergast, A. J. (2015). The expanding role of co-trimoxazole in developing countries. *The Lancet Infectious Diseases*, 15:327–339.

[Cross et al., 2015] Cross, M. J., Berridge, B. R., Clements, P. J. M., Cove-Smith, L., Force, T. L., Hoffmann, P., Holbrook, M., Lyon, A. R., Mellor, H. R., Norris, A. A., Pirmohamed, M., Tugwood, J. D., Sidaway, J. E., and Park, B. K. (2015). Physiological, pharmacological and toxicological considerations of drug-induced structural cardiac injury. *British Journal of Pharmacology*, 172:957–974.

[Dally, 1998] Dally, A. (1998). Thalidomide: was the tragedy preventable? *The Lancet*, 351(9110):1197–1199.

[Davidson et al., 2005] Davidson, M. M., Nesti, C., Palenzuela, L., Walker, W. F., Hernandez, E., Protas, L., Hirano, M., and Isaac, N. D. (2005). Novel cell lines derived from adult human ventricular cardiomyocytes. *Journal of Molecular and Cellular Cardiology*, 39:133–147.

[Drakhlis et al., 2021] Drakhlis, L., Biswanath, S., Farr, C.-M., Lupanow, V., Teske, J., Ritzenhoff, K., Franke, A., Manstein, F., Bolesani, E., Kempf, H., Liebscher, S., Schenke-Layland, K., Hegermann, J., Nolte, L., Meyer, H., de la Roche, J., Thiemann, S., Wahl-Schott, C., Martin, U., and Zweigerdt, R. (2021). Human heart-forming organoids recapitulate early heart and foregut development. *Nature Biotechnology*, 39:737–746.

[Eder et al., 2016] Eder, A., Vollert, I., Hansen, A., and Eschenhagen, T. (2016). Human engineered heart tissue as a model system for drug testing. *Advanced Drug Delivery Reviews*, 96:214–224.

[Eghbali, 1992] Eghbali, M. (1992). Cardiac fibroblasts: Function, regulation of gene expression, and phenotypic modulation. *Basic Research in Cardiology*, 87:183–189.

[Evans and Kaufman, 1981] Evans, M. J. and Kaufman, M. H. (1981). Establishment in culture of pluripotential cells from mouse embryos. *Nature*, 292:154–156.

[FDA, NA] FDA (NA). Fda approved drug products: Primsol (trimethoprim) oral solution.

[Fisher et al., 2016] Fisher, D. I., Mayr, L. M., and Roth, R. G. (2016). Expression systems. *Encyclopedia of Cell Biology*, 1:54–65.

[Genschow et al., 2004] Genschow, E., Spielmann, H., Scholz, G., Pohl, I., Seiler, A., Clemann, N., Bremer, S., and Becker, K. (2004). Validation of the embryonic stem cell test in the international

ecvam validation study on three ¡i¿in vitro¡/i¿ embryotoxicity tests. *Alternatives to Laboratory Animals*, 32:209–244.

[Ghafouri-Fard et al., 2021] Ghafouri-Fard, S., Abak, A., Anamag, F. T., Shoorei, H., Fattahi, F., Javadinia, S. A., Basiri, A., and Taheri, M. (2021). 5-fluorouracil: A narrative review on the role of regulatory mechanisms in driving resistance to this chemotherapeutic agent. *Frontiers in Oncology*, 11:1210.

[Guo and Pu, 2020] Guo, Y. and Pu, W. T. (2020). Cardiomyocyte maturation. *Circulation Research*, pages 1086–1106.

[Heijman et al., 2014] Heijman, J., Voigt, N., Carlsson, L. G., and Dobrev, D. (2014). Cardiac safety assays. *Current Opinion in Pharmacology*, 15(1):16–21.

[Hernández-Díaz et al., 2012] Hernández-Díaz, S., Smith, C. R., Shen, A., Mittendorf, R., Hauser, W. A., Yerby, M., and Holmes, L. B. (2012). Comparative safety of antiepileptic drugs during pregnancy. *Neurology*, 78:1692–1699.

[Hoang et al., 2021] Hoang, P., Kowalczewski, A., Sun, S., Winston, T. S., Archilla, A. M., Lemus, S. M., Ercan-Sencicek, A. G., Gupta, A. R., Liu, W., Kontaridis, M. I., Amack, J. D., and Ma, Z. (2021). Engineering spatial-organized cardiac organoids for developmental toxicity testing. *Stem Cell Reports*, 16:1228–1244.

[Hofbauer et al., 2021] Hofbauer, P., Jahnel, S. M., Papai, N., Giesshammer, M., Deyett, A., Schmidt, C., Penc, M., Tavernini, K., Grdseloff, N., Meledeth, C., Ginistrelli, L. C., Ctortecka, C., Šejla Šalic, Novatchkova, M., and Mendjan, S. (2021). Cardioids reveal self-organizing principles of human cardiogenesis. *Cell*, 184:3299–3317.e22.

[Hoffmann and Warner, 2006] Hoffmann, P. and Warner, B. (2006). Are herg channel inhibition and qt interval prolongation all there is in drug-induced torsadogenesis? a review of emerging trends. *Journal of Pharmacological and Toxicological Methods*, 53(2):87–105.

[Jamalpoor et al., 2022] Jamalpoor, A., Hartvelt, S., Dimopoulou, M., Zwetsloot, T., Brandsma, I., Racz, P. I., Osterlund, T., and Hendriks, G. (2022). A novel human stem cell [U+2010] based biomarker assay for in vitro assessment of developmental toxicity. *Birth Defects Research*, 114:1210–1228.

[Jamieson et al., 2006] Jamieson, D., Theiler, R., and Rasmussen, S. (2006). Emerging Infections and Pregnancy. *Emerging Infectious Diseases*, 12(11):1638–1643.

[Jentink et al., 2010] Jentink, J., Loane, M. A., Dolk, H., Barisic, I., Garne, E., Morris, J. K., and de Jong-van den Berg, L. T. (2010). Valproic acid monotherapy in pregnancy and major congenital malformations. *The New England Journal of Medicine*, 362:2185–2193.

[Kameoka et al., 2014] Kameoka, S., Babiarz, J., Kolaja, K., and Chiao, E. (2014). A high-throughput screen for teratogens using human pluripotent stem cells. *Toxicological Sciences*, 137:76–90.

[Kazuki et al., 2016] Kazuki, Y., Akita, M., Kobayashi, K., Osaki, M., Satoh, D., Ohta, R., Abe, S., Takehara, S., Kazuki, K., Yamazaki, H., Kamataki, T., and Oshimura, M. (2016). Thalidomide-induced limb abnormalities in a humanized cyp3a mouse model. *Scientific Reports*, 6:21419.

[Kehat et al., 2001] Kehat, I., Kenyagin-Karsenti, D., Snir, M., Segev, H., Amit, M., Gepstein, A., Livne, E., Binah, O., Itskovitz-Eldor, J., and Gepstein, L. (2001). Human embryonic stem cells can differentiate into myocytes with structural and functional properties of cardiomyocytes. *Journal of Clinical Investigation*, 108:407–414.

[Khalil et al., 2017] Khalil, A., Tanos, R., El-Hachem, N., Kurban, M., Bouvagnet, P., Bitar, F., and Nemer, G. (2017). A hand to tbx5 explains the link between thalidomide and cardiac diseases. *Scientific Reports*, 7:1416.

[Kheradvar et al., 2017] Kheradvar, A., Zareian, R., Kawauchi, S., Goodwin, R. L., and Rugonyi, S. (2017). Animal models for heart valve research and development. *Drug Discovery Today: Disease Models*, 24(xx):55–62.

[Kim and Scialli, 2011] Kim, J. H. and Scialli, A. R. (2011). Thalidomide: The Tragedy of Birth Defects and the Effective Treatment of Disease. *Toxicological Sciences*, 122(1):1–6.

[Klabunde, 2011] Klabunde, R. (2011). *Cardiovascular Physiology Concepts*. Lippincott Williams & Wilkins/Wolters Kluwer.

[Krishnan et al., 2014] Krishnan, A., Samtani, R., Dhanantwari, P., Lee, E., Yamada, S., Shiota, K., Donofrio, M. T., Leatherbury, L., and Lo, C. W. (2014). A detailed comparison of mouse and human cardiac development. *Pediatric Research*, 76(6):500–507.

[Kumar et al., 2004] Kumar, S., Witzig, T. E., and Rajkumar, S. V. (2004). Thalidomide: Current role in the treatment of non-plasma cell malignancies. *Journal of Clinical Oncology*, 22:2477–2488.

[Lachmann, 2012] Lachmann, P. J. (2012). The penumbra of thalidomide, the litigation culture and the licensing of pharmaceuticals. *QJM*, 105(12):1179–1189.

[Lauschke et al., 2020] Lauschke, K., Rosenmai, A. K., Meiser, I., Neubauer, J. C., Schmidt, K., Rasmussen, M. A., Holst, B., Taxvig, C., Emnéus, J. K., and Vinggaard, A. M. (2020). A novel human pluripotent stem cell-based assay to predict developmental toxicity. *Archives of Toxicology*, 94:3831–3846.

[Laverty et al., 2011] Laverty, H., Benson, C., Cartwright, E., Cross, M., Garland, C., Hammond, T., Holloway, C., McMahon, N., Milligan, J., Park, B., Pirmohamed, M., Pollard, C., Radford, J., Roome, N., Sager, P., Singh, S., Suter, T., Suter, W., Trafford, A., Volders, P., Wallis, R., Weaver, R., York, M., and Valentin, J. (2011). How can we improve our understanding of cardiovascular safety liabilities to develop safer medicines? *British Journal of Pharmacology*, 163:675–693.

[Leek and Arif, 2022] Leek, J. C. and Arif, H. (2022). Pregnancy medications. *StatPearls*.

[Lewis-Israeli et al., 2021] Lewis-Israeli, Y. R., Wasserman, A. H., Gabalski, M. A., Volmert, B. D., Ming, Y., Ball, K. A., Yang, W., Zou, J., Ni, G., Pajares, N., Chatzistavrou, X., Li, W., Zhou, C., and Aguirre, A. (2021). Self-assembling human heart organoids for the modeling of cardiac development and congenital heart disease. *Nature Communications*, 12:5142.

[Li et al., 2018] Li, R. A., Keung, W., Cashman, T. J., Backeris, P. C., Johnson, B. V., Bardot, E. S., Wong, A. O., Chan, P. K., Chan, C. W., and Costa, K. D. (2018). Bioengineering an electro-mechanically functional miniature ventricular heart chamber from human pluripotent stem cells. *Biomaterials*, 163:116–127.

[Lian et al., 2012] Lian, X., Hsiao, C., Wilson, G., Zhu, K., Hazeltine, L. B., Azarin, S. M., Raval, K. K., Zhang, J., Kamp, T. J., and Palecek, S. P. (2012). Robust cardiomyocyte differentiation from human pluripotent stem cells via temporal modulation of canonical wnt signaling. *Proceedings of the National Academy of Sciences of the United States of America*, 109.

[Lilienblum et al., 2008] Lilienblum, W., Dekant, W., Foth, H., Gebel, T., Hengstler, J. G., Kahl, R., Kramer, P.-J., Schweinfurth, H., and Wollin, K.-M. (2008). Alternative methods to safety studies in experimental animals: role in the risk assessment of chemicals under the new European Chemicals Legislation (REACH). *Archives of Toxicology*, 82(4):211–236.

[Lim et al., 2008] Lim, C. Y., Tam, W.-L., Zhang, J., Ang, H. S., Jia, H., Lipovich, L., Ng, H.-H., Wei, C.-L., Sung, W. K., Robson, P., Yang, H., and Lim, B. (2008). Sall4 regulates distinct transcription circuitries in different blastocyst-derived stem cell lineages. *Cell Stem Cell*, 3:543–554.

[Liu et al., 2018] Liu, Q., Bortle, K. V., Zhang, Y., Zhao, M.-T., Zhang, J. Z., Geller, B. S., Gruber, J. J., Jiang, C., Wu, J. C., and Snyder, M. P. (2018). Disruption of mesoderm formation during cardiac differentiation due to developmental exposure to 13-cis-retinoic acid. *Scientific Reports*, 8:12960.

[Lough and Sugi, 2000] Lough, J. and Sugi, Y. (2000). Endoderm and heart development. *Developmental Dynamics*, 217:327–342.

[Lynch and Abel, 2015] Lynch, T. A. and Abel, D. E. (2015). Teratogens and congenital heart disease. *Journal of Diagnostic Medical Sonography*, 31:301–305.

[Mahler and Butcher, 2011] Mahler, G. J. and Butcher, J. T. (2011). Cardiac developmental toxicity. *Birth Defects Research Part C: Embryo Today: Reviews*, 93(4):291–297.

[Mahmood and Chamberlin, 1998] Mahmood, I. and Chamberlin, N. (1998). A limited sampling method for the estimation of auc and cmax of carbamazepine and carbamazepine epoxide following a single and multiple dose of a sustained release product. *British Journal of Clinical Pharmacology*, 45:241–246.

[Mandenius et al., 2011] Mandenius, C.-F., Steel, D., Noor, F., Meyer, T., Heinzle, E., Asp, J., Arain, S., Kraushaar, U., Bremer, S., Class, R., and Sartipy, P. (2011). Cardiotoxicity testing using pluripotent stem cell-derived human cardiomyocytes and state-of-the-art bioanalytics: a review. *Journal of Applied Toxicology*, 31:191–205.

[Mantziou et al., 2021] Mantziou, V., Baillie-Benson, P., Jaklin, M., Kustermann, S., Arias, A. M., and Moris, N. (2021). In vitro teratogenicity testing using a 3d, embryo-like gastruloid system. *Reproductive Toxicology*, 105:72–90.

[Matalon et al., 2002] Matalon, S., Schechtman, S., Goldzweig, G., and Ornoy, A. (2002). The teratogenic effect of carbamazepine: a meta-analysis of 1255 exposures. *Reproductive Toxicology*, 16(1):9–17.

[McBride, 1961] McBride, W. (1961). Thalidomide and Congenital Abnormalities. *The Lancet*, 278(7216):1358.

[Meilhac and Buckingham, 2018] Meilhac, S. M. and Buckingham, M. E. (2018). The deployment of cell lineages that form the mammalian heart. *Nature Reviews Cardiology*, 15(11):705–724.

[Miller et al., 2016] Miller, A., Ralser, M., Kloet, S. L., Loos, R., Nishinakamura, R., Bertone, P., Vermeulen, M., and Hendrich, B. (2016). Sall4 controls differentiation of pluripotent cells independently of the nucleosome remodelling and deacetylation (nurd) complex. *Development*, 143:3074–3084.

[Mills et al., 2017] Mills, R. J., Titmarsh, D. M., Koenig, X., Parker, B. L., Ryall, J. G., Quaife-Ryan, G. A., Voges, H. K., Hodson, M. P., Ferguson, C., Drowley, L., Plowright, A. T., Needham, E. J., Wang, Q.-D., Gregorevic, P., Xin, M., Thomas, W. G., Parton, R. G., Nielsen, L. K., Launikonis, B. S., James, D. E., Elliott, D. A., Porrello, E. R., and Hudson, J. E. (2017). Functional screening in human cardiac organoids reveals a metabolic mechanism for cardiomyocyte cell cycle arrest. *Proceedings of the National Academy of Sciences*, 114:E8372–E8381.

[Miyamoto et al., 2021] Miyamoto, M., Nam, L., Kannan, S., and Kwon, C. (2021). Heart organoids and tissue models for modeling development and disease. *Seminars in Cell and Developmental Biology*, 118(March):119–128.

[Mohammed and Pratten", 2019] Mohammed, O. J. and Pratten", M. K. ("2019"). *"Micromass Methods for the Evaluation of Developmental Toxicants"*, pages "49–72". "Springer New York", "New York, NY".

[Muanda et al., 2017] Muanda, F. T., Sheehy, O., and Bérard, A. (2017). Use of antibiotics during pregnancy and the risk of major congenital malformations: a population based cohort study. *British Journal of Clinical Pharmacology*, 83:2557–2571.

[Muanda et al., 2020] Muanda, F. T., Sheehy, O., and Bérard, A. (2020). Response to letter 'challenges in assessing the use of antibiotics during pregnancy and risk of congenital malformations'. *British Journal of Clinical Pharmacology*, 86:531–532.

[Nagelschmitz et al., 2014] Nagelschmitz, J., Blunck, M., Kraetzschmar, J., Ludwig, M., Wensing, G., and Hohlfeld (2014). Pharmacokinetics and pharmacodynamics of acetylsalicylic acid after intravenous and oral administration to healthy volunteers. *Clinical Pharmacology: Advances and Applications*, 6:51.

[Olson et al., 2000] Olson, H., Betton, G., Robinson, D., Thomas, K., Monro, A., Kolaja, G., Lilly, P., Sanders, J., Sipes, G., Bracken, W., Dorato, M., Deun, K. V., Smith, P., Berger, B., and Heller, A. (2000). Concordance of the toxicity of pharmaceuticals in humans and in animals. *Regulatory Toxicology and Pharmacology*, 32:56–67.

[Ovics et al., 2020] Ovics, P., Regev, D., Baskin, P., Davidor, M., Shemer, Y., Neeman, S., Ben-Haim, Y., and Binah, O. (2020). Drug Development and the Use of Induced Pluripotent Stem Cell-Derived Cardiomyocytes for Disease Modeling and Drug Toxicity Screening. *International Journal of Molecular Sciences*, 21(19):7320.

[Paine, 2017] Paine, M. (2017). Therapeutic disasters that hastened safety testing of new drugs. *Clinical Pharmacology & Therapeutics*, 101(4):430–434.

[Palmer et al., 2013] Palmer, J. A., Smith, A. M., Egnash, L. A., Conard, K. R., West, P. R., Burrier, R. E., Donley, E. L., and Kirchner, F. R. (2013). Establishment and assessment of a new human embryonic stem cell-based biomarker assay for developmental toxicity screening. *Birth Defects Research Part B: Developmental and Reproductive Toxicology*, 98:343–363.

[Pfister et al., 2011] Pfister, S., Jones, V. J., Power, M., Truisi, G. L., Khoo, P.-L., Steiner, K. A., Kanai-Azuma, M., Kanai, Y., Tam, P. P., and Loebel, D. A. (2011). Sox17-dependent gene expression and early heart and gut development in sox17-deficient mouse embryos. *The International Journal of Developmental Biology*, 55:45–58.

[Protze et al., 2019] Protze, S. I., Lee, J. H., and Keller, G. M. (2019). Human Pluripotent Stem Cell-Derived Cardiovascular Cells: From Developmental Biology to Therapeutic Applications. *Cell Stem Cell*, 25(3):311–327.

[Qian et al., 2016] Qian, X., Nguyen, H. N., Song, M. M., Hadiono, C., Ogden, S. C., Hammack, C., Yao, B., Hamersky, G. R., Jacob, F., Zhong, C., Yoon, K. J., Jeang, W., Lin, L., Li, Y., Thakor, J., Berg, D. A., Zhang, C., Kang, E., Chickering, M., Nauen, D., Ho, C. Y., Wen, Z., Christian, K. M., Shi, P. Y., Maher, B. J., Wu, H., Jin, P., Tang, H., Song, H., and Ming, G. L. (2016). Brain-region-specific organoids using mini-bioreactors for modeling zikv exposure. *Cell*, 165:1238–1254.

[Reeves and Wilkinson, 1979] Reeves, D. S. and Wilkinson, P. J. (1979). The pharmacokinetics of trimethoprim and trimethoprim/sulphonamide combinations, including penetration into body tissues. *Infection*, 7:S330–S341.

[Richards et al., 2017] Richards, D. J., Coyle, R. C., Tan, Y., Jia, J., Wong, K., Toomer, K., Menick, D. R., and Mei, Y. (2017). Inspiration from heart development: Biomimetic development of functional human cardiac organoids. *Biomaterials*, 142:112–123.

[Richards et al., 2020] Richards, D. J., Li, Y., Kerr, C. M., Yao, J., Beeson, G. C., Coyle, R. C., Chen, X., Jia, J., Damon, B., Wilson, R., Hazard, E. S., Hardiman, G., Menick, D. R., Beeson, C. C., Yao, H., Ye, T., and Mei, Y. (2020). Human cardiac organoids for the modelling of myocardial infarction and drug cardiotoxicity. *Nature Biomedical Engineering*, 4:446–462.

[Sasseville et al., 2004] Sasseville, V., Lane, J., Kadambi, V., Bouchard, P., Lee, F., Balani, S., Miwa, G., Smith, P., and Alden, C. (2004). Testing paradigm for prediction of development-limiting barriers and human drug toxicity. *Chemico-Biological Interactions*, 150:9–25.

[Sayed et al., 2016] Sayed, N., Liu, C., and Wu, J. C. (2016). Translation of human-induced pluripotent stem cells. *Journal of the American College of Cardiology*, 67:2161–2176.

[Scialli, 2008] Scialli, A. R. (2008). The challenge of reproductive and developmental toxicology under REACH. *Regulatory Toxicology and Pharmacology*, 51(2):244–250.

[Seiler and Spielmann, 2011] Seiler, A. E. and Spielmann, H. (2011). The validated embryonic stem cell test to predict embryotoxicity in vitro. *Nature Protocols*, 6:961–978.

[Sharma et al., 2017] Sharma, A., Burridge, P. W., McKeithan, W. L., Serrano, R., Shukla, P., Sayed, N., Churko, J. M., Kitani, T., Wu, H., Holmström, A., Matsa, E., Zhang, Y., Kumar, A., Fan, A. C., del Álamo, J. C., Wu, S. M., Moslehi, J. J., Mercola, M., and Wu, J. C. (2017). High-throughput screening of tyrosine kinase inhibitor cardiotoxicity with human induced pluripotent stem cells. *Science Translational Medicine*, 9.

[Sharma et al., 2018] Sharma, A., McKeithan, W. L., Serrano, R., Kitani, T., Burridge, P. W., del Álamo, J. C., Mercola, M., and Wu, J. C. (2018). Use of human induced pluripotent stem cell–derived cardiomyocytes to assess drug cardiotoxicity. *Nature Protocols*, 13:3018–3041.

[Shi et al., 2020] Shi, M., Tien, N. T., de Haan, L., Louisse, J., Rietjens, I. M., and Bouwmeester, H. (2020). Evaluation of in vitro models of stem cell-derived cardiomyocytes to screen for potential cardiotoxicity of chemicals. *Toxicology in Vitro*, 67:104891.

[Shields and Lyerly, 2013] Shields, K. E. and Lyerly, A. D. (2013). Exclusion of Pregnant Women From Industry-Sponsored Clinical Trials. *Obstetrics & Gynecology*, 122(5):1077–1081.

[Später et al., 2014] Später, D., Hansson, E. M., Zangi, L., and Chien, K. R. (2014). How to make a cardiomyocyte. *Development*, 141(23):4418–4431.

[Stein et al., 2022] Stein, J. M., Arslan, U., Franken, M., de Greef, J. C., Harding, S. E., Mohammadi, N., Orlova, V. V., Bellin, M., Mummery, C. L., and van Meer, B. J. (2022). Software tool for automatic quantification of sarcomere length and organization in fixed and live 2d and 3d muscle cell cultures ¡i¿in vitro¡/i¿. *Current Protocols*, 2.

[Stephens et al., 2000] Stephens, T. D., Bunde, C. J., and Fillmore, B. J. (2000). Mechanism of action in thalidomide teratogenesis. *Biochemical Pharmacology*, 59:1489–1499.

[Takahashi et al., 2007] Takahashi, K., Tanabe, K., Ohnuki, M., Narita, M., Ichisaka, T., Tomoda, K., and Yamanaka, S. (2007). Induction of pluripotent stem cells from adult human fibroblasts by defined factors. *Cell*, 131:861–872.

[Takahashi and Yamanaka, 2006] Takahashi, K. and Yamanaka, S. (2006). Induction of pluripotent stem cells from mouse embryonic and adult fibroblast cultures by defined factors. *Cell*, 126:663–676.

[Takeda et al., 2018] Takeda, M., Miyagawa, S., Fukushima, S., Saito, A., Ito, E., Harada, A., Matsuura, R., Iseoka, H., Sougawa, N., Mochizuki-Oda, N., Matsusaki, M., Akashi, M., and Sawa, Y. (2018). Development of ¡i¿in vitro¡/i¿ drug-induced cardiotoxicity assay by using three-dimensional cardiac tissues derived from human induced pluripotent stem cells. *Tissue Engineering Part C: Methods*, 24:56–67.

[Teo et al., 2004] Teo, S. K., Colburn, W. A., Tracewell, W. G., Kook, K. A., Stirling, D. I., Jaworsky, M. S., Scheffler, M. A., Thomas, S. D., and Laskin, O. L. (2004). Clinical pharmacokinetics of thalidomide. *Clinical Pharmacokinetics*, 43:311–327.

[Thomson et al., 1998] Thomson, J. A., Itskovitz-Eldor, J., Shapiro, S. S., Waknitz, M. A., Swiergiel, J. J., Marshall, V. S., and Jones, J. M. (1998). Embryonic stem cell lines derived from human blastocysts. *Science*, 282:1145–1147.

[Trinkley et al., 2013] Trinkley, K. E., Page, R. L., Lien, H., Yamanouye, K., and Tisdale, J. E. (2013). Qt interval prolongation and the risk of torsades de pointes: essentials for clinicians. *Current Medical Research and Opinion*, 29:1719–1726.

[van Meer et al., 2019] van Meer, B. J., Krotenberg, A., Sala, L., Davis, R. P., Eschenhagen, T., Denning, C., Tertoolen, L. G. J., and Mummery, C. L. (2019). Simultaneous measurement of excitation-contraction coupling parameters identifies mechanisms underlying contractile responses of hipsc-derived cardiomyocytes. *Nature Communications*, 10:4325.

[van Meer et al., 2016] van Meer, B. J., Tertoolen, L. G., and Mummery, C. L. (2016). Concise Review: Measuring Physiological Responses of Human Pluripotent Stem Cell Derived Cardiomyocytes to Drugs and Disease. *Stem Cells*, 34(8):2008–2015.

[Walker et al., 2021] Walker, L. M., Sparks, N. R. L., Puig-Sanvicens, V., Rodrigues, B., and zur Nieden, N. I. (2021). An evaluation of human induced pluripotent stem cells to test for cardiac developmental toxicity. *International Journal of Molecular Sciences*, 22:8114.

[Walker et al., 2016] Walker, T., Harris, K., Maifoshie, E., and Chaudhary, K. (2016). *Human Stem Cell-Derived Cardiomyocyte In Vitro Models for Cardiotoxicity Screening*, chapter 6, pages 85–121. John Wiley & Sons, Ltd.

[Xia et al., 2020] Xia, J., Meng, Z., Ruan, H., Yin, W., Xu, Y., and Zhang, T. (2020). Heart Development and Regeneration in Non-mammalian Model Organisms. *Frontiers in Cell and Developmental Biology*, 8(October):1–7.

[Xing et al., 2015] Xing, J., Toh, Y.-C., Xu, S., and Yu, H. (2015). A method for human teratogen detection by geometrically confined cell differentiation and migration. *Scientific Reports*, 5:10038.

[Ye et al., 2020] Ye, D., Bao, Z., Yu, Y., Han, Z., Yu, Y., Xu, Z., Ma, W., Yuan, Y., Zhang, L., Xu, Y., Ma, T., Liu, S., Gao, X., Yan, G., Huang, Q., Wang, X., Hua, B., Yang, F., Li, Y., and Cai, B. (2020). Inhibition of cardiomyocyte differentiation of human induced pluripotent stem cells by ribavirin: Implication for its cardiac developmental toxicity. *Toxicology*, 435:152422.

[Yoon et al., 2019] Yoon, C. S., Kim, H. K., Mishchenko, N. P., Vasileva, E. A., Fedoreyev, S. A., Stonik, V. A., and Han, J. (2019). Spinochrome d attenuates doxorubicin-induced cardiomyocyte death via improving glutathione metabolism and attenuating oxidative stress. *Marine Drugs*, 17.

[Zakaria et al., 2018] Zakaria, Z. Z., Benslimane, F. M., Nasrallah, G. K., Shurbaji, S., Younes, N. N., Mraiche, F., Da'as, S. I., and Yalcin, H. C. (2018). Using Zebrafish for Investigating the Molecular Mechanisms of Drug-Induced Cardiotoxicity. *BioMed Research International*, 2018:1–10.

[Zhang et al., 2019] Zhang, J., Tao, R., Campbell, K. F., Carvalho, J. L., Ruiz, E. C., Kim, G. C., Schmuck, E. G., Raval, A. N., da Rocha, A. M., Herron, T. J., Jalife, J., Thomson, J. A., and Kamp, T. J. (2019). Functional cardiac fibroblasts derived from human pluripotent stem cells via second heart field progenitors. *Nature Communications*, 10:2238.

[Öman et al., 2005] Öman, M., Lundqvist, S., Gustavsson, B., Hafström, L., and Naredi, P. (2005). Phase i/ii trial of intraperitoneal 5-fluorouracil with and without intravenous vasopressin in non-resectable pancreas cancer. *Cancer Chemotherapy and Pharmacology*, 56:603–609.

Suplemental Data

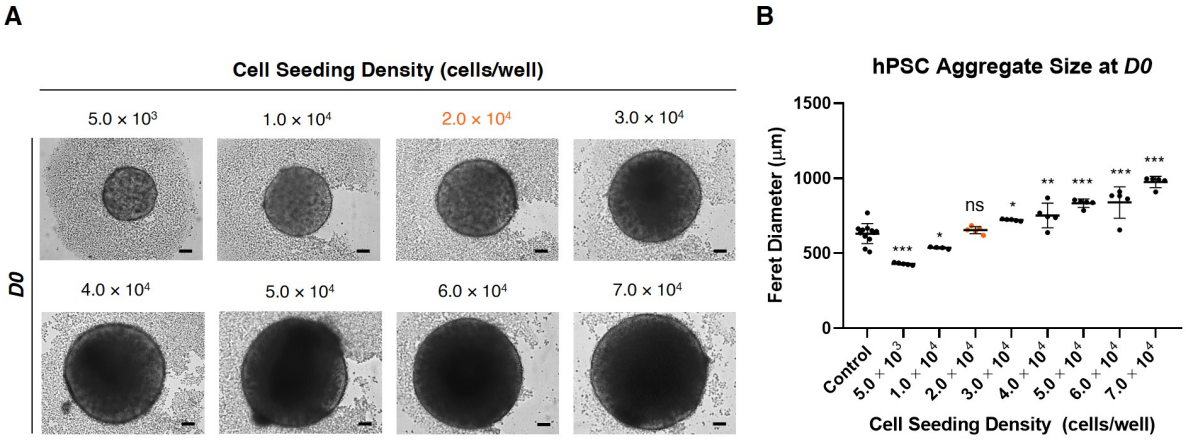

Figure A.1: Optimization of cell seeding density for formation of hiPSC aggregates for cytotoxicity testing. **A** - Representative bright-field images of the size of hiPSC aggregates on Day 0 of the citotoxicity assay. Formation of the aggregates occurred on Day –2 using cell seeding densities of 5.0×10^3, 1.0×10^4, 2.0×10^4, 3.0×10^4, 4.0×10^4, 5.0×10^4, 6.0×10^4, and 7.0×10^4 cells/well. Scale bars represent 100 µm. **B** - hiPSC aggregate size on Day 0 by Feret diameter measurement. Control condition corresponds to CM aggregates on Day 9 of differentiation. Mean $\pm$ SD; n $= 1$ experiment for each condition with technical replicates ranging from N $= 4 - 12$. Statistical analysis was performed based on ANOVA with Dunnett's multiple comparisons test comparing each condition with the control condition (***p <0.001 between 5.0×10^3, 5.0×10^4, 6.0×10^4, and 7.0×10^4 cells/well and control; *p = 0.040 between 1.0×10^4 cells/well and control; *p = 0.040 between 3.0×10^4 cells/well and control; *p = 0.002 between 4.0×10^4 cells/well and control). A cell seeding density of 2.0×10^4 (orange) was chosen.

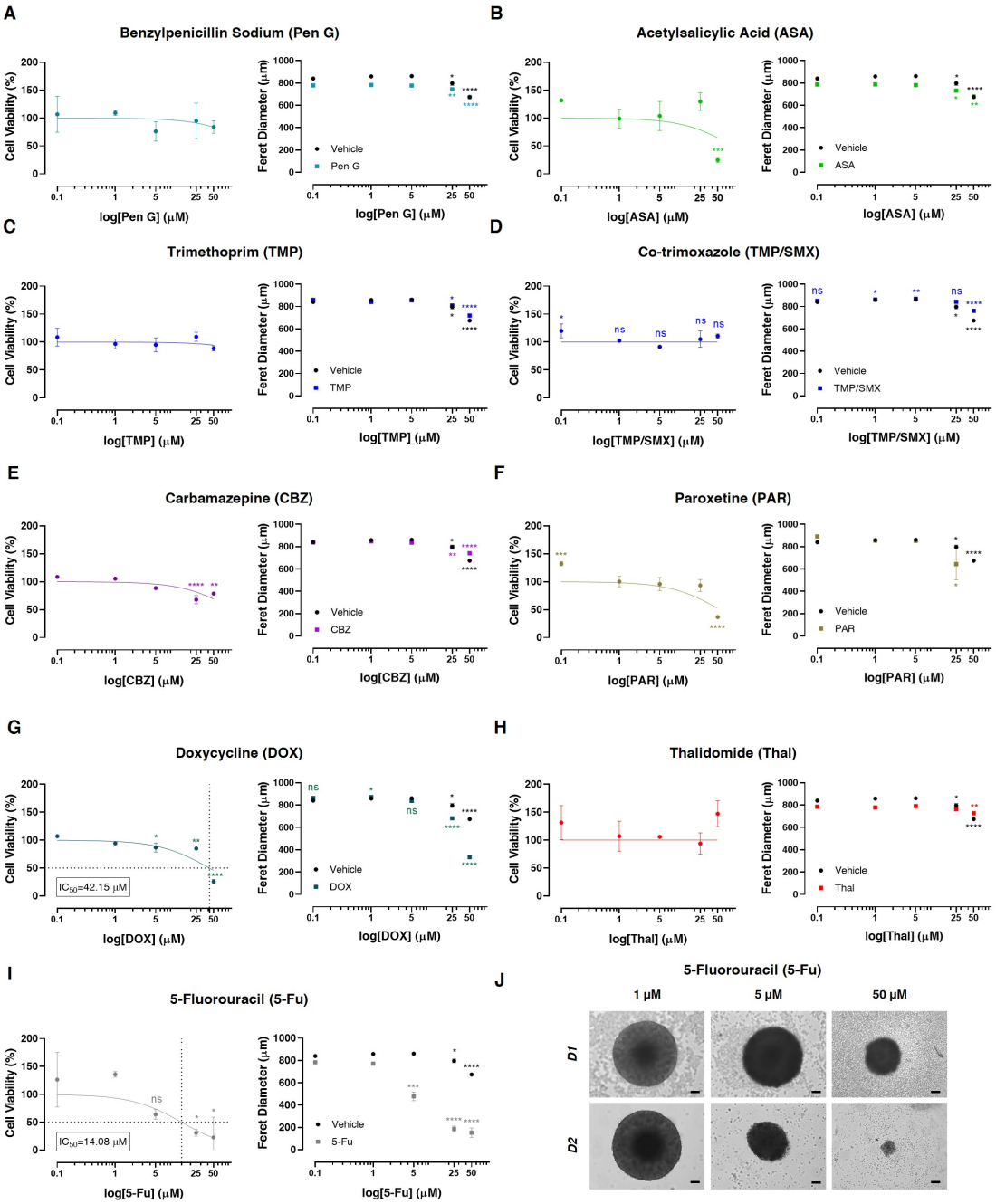

Figure A.2: Comparison between cell viability and hiPSC aggregate size on the day of the cytotoxicity experiment after exposure to the nine selected drugs. Usually, a trend of decrease in cell viability was accompanied by reduced aggregate size. An effect of vehicle-induced toxicity was also detected. **A-I** - Cell viability (**left**) and hiPSC aggregate size (**right**) of Pen G, ASA, TMP, TMP/SMX, CBZ, PAR, DOX, Thal, and 5-Fu, respectively, measured on Day 2 of the cytoxicity experiment. Mean $\pm$ SD; n $= 1$ experiment for each condition with technical replicates ranging from N $= 2 - 3$. Statistical analysis was performed based on ANOVA with Dunnett's multiple comparisons test comparing each condition with the control condition. **J** - Representative bright-field images of the evolution of hiPSC aggregates during drug exposure. Each photo corresponds to the evolution of the same aggregate throughout time within conditions. n $= 1$ experiment. Scale bars represent 100 µm.

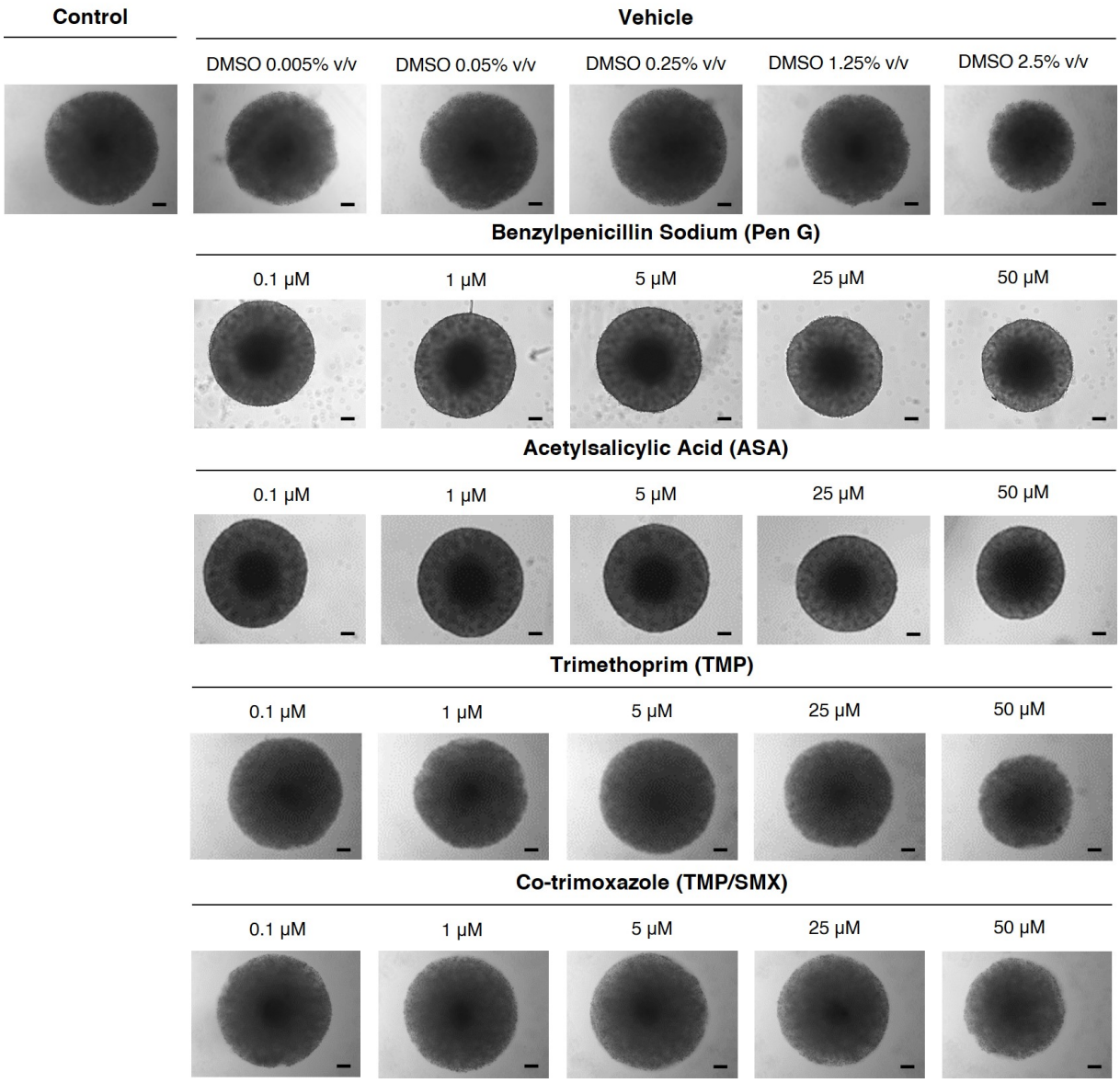

Figure A.3: Representative bright-field images of the impact of exposure to increasing doses of vehicle, Pen G, ASA, TMP, and TMP/SMX on hiPSC aggregates on Day 2 of the cytoxocity experiment. n $= 1$ experiment. Scale bars represent 100 µm.

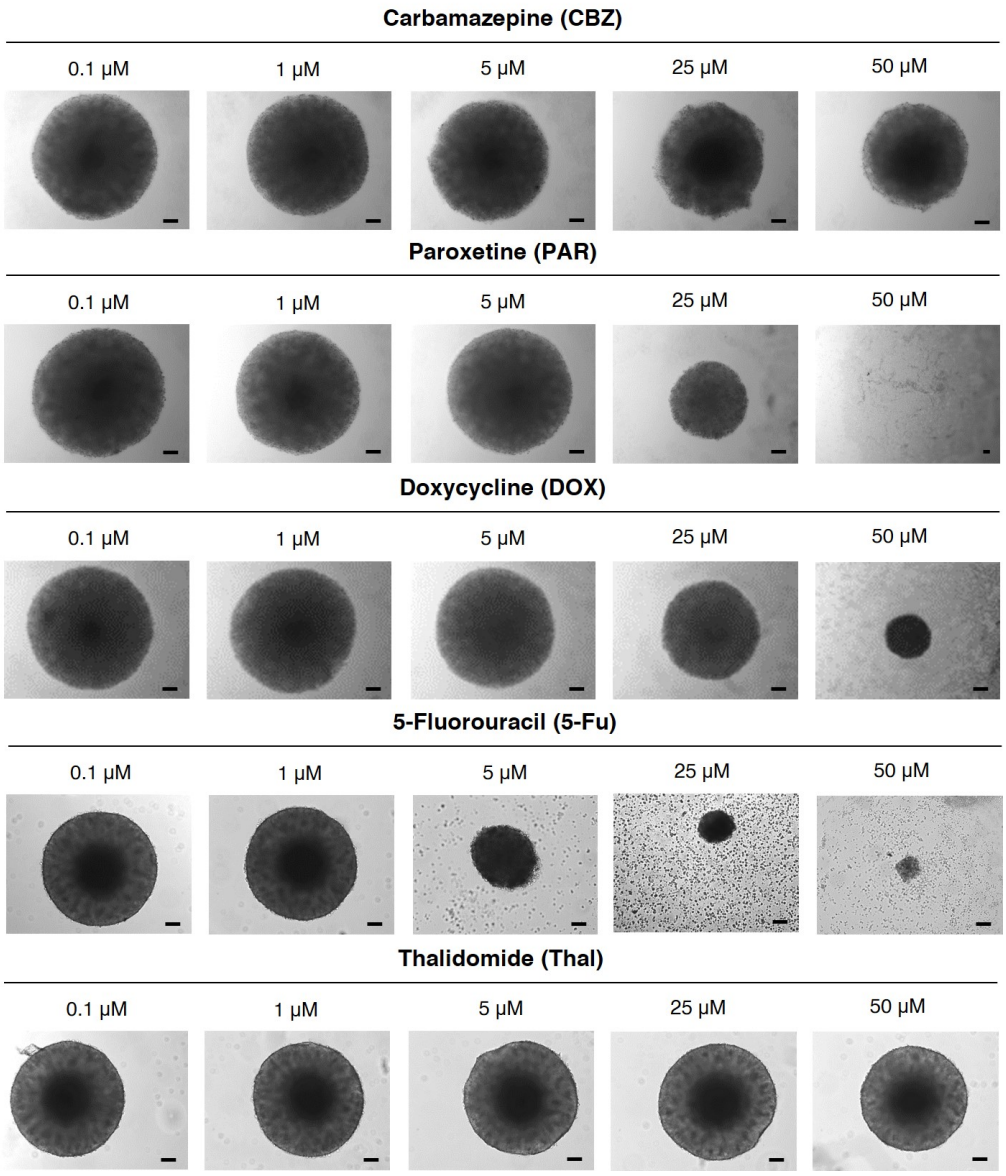

Figure A.4: Representative bright-field images of the impact of exposure to increasing doses of CBZ, PAR, DOX, 5-Fu, and Thal on hiPSC aggregates on Day 2 of the cytoxocity experiment. n $= 1$ experiment. Scale bars represent 100 µm.

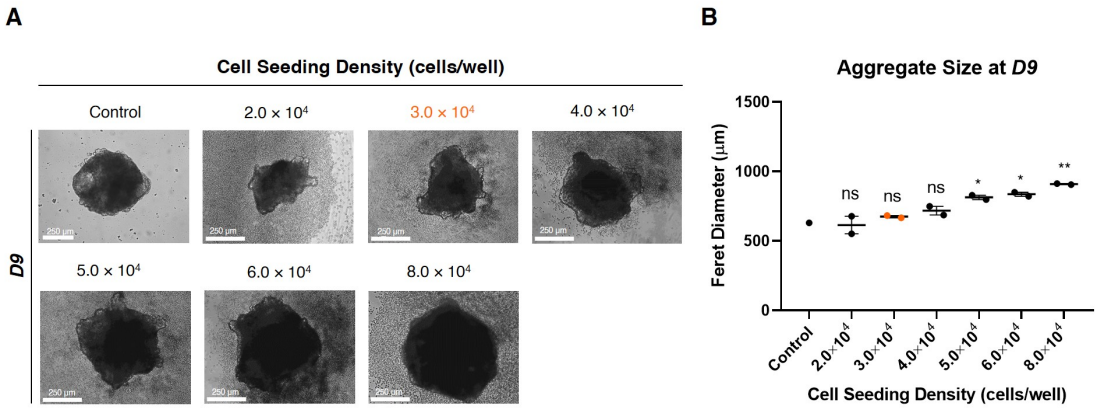

Figure A.5: Optimization of cell seeding density for re-aggregation on Day 5 of differentiation. **A** - Representative bright-field images of the size of aggregates on Day 9 of differentiation. Re-aggregation was performed using cell seeding densities of 2.0×10^4, 3.0×10^4, 4.0×10^4, 5.0×10^4, 6.0×10^4, and 8.0×10^4 cells/well. Scale bars represent 250 µm. **B** - Aggregate size on Day 9 by Feret diameter measurement. Control condition corresponds to non-re-aggregated aggregates on the same day of differentiation. Mean ± SEM; n $= 2$ independent experiments for each condition, except control (n $= 1$), with technical replicates ranging from N $= 6 - 12$. Statistical analysis was performed based on ANOVA with Dunnett's multiple comparisons test comparing each condition with the control condition (*p = 0.0432 between 5.0×10^4 cells/well and control; *p = 0.0266 between 6.0×10^4 cells/well and control; **p = 0.0064 between 8.0×10^4 cells/well and control). A cell seeding density of 3.0×10^4 (orange) was chosen.

Table A.1: Composition of Day 5 hiPSC-derived aggregates in terms of progenitor populations after exposure to the nine selected drugs as assessed by flow cytometry analysis. Mean ± SEM. n $= 2 - 3$ independent experiments.

Drug	**Mesoderm ($CXCR4^+c\text{-}KIT^-$, %)**	**Endoderm ($CXCR4^+c\text{-}KIT^+$, %)**	**Other ($CXCR4^-c\text{-}KIT^-$, %)**
Control	78.3 ± 1.83	17.2 ± 2.10	3.79 ± 2.03
Vehicle	85.7 ± 0.55	12.3 ± 1.10	1.75 ± 0.35
Pen G	86.2 ± 1.56	7.87 ± 0.61	5.64 ± 0.74
ASA	85.7 ± 0.74	7.60 ± 0.33	6.37 ± 0.48
TMP	80.9 ± 0.30	17.0 ± 0.30	1.64 ± 0.14
TMP/SMX	79.5 ± 3.80	17.8 ± 4.80	2.33 ± 0.90
CBZ	84.8 ± 0.90	12.3 ± 1.20	2.60 ± 0.37
PAR	87.4 ± 0.15	5.91 ± 1.08	6.48 ± 1.20
DOX	87.3 ± 3.85	8.33 ± 5.27	4.13 ± 1.53
5-Fu	90.1 ± 1.51	8.42 ± 1.39	1.44 ± 0.14
Thal	87.4 ± 1.28	6.97 ± 1.39	5.36 ± 0.97

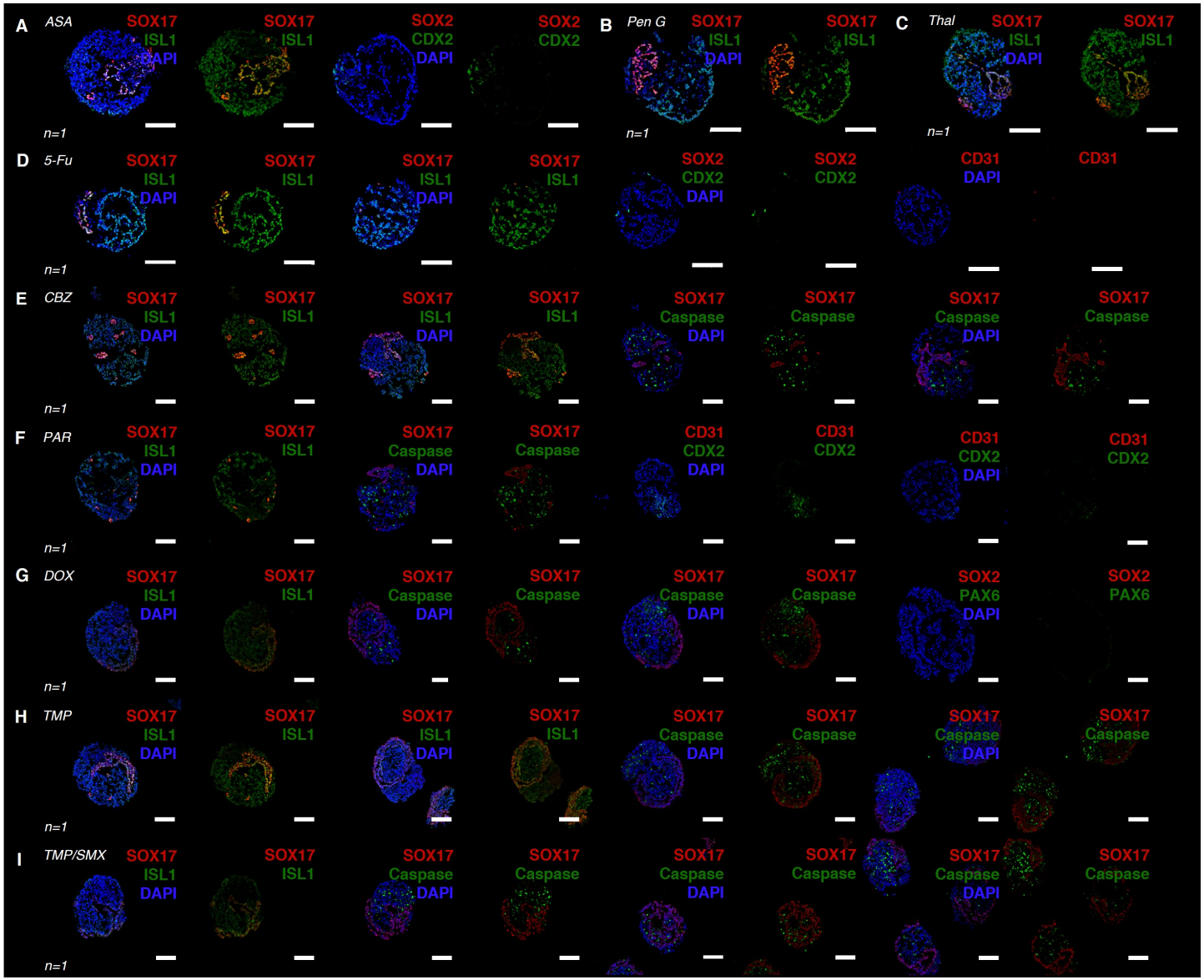

Figure A.6: Exposure to the nine selected drugs was able the impact the spatial organization of progenitor populations. DOX, TMP, and TMP/SMX treatment led to increased levels of SOX 17 expression. Exposure to ASA, Pen G, Thal, 5-Fu, and PAR disrupted the spatial organization of endoderm progenitors. **A-I** - Representative immunostained sections of Day 5 aggregates treated with ASA, Pen G, Thal, 5-Fu, CBZ, PAR, DOX, TMP, and TMP/SMX. n $= 1$ experiment. Scale bars represent 100 µm.

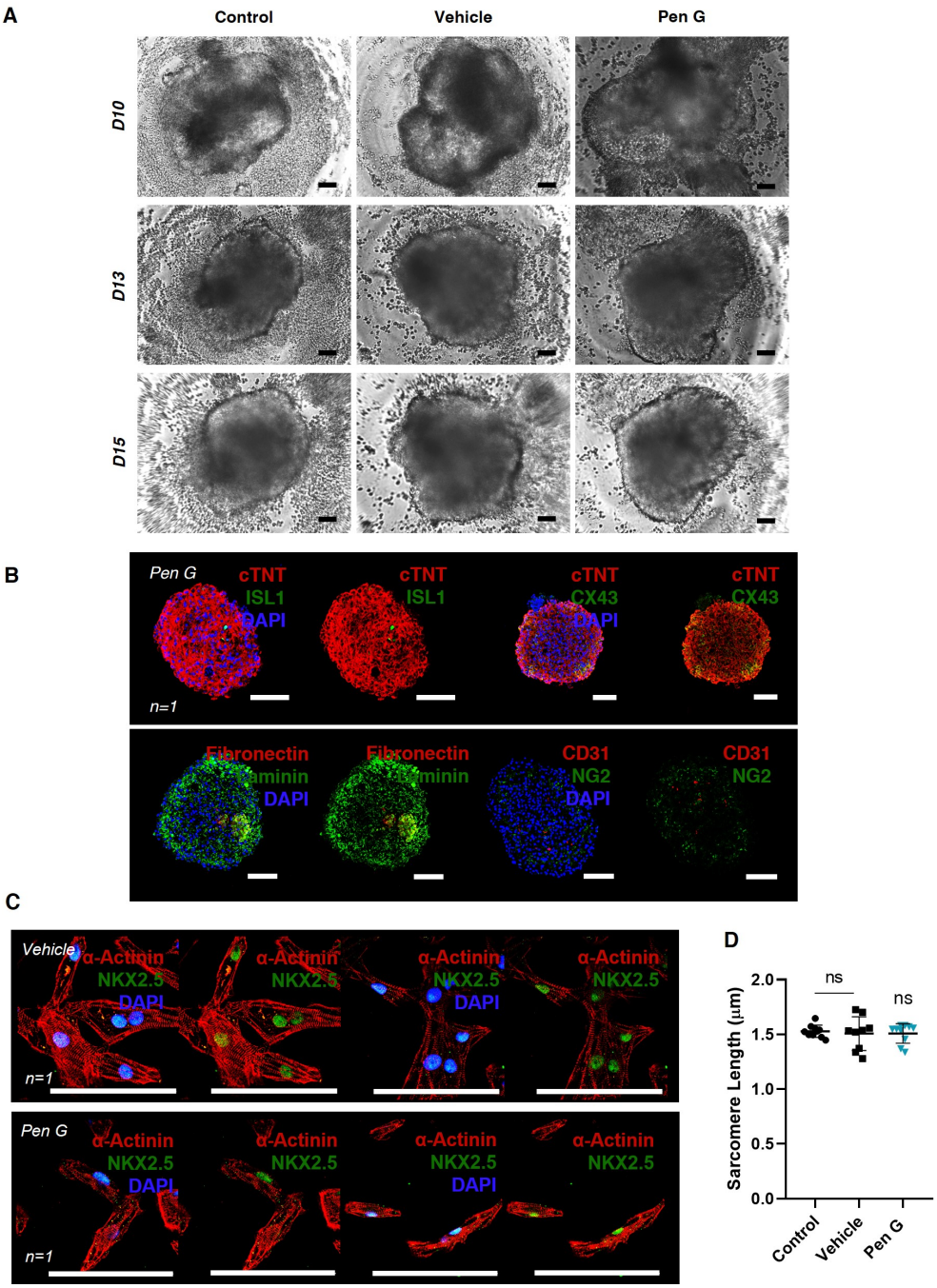

Figure A.7: Effects of Pen G exposure with onset after mesendoderm specification on aggregate and cell morphology, and sarcomere length. No major abnormalities were detected after Pen G treatment from Day 6 to Day 15, as expected due to the drug's proven non-teratogenicity. **A** - Representative bright-field images of the evolution of aggregates treated with Pen G from Day 6 to Day 15. Each photo corresponds to the evolution of the same aggregate throughout time within conditions. **B** - Representative immunostained sections of Day 15 aggregates treated with Pen G from Day 6 to Day 15. n $= 1$ experiment. **C** - Representative immunostaining images of replated cells on Day 15 $+$ 2 after treatment with Pen G from Day 6 to Day 15. n $= 1$ experiment. Scale bars represent 100 µm. **D** - Sarcomere length quantification of Day 15 $+$ 2 cells of the control condition and after treatment with vehicle and Pen G from Day 6 to Day 15. Mean $\pm$ SD. n $= 1$ experiment with technical replicates ranging from N $= 9 - 10$. Statistical analysis was performed using Student's t-test comparing each condition with vehicle.